MODELLING THE TOTAL APPEARANCE OF GONIO-APPARENT SURFACES USING STEREO VISION

Min-Ho Jung

Submitted in accordance with the requirements for the degree of
Doctor of Philosophy

The University of Leeds
Colour & Imaging Group, School of Design

March 2015

The candidate confirms that the work submitted is his own and that appropriate credit has been given where reference has been made to the work of others.

Acknowledgements

First of all, I would like to express my deepest gratitude to my supervisor Dr Peter A. Rhodes and Dr Vien Cheung for his continuous guidance, sincerely support and encouragement. This research work would not have been possible without his support and valuable advice.

I thank the members of my thesis committee: Professor Stephen Westland, Dr Sori Kitaguchi and Professor Ronnier M Luo.

Thanks to all my colleagues and friends who participated in my long-term psychophysical experiments. The following people who–Yiting Duan, Dr Chryseitha Kitsara, Dr Jason Kao,Ziyeoung Kang, Dr seahwa Won, Mengmeng Wang, Dr Qianqian Pan, Dr Caroline Suzanne, Dr Maria Georgoula, Majan Vazirian, Dr Phannaphat Phromphen, Dr Mattew Fuller, Dr Nick Edwards, Chaoran Wang, Al Memari, Dr Maju Sugathan and Martin Douglas Hendry –are my good friends

Whole-hearted thanks to my friends Dr Heeyong Min, Dr JeaHwan You and Dr Kiwoong Nam. Their sincerely advice, beer and coffee were very valuable to carrying out my study.

Finally, I am extremely grateful to my parents, my sister for their patience, support and love during this long period away from home.

I would like to express my profound gratitude to my wife and daughter.

ABSTRACT

Over recent decades, the textured coating provided by metallic surfaces has been an important factor in attracting customers of the automobile industry. This has meant that quantifying the appearance of coating products is essential for product development and quality control. The appearance of these coated products strongly depends on the viewing geometry, giving rise to a variety of properties of perceptual attributes such as texture, colour and gloss. Due to the visually-complex nature of such coatings, there remains an unsatisfied demand to develop techniques to measure the total appearance of metallic coatings.

This study describes which aims to define the total appearance of metallic coatings and then objectively characterise it. Total appearance here refers to the combination of three properties of perceptual attributes of the surface: glint, coarseness and brightness. A number of metallic panels were visually scaled and a computational model capable for predicting three perceptual attributes was developed.

A computational model was developed to relate the results from this psychophysical experiment to data obtained from a stereo image capture system. This is a new alternative technique aimed at solving one of the most challenging problems in computer vision: stereo matching. In the system, two images are captured by a same camera under two different lighting conditions to mimic stereoscopic vision. This not only addresses the problem of stereo matching (i.e. to find the corresponding pixels between two images) but also enhances the effect of perceptual attributes. After linearisation of camera response, spatial uniformity correction was performed to minimise the effect of uneven illumination. A characterisation method was then used to transfer the *RGB* to device-independent values. Two images captured under different lighting conditions were merged to obtain stereo data. In glint feature extraction, the pixels in the final image were segmented into two regions: bright spots and dark background. Next, statistical analyses were applied to extract features. Finally a model was created to predict the glint attribute of the metallic coating panels based on an image captured by the stereo capture system. In coarseness feature extraction, the merged image transformed to frequency domain using a discrete Fourier Transform. An octave bandpass filter was then applied to the Fourier Spectra image and data analysis was carried out to achieve the “image variance value” for each band. In similar to final step of glint, a model was created to predict the coarseness attribute.

CONTENTS

LIST OF FIGURES

LIST OF TABLES

CHAPTER 1
INTRODUCTION

CHAPTER 1. Introduction

1.1. Background of the research

Recent developments in automobile industry and automobile finishing industries have enhanced the efficient product development and quality control of metallic coating panels. The appearance of the coating surface can be strongly changeable according to illumination and viewing angle and present the visually various properties such colour, glint, coarseness, etc. This complex appearance poses the question, "how can the visual texture properties of metallic-coatings be visually assessed". With regard to the study, it should be considered that the appearance of coatings is the interaction effect between various attributes of visual texture and human stereoscopic vision.

1.2. Aim and objectives

The aim of this study was to investigate which appearance properties of gonio-apparent surfaces are influenced by stereoscopic and monocular vision using a psychophysical approach. In general, many studies have been carried out on measurements and visualisation or preproduction of gonio-apparent properties in terms of a single parameter mainly (Alman, 1984; ASTM,2003; McCamy, 1996; Venable, 1987; Westlund & Meyer, 2001). However gonio-apparent properties cannot be explained by a single or a few parameters because it consists of a combination of various spatially related attributes or has a specific property. A further important consideration is to study how these properties play a role in real human perception.

- To design specific experiments to visually assess according to different properties of gonio-apparent attributes
- To find out and verify the difference between stereoscopic and monocular vision in terms of appearance of various gonio-apparent materials.
- To develop the image acquisition to mimic stereoscopic vision.
- To develop computation models to predict the total appearance of the metallic coating panels.

1.3. Publications

The following publications relate to study presented in this thesis

- Min-Ho JUNG, Vien CHEUNG, and Peter A. RHODES (2012). Difference of Stereoscopic and Monocular Vision on Gonio-apparent Surfaces, *Proceedings of the AIC conference*, Taipei, Taiwan.

- Min-Ho JUNG, Vien CHEUNG, and Peter A. RHODES (2015). Total appearance of metallic coatings using a stereo capture system *Proceedings of the AIC conference*, Tokyo, Japan.

CHAPTER 2

LITERATURE SURVEY

CHAPTER 2. Literature survey

A comprehensive literature survey was carried out at the beginning of the study. It includes appearance and also the topic of stereoscopic vision. This chapter explains a summary of the topic.

2.1. Human visual system

2.1.1. Optical component

Human perception passes through the process that the eye converts physical energy, light, into nerve impulses to be interpreted by the brain. It is, therefore, necessary to understand the construction of the human eye. Figure 2-1 shows a simplified cross-sectional diagram of the human eye. The human eye is nearly spherical with a diameter of approximately 20mm (Gonzalez, 2002). Light passes through several membranes, mainly the cornea, the pupil and lens, then is imaged onto the back of the eyeball, retina. The cornea, a transparent tissue without blood vessels, covers the anterior surface of the eye so that receives most of the optical information. The pupil is an optical aperture. The circular opening of the pupil is controlled by the iris which is a circular coloured part of the eye enclosing the pupil. The membrane, the iris, consists of muscles that adjust the pupil size from about 2mm in diameter in bright light to the maximum diameter of about 8mm in dim light. By changing its size, the pupil provides some compensation for changes in overall light intensity and the process is termed adaptation. The lens performs a function to focus on objects by changing its thickness, being thinner for distant objects and thicker for near. The change of lens-shape is controlled by tension in the fibers of the cilary body and provides the fovea of the retina with the image of an external object sharply focused on. The light energy via the process is transformed to electrical impulses by the retina.

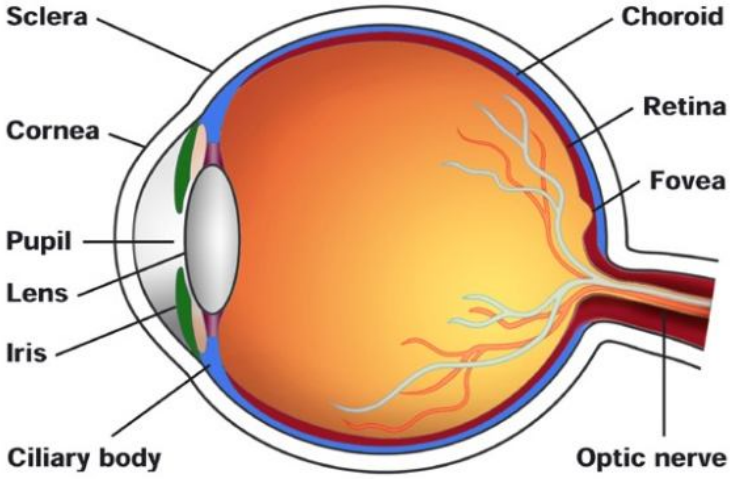

Figure 2-1 Structure of the eye (Tatler, 2007)

2.1.2. The retina

The retina is the portion of eye that light entering the eye is imaged onto and generates an electrical signal eventually interpreted by the brain. The membrane lines most of the interior of the wall's entire posterior portion. Pattern vision is provided by the distribution of discrete light receptors over the surface of the retina. Receptors can be divided into two classes of, rods and cones, named according to their shape. The rods are sensitive to low levels of illumination and detect very small amount of light. The rods have only one pigment type and provide images in monochromatic. As the level of illumination increases, the rods become desensitized and finally stop sending signals to the brain. The number of rods in each eye is between 75 to 150 million and is distributed over the whole area of the retinal surface except the blind spot as shown in Figure 2-2. Particularly, they increase in density from the centre out to approximately 20 degree. On the other hand, cones between 6 and 7 million are concentrated in the central portion of the retina called the fovea. The cones have much lower sensitivity to high level of illumination than the rods. Therefore, they are inactive during the night or in a dimly-lit room. As the amount of light increases, the cones begin sending neural signals to the brain. It means that they are highly sensitive to colour. Cone vision is thus called photopic or bright-light vision.

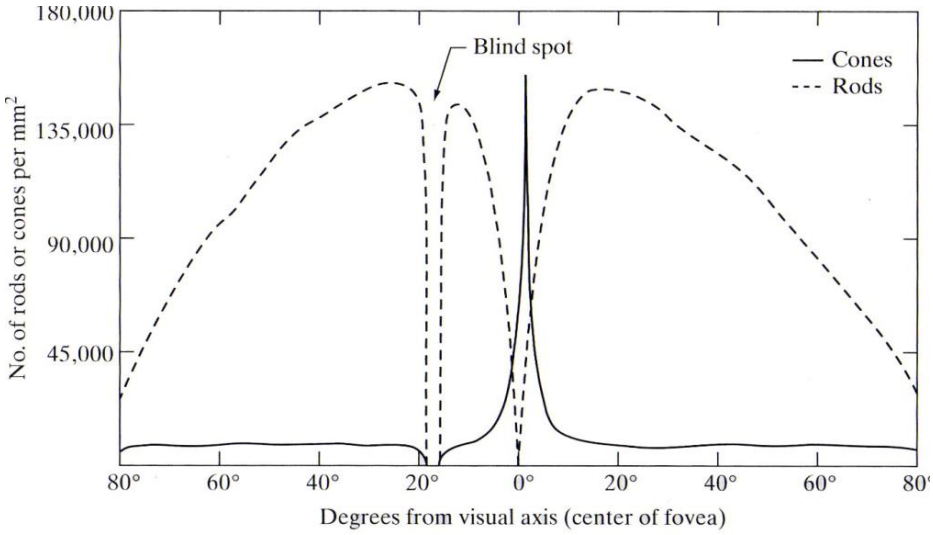

Figure 2-2 The distribution of the rods and cones on the retina

The cones consist of three types of receptors responding differently to light of various wavelengths. The three receptors are represented by the letters L, M, and S with their peak sensitivities in the long, middle, and short wavelength regions, respectively.

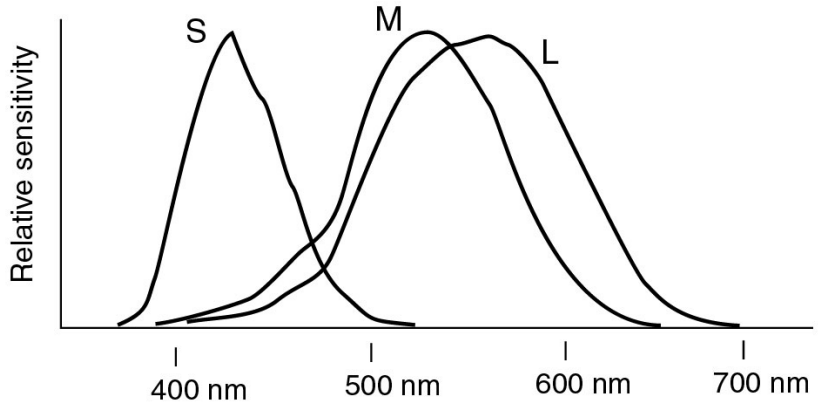

Figure 2-3 The relative spectral sensitivity of the L, M, and S cones

Figure 2-3 shows the spectral sensitivities of the three cones which have maximum sensitivities, 420nm for the S-cone, 530nm for the M-cone, and 560nm for the L-cone (Dartnall *et al.*, 1983) The wavelength sensitivities of the L- and M-cones are very similar, whereas the sensitivity of the S-cone is higher than those of the L- and M-cones in the

short-wavelength region. The L- and M-cones are mostly present in the fovea central while S-cones are mostly found outside the fovea. Their relative population is 40 : 20 : 1 for L-cone : M-cone : S-cone.

2.1.3. Mechanisms of colour vision

Many theories have been developed to explain the mechanisms of colour vision. In this section, three theories are introduced, the trichromatic, Hering's opponent-colours theory and the modern opponent-colours theory.

The trichromatic theory, also known as the three-component theory, was developed based on the work of Maxwell, Young and Helmholtz. The trichromatic theory assumes that signals are generated by three types of independent cones with different spectral sensitivities and are then transmitted to the brain. However, this theory fails to explain several visually observed phenomena. For example, it cannot explain the concept of there being four unique colours: red, green, yellow and blue (Hunt, 1998).

The opponent-colours theory was proposed by Hering in 1872. He noted that certain hues were never perceived to occur together and assumed that colour was encoded into three channels, red-green, yellow-blue, and black-white, with each responding in an antagonistic way. However, this was thought to be physiologically implausible at the time, and Hering's opponent theory did not receive appropriate acceptance (Fairchild, 2005)

The modern opponent-colours theory incorporates both the trichromatic theory and the opponent-colours theory into two stages as shown in Figure 2-5. The first stage can be considered as the receptor stage, in which the three photopigments (red, green and blue cones) absorb the light independently as hypothesized by Maxwell, Young and Helmholtz. However, contrary to the trichromatic theory, the absorptions of the light are not transmitted directly to the brain. Instead, they are converted into the opponent signals in the second stage. The outputs of the three new signals are: one achromatic signal and two antagonistic chromatic signals. The achromatic response is derived from the sum (L+M+S) of cone signals, while the red-green and yellow-blue opponent signals are created by different cone signals L-M and L+M-S, respectively. The transformation from trichromatic to opponent signals for colour appearance can be found within the formulation of all colour appearance models.

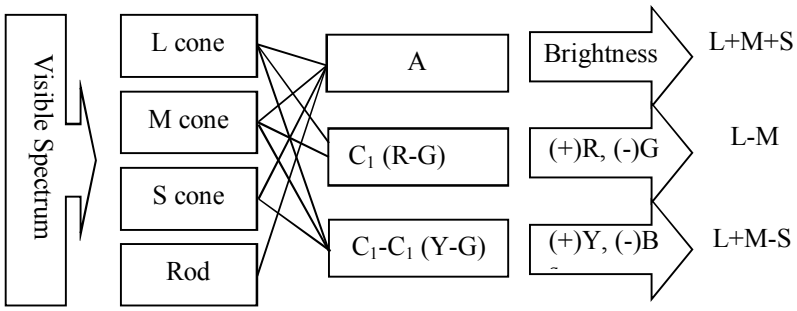

Figure 2-4 Diagram of the opponent colour theory

2.1.4. Mechanisms of adaptation

Adaptation occurs when colour is perceived under changing viewing conditions. It can be mainly explained by chromatic and luminance adaptation.

The human visual system can operate, although not with equal visibility, over an enormous range of illumination, i.e. from bright sunlight to dim star light; it compensates and optimises the response of the eye for changing levels of illumination. This is called luminance adaptation. As explained in section 2.1.1, changing the pupil size is a process to control the amount of light entering the eye. In particular, a function of changes in pupil diameter plays an important role in the reduction of the effects caused by sudden changes in the level of illumination. While both rods and cones take several minutes for the adaptation to complete, as shown in Figure 2-5. In the worst case, the dark adaptation from light adaptation, it takes about 30 minutes to completely accomplish a reasonable level of adaptation. They function under different luminance levels because of different sensitivity. The rods, being more sensitive and more numerous than cones, operate alone at low levels of illumination, less than 0.1 lux. The cones are only active at high luminance levels, higher than 10 lux.

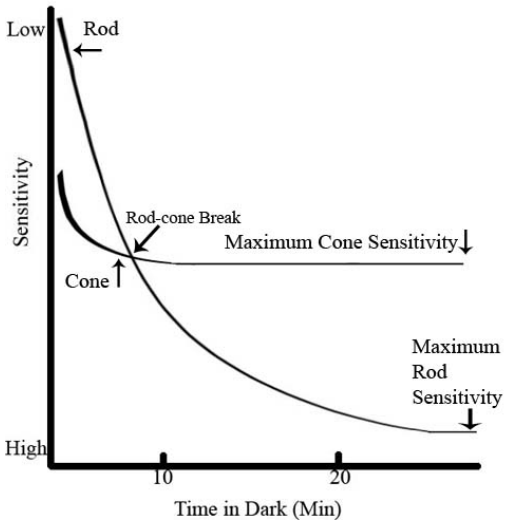

Figure 2-5 The length of adaptation time in for cones and rods
(Department of Psychology University of Calgary, 2005)

Another mechanism is chromatic adaptation, a visual mechanism for adapting to changes in the spectral composition of the illumination entering the eye. Chromatic adaptation leads to the effect known as colour constancy. The effect of chromatic adaptation is a two-stage process: a chromatic shift and an adaptive shift. The colour appearances of the objects become normal after a certain adaptation period even though colorimetric shifts for objects are caused by the changes of a light source, which has the different spectral power distribution. For example, white paper always appears white regardless of which illuminant it is viewed under. In other words, colour appearance of objects doesn't change under different illuminants. The second adaptive shift is caused by physiological changes and a cognitive mechanism. Judd (1940) explained that 'the processes by means of which an observer adapts to the illuminant or discounts most of the effect of non-daylight illumination are complicated; they are known to be partly retinal and partly cortical'.

2.2. Colorimetry

Colorimetry is a method of specifying numerically the colour of a physically-defined visual stimulus in such a manner that (Wyszecki et al. 1982):

a) stimuli with the same specification look alike when viewed by an observer with normal colour vision under the same observing conditions;

b) stimuli that look alike have the same specification; and

c) the numbers comprising the specification are continuous functions of the physical parameters defining the spectral radiant power distribution of the stimulus.

The technology began to answer one question, 'Does this colour match this reference colour?'. The easiest method of quantifying the colour was to use the Munsell system which includes several hundred colour chips at equal intervals of visual spacing. The sample is assigned the notation of the colour chips closest to it in colour. Visual colour matching is very subjective since a human observer is the judge of the match. CIE Tristimulus colorimetry is the most common system used to quantify the colour of displays, and it is based on the assumption that any colour can be matched by a suitable combination of three primary colours. This is a colour matching experiment, known as the colour matching functions. In 1931, the Commission Internationale de l'Eclairage(CIE) defined Standard Illuminant and Standard Observer functions.

The CIE Standard Illuminants are a series of spectral power distributions recommended as standard light sources for measuring colours. In 1931, The CIE defined the three standard illuminants, A, B and C. The standard source A represents an incandescent light having colour temperature of 2856K. Standard sources B and C indicate direct sunlight and average daylight respectively. They can be produced by filtering the standard source A and operate 4874 and 6774K respectively. In 1964, CIE recommended a series of the D illuminants. It is useful for measuring materials with fluorescent colorants since it has more power in the ultraviolet region then standard sources B and C. D65 and D50 of D illuminant are the most widely used in surface colour industry and display industry respectively.

2.2.1. CIE Standard Colorimetric Observer

The CIE standard colorimetric observer is recommended as representative of an average human viewer with normal colour vision and defined by a set of colour-matching functions. Colour matching experiment is based on the assumption that any colours may be visually matched by a suitably-adjusted additive mixture of three primary colours- Red, Green and Blue. As illustrated in Figure 2-6, the left half of the circle provides the target stimulu produced by passing incandescent light through a filter. The other half of the circle

provides a mixture of red, green and blue stimuli originating from three spotlights. Observers attempted to match the colour appearance of test stimuli by adjusting the radiant powers of the primary stimuli.

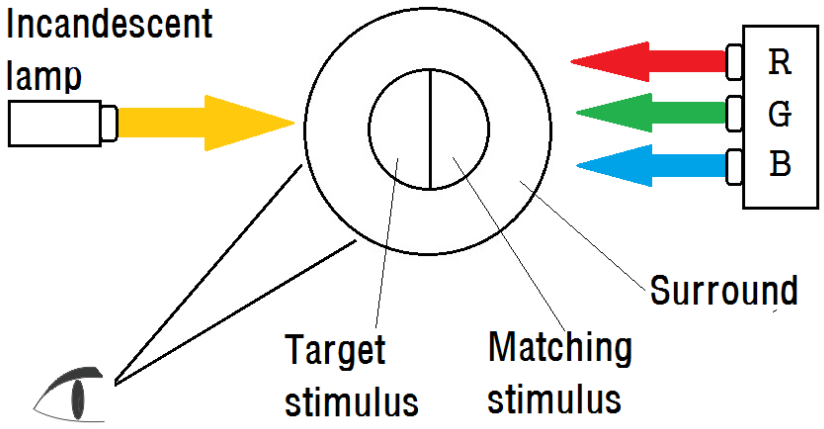

Figure 2-6 A typical experimental setup for additive colour mixing

2.2.1.1.CIE 1931 Standard Colorimetric Observer

The CIE 1931 Standard Colorimetric Observer was recommended as the colour matching functions $\bar{x}(\lambda)$, $\bar{y}(\lambda)$ and $\bar{z}(\lambda)$ of the standard observer for a 2° viewing field. In 1920s, two experiments were performed to measure the color matching function of a small number of color normal observers. Guild measured colour matching functions of the seven observers and three primaries that were generated by placing suitable coloured filters over an incandescent tungsten lamp. Wright collected data from ten observers and three monochromatic primaries at 650, 530 and 460 nm. Both experiments employed the same viewing conditions, a bipartite field subtending a 2° visual angle that was surrounded by darkness for adaptation purposes. In 1931, Colorimetry Committee of the CIE agreed to adopt a color matching system based on the Guild and Wright experimental results. Both sets of colour matching data were transformed into a system in which the RGB primary stimuli, $\bar{r}(\lambda)$, $\bar{g}(\lambda)$ and $\bar{b}(\lambda)$, were monochromatic primaries at wavelengths of 700, 546.1 and 435.8 nm respectively. The colour matching function of the CIE 1931 standard colorimetric observer are shown in Figure 2.7 (a). The $\bar{r}(\lambda)$ curve shows strongly negative in the bleu-green part of the spectrum and $\bar{g}(\lambda)$, $\bar{b}(\lambda)$ curves have a small negative part in the violet and yellow respectively. The negative lobes in the curves indicate that a match

can only be accomplished by adding one of the matching primaries to the test stimulus. The negative part of $\bar{r}(\lambda)$ arise because some amount of R is added to the test colour, with spectral colour matched by G and B only. The existence of the negative lobes in the colour-matching functions caused difficulties in many colorimetric calculations at that time of standardizing the trichromatic system (Schanda 2007). The $\bar{r}(\lambda)$, $\bar{g}(\lambda)$, $\bar{b}(\lambda)$ function were, thus, linearly transformed to a new set of function, $\bar{x}(\lambda)$, $\bar{y}(\lambda)$ and $\bar{z}(\lambda)$ function in order to avoid negative coefficients in the former set of functions. These imaginary stimuli exists only a mathematical constructs and are not physical realisable. However, The International Commission on Illumination (Commission Internationale de l'Éclairage,CIE) recommended the alternative function for reasons of more convenient application in practical colorimery. The $\bar{r}(\lambda)$, $\bar{g}(\lambda)$, $\bar{b}(\lambda)$ functions fo the CIE 1931 standard colour observer are shown in Figure 2.7 (b) using solid lines.

These colour matching function shown by solid lines in Figure 2.7(b) determine the properties of the the CIE 1931 Standard Colorimetric Observer or 2° observer which serves for visual field sizes of 1° to 4°. The colour-matching functions, $\bar{x}(\lambda)$, $\bar{y}(\lambda)$ and $\bar{z}(\lambda)$ function were defined in the wavelength range 380 – 780 nm at 5 nm wavelength intervals.

2.2.1.2.CIE 1964 Standard Colorimetric Observer

In 1964, the CIE recommended an alternative set of standard colour matching functions, the 1964 Standard Colorimetric Observer denoted by $\bar{x}\_10(\lambda)$, $\bar{y}\_10(\lambda)$ and $\bar{z}\_10(\lambda)$ for 10° viewing field which means a visual field greater than 4°. Since the experiments in the 1931 CIE standard observer were performed using only the fovea which covers only about a 2° angle of viewing field, there are limitations for a number of applications in which stimuli subtend a much larger visual angle.

Stiles and Burch measured the color matching functions of 49 observers with a 10° field of view. The results were transformed to refer to primaries at 645.2 nm, 526.3 nm and 444.4 nm. In the experiment, the very high levels of illumination used as a light source were to reduce rod intrusion, and computational techniques eliminated nearly negligible rod effect. Speranskaya measured the color matching functions of 27 observers, also with a 10° field of view using considerably lower levels of illumination. The CIE removed the effects of rod intrusion caused by Speranskaya's light source and weight-averaged the two

data sets. The calculated result is the 1964 CIE supplementary standard observer(Wyszecki 1982) and usually referred to as the 1964 CIE standard observer or the 10° observer.

The 1964 colour matching functions by $\bar{x}_{10}(\lambda)$, $\bar{y}_{10}(\lambda)$ and $\bar{z}_{10}(\lambda)$ are shown in Figure 2-7(b) by dashed line and compared to the 1931 colour matching functions $\bar{x}(\lambda)$, $\bar{y}(\lambda)$ and $\bar{z}(\lambda)$ by dashed lines.

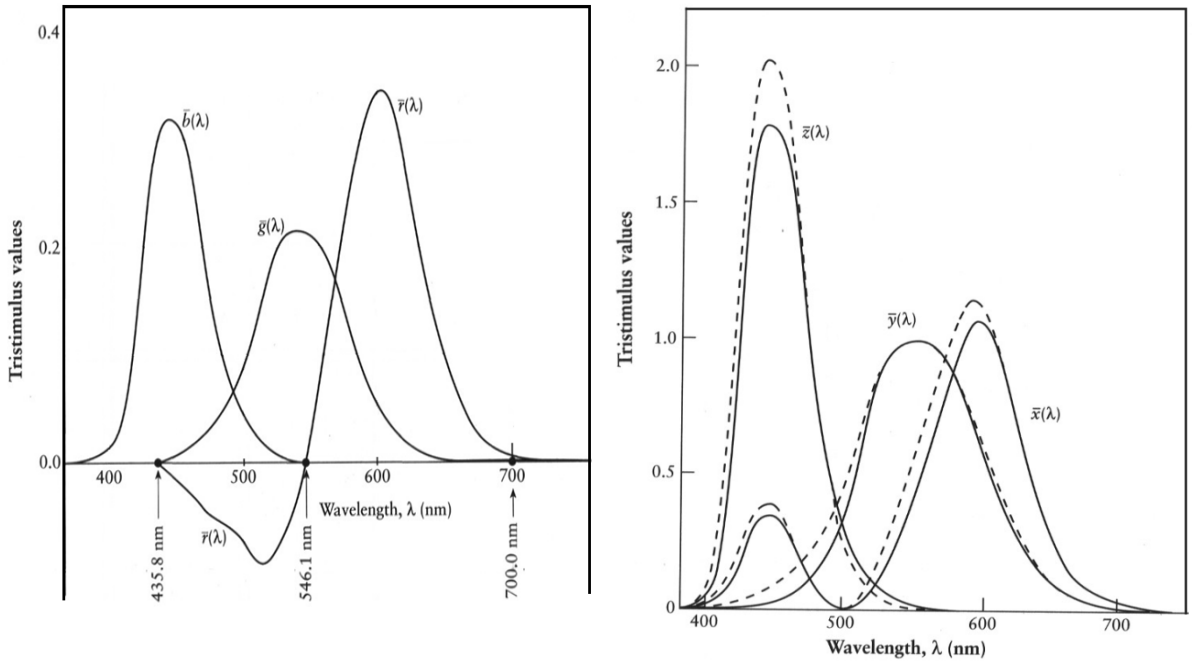

Figure 2-7 (a) Colour matching function; $\bar{r}(\lambda)$, $\bar{g}(\lambda)$ and $\bar{b}(\lambda)$, (b) CIE 1931 standard colorimetric observer (full lines) and CIE 1964 standard colorimetric observer (dashed lines).

2.2.2. Tristimulus Values and Chromaticity Coordinates

The amount of primaries to be matched with the monochromatic test stimuli are referred as tristimulus values. The CIE defined the XYZ tristimulus values of a colour stimulus $S(\lambda)$ using the colour matching Functions by following Equation 2-1

$$X = k\sum S(\lambda)R(\lambda)\bar{x}(\lambda)\Delta(\lambda)$$
$$Y = k\sum S(\lambda)R(\lambda)\bar{y}(\lambda)\Delta(\lambda)$$
$$Z = k\sum S(\lambda)R(\lambda)\bar{z}(\lambda)\Delta(\lambda) \qquad \text{Equation 2-1}$$
$$k = \frac{100}{\sum S(\lambda)\bar{y}(\lambda)\Delta\lambda}$$

where, k is a scaling constant used to normalize the tristimulus value such that a object will have 100 illuminance(Y). S(λ) is the relative spectral power distribution of a CIE standard illuminant or a used light source and R(λ) is a spectral reflectance factor or a spectral transmittance factor of the object. For transmitting objects, R(λ) may be represented as T(λ). $\bar{x}(\lambda)$, $\bar{y}(\lambda)$ and $\bar{z}(\lambda)$ are the colour matching function of the CIE standard observer and Δ(λ) specify the wavelength interval.

For self-luminous objects or illumination such as colours on displays, the multiplication of relative spectral power distribution of a CIE standard illuminant and a spectral reflectance factor of the object, S(λ)·R(λ), may be substituted as the spectral radiance of the colour stimulus in which the maximum luminous efficacy K is set to 683 lm/W.

The CIE 1964XYZ tristimulus values can be calculated in a similar manner using the CIE 1964 colour matching function of the Standard Colorimetric Observer $\bar{x}\_10(\lambda)$, $\bar{y}\_10(\lambda)$ and $\bar{z}\_10(\lambda)$ instead of the the CIE 1931 colour matching function $\bar{x}(\lambda)$, $\bar{y}(\lambda)$ and $\bar{z}(\lambda)$. However, unlike $\bar{y}(\lambda)$, $\bar{y}\_10(\lambda)$ not adjusted to the luminous efficiency so Y value does not represent the luminance in cd/m2.

A way to represent tristimulus values XYZ is to use a chromaticity diagram which is two dimensional colour space called the 1931 or 1964 chromaticity coordinates. Chromaticity coordinates are defined as the ration of the tristimulus values to their sum as shown in Equation 2-2.

$$x = \frac{X}{X+Y+Z}$$
$$y = \frac{Y}{X+Y+Z} \qquad \text{Equation 2-2}$$
$$z = \frac{Z}{X+Y+Z} = 1-x-y$$

where $x + y + z = 1$

hence, z can be calculated from $1 - x - y$ if x and y are given. Only two of three coordinates, x and y, can describe a colour stimulus. For chromaticity coordinates of colour stimuli subtending greater than 4° visual field, the tristimulus values X_{10}, Y_{10} and Z_{10} are replaced in Equation 2-2 instead of the tristimulus value XYZ.

Figure 2-8 shows the CIE 1931 chromaticity diagram in a two-dimensional space giving the *x, y* Chromaticity coordinates of the XYZ colour specification system. In the plot, three points of the triangulation indicate the RGB primaries of the CIE 1931 RGB trichromatic system: 700 nm, 546.1 nm and 435.8 nm for RGB, respectively. The equi-energy stimuls has tristimulus values that are equal to one another. The curved line called the *spectral locus* in the *x, y* chromaticity diagram represents where the colours of the spectrum lie. The straight line called the purple boundary is connected the two ends of the spectral locus. The area inside the spectral locus and the purple boundary represent the domain of all human visible colours. The area within triangle formed by the three lines describes all the colours that can be matched by additive mixtures of these three stimuli. The three lines on the triangle means that two colour stimuli related to each line are mixed together.

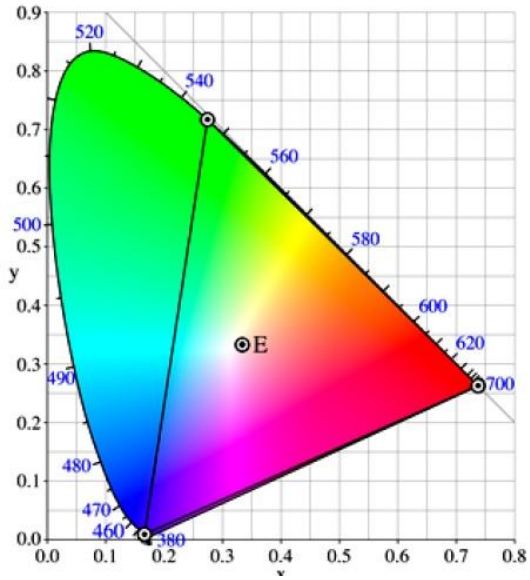

Figure 2-8 x, y chromaticity coordinate diagram of the CIE 1931 trichromatic system.
(http://content.answers.com/main/content/wp/en-commons/thumb/b/ba/325px-CIExy1931_CIERGB.png)

The x, y chromaticity diagrams only represent the proportions of the tristimulus values. Hence, whites, greys, and blacks having tristimulus values in the same ratios to one

another are plotted on same point of the x, y chromaticity diagram regardless of different colour stimuli. This disadvantage is derived from the nature of two dimensional space.

Another problem of the x, y chromaticity diagrams is that the diagram does not well represent the colour differences between the two pairs having the same perceived colour difference. In Figure 2-9(a), each of the short lines represents perceptually the same proportion of colour difference. Thus, the distance of each line should be perceptually the same according to the 1931 CIE standard colorimetric observer. However, the lengths of the lines vary.

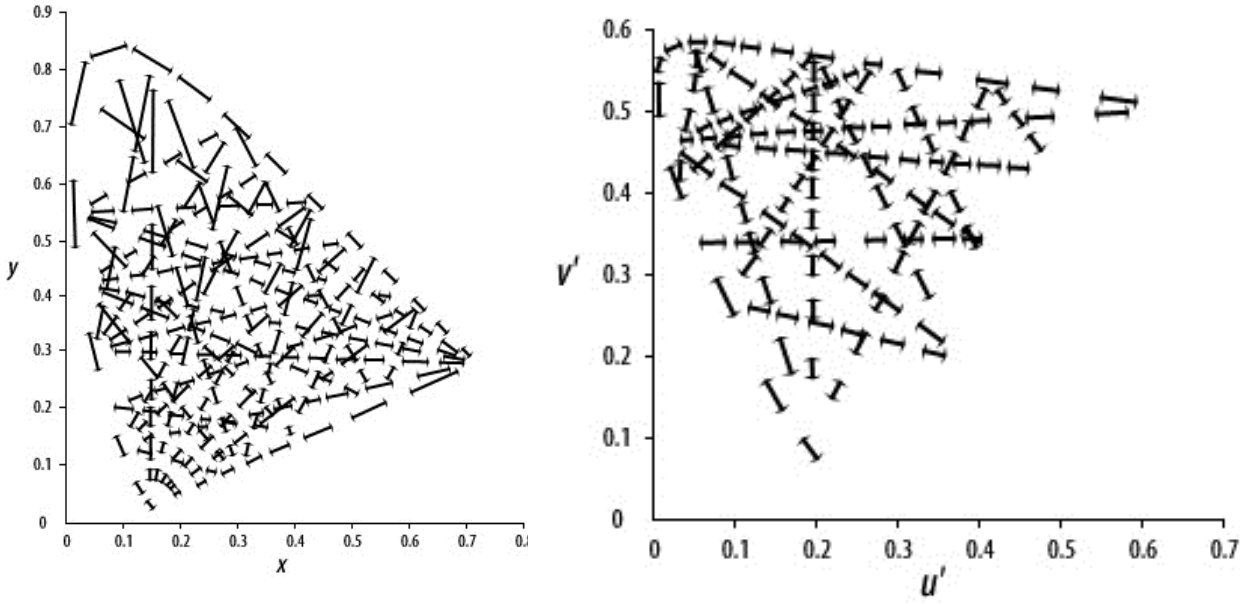

Figure 2-9 x, Equally-perceived colour difference (a) The CIE 1931 x, y chromaticity diagram (b) The CIE 1976 u^',v^'chromaticity diagram (http://dba.med.sc.edu/price/irf/Adobe_tg/models/cieluv.html)

As mentioned in 2.2.2, there is serious disadvantage which the distribution of the colours on the x, y chromaticity diagrams is non-uniform. The equal changes on chromaticity coordinates do not match to equal perceptual differences. As shown in Figure 2-9, there is an alternative diagram called as he CIE 1976 uniform chromaticity scale diagram or CIE 1976 UCS diagram, commonly referred to as the u', v'diagram which has a more perceptually uniform representation for equal colour differences. The CIE 1976 chromaticity coordinates, u', v' was defined from the CIE 1931 tristimulus or chromaticity values as given in Equation 2-3

$$u' = \frac{4X}{X + 15Y + 3Z} = \frac{4x}{-2x + 12y + 3z}$$
$$v' = \frac{9Y}{X + 15Y + 3Z} = \frac{9y}{-2x + 12y + 3z}$$

Equation 2-3

2.2.3. Uniform Colour Spaces

The CIE recommended two uniform colour systems, CIELAB and CIELUV, which give perceptually uniform spaces. The CIELAB and CIELUV spaces are intended to be applied to comparisons of differences between object colours of the same size and shape, viewed in white to middle-grey surroundings, by an observer photopically adapted to a field whose chromaticity is not too different from that of average daylight.

In Figue 2-9, the CIELAB is illustrated with three dimensional orthogonal coordinates; L^* axis being considered vertical, and a^* and b* lying in a horizontal plane. The L^* values of 0 and 100 represent a black and white reference respectively. The a^* and b* indicate redness.-greenness and blueness-yellowness respectively. The C^*_{ab} scale is an open scale with a zero origin and the hue angle, h_{ab}, has the range between 0° and 360°. The L^*, a^* and b* are defined by Equation 2-4

$$L^* = 116 \cdot f\left(\frac{Y}{Y_n}\right) - 16$$
$$a^* = 500 \cdot \left[f\left(\frac{X}{X_n}\right) - f\left(\frac{Y}{Y_n}\right) \right]$$
$$b^* = 200 \cdot \left[f\left(\frac{Y}{Y_n}\right) - f\left(\frac{Z}{Z_n}\right) \right]$$

Equation 2-4

where

$$f\left(\frac{F}{F_n}\right) = \begin{cases} \left(\frac{F}{F_n}\right)^{1/3}, \ldots\ldots\ldots\ldots\left(\frac{F}{F_n}\right) > 0.008856 \\ 7.787 \cdot \left(\frac{F}{F_n}\right) + \frac{16}{116}, \ldots\ldots\left(\frac{F}{F_n}\right) \le 0.008856 \end{cases}$$

and $F \in \{ X, Y, Z \}$

Xn, Yn, Zn represent the reference white.

The hue angle hab and chroma C*ab of CIELAB can be calculated from following formulae.

$$h_{ab} = \tan^{-1}\left(\frac{a^*}{b^*}\right)$$
$$C^*_{ab} = \sqrt{a^{*2} + b^{*2}}$$

Equation 2-5

The hue angle h_{ab} should be defined in the range of 0o $\leq h_{ab} \leq$ 360°.

$$h_{ab} = \begin{cases} \tan^{-1}\left(\frac{b^*}{a^*}\right) + 180° & a^* < 0 \\ \tan^{-1}\left(\frac{b^*}{a^*}\right) + 360° & a^* < 0, \quad and \quad b^* < 0 \\ \tan^{-1}\left(\frac{b^*}{a^*}\right) & otherwise \end{cases}$$

Equation 2-6

The CIELAB does not associated with saturation because of the non-linear nature of the a^* and b^* formulae.

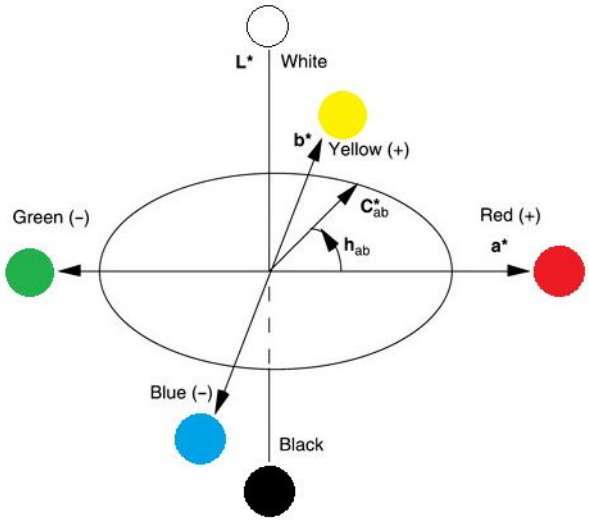

Figure 2-10 A three dimensional representation of the CIELAB space

Unlike the CIELAB, the CIELUV colour space has a correlate of saturation. In Figure 2-10, the sturcture of surfaces of constant CIE hue-angle, saturation and chroma are illustrated. Surfaces of constant hue-angle, h_{uv}, chroma, C^*_{uv}, saturation, s_{uv}, are planes,

cylinders and cones having the are planes, cylinders cones having the L^* axis as one edge or axes respectively. CIELUV colour space is defined by Equation 2-7

$$L^* = 116 \cdot f\left(\frac{Y}{Y_n}\right) - 16 \qquad for \qquad x > 0.008856$$

$$L^* = 903.3 \cdot f\left(\frac{Y}{Y_n}\right) - 16 \qquad for \qquad x \le 0.008856$$

$$u^* = 13L^*(u' - u'_n)$$

$$v^* = 13L^*(v' - v'_n) \qquad \text{Equation 2-7}$$

$$C^*_{uv} = \sqrt{u^{*2} + v^{*2}}$$

$$s^*_{uv} = 13\sqrt{(u' - u'_n)^2 + (v' - v'_n)^2}$$

$$h_{uv} = \tan^{-1}\left(\frac{v^*}{u^*}\right)$$

Euclidean distance in CIELAB colour space can be used to examine approximately the perceived magnitude of colour difference between object colour stimuli. Two equations of CIELAB colour difference are defined by Equation 2-8

$$\Delta E^*_{ab} = \sqrt{(\Delta L^*)^2 + (\Delta a^*)^2 + (\Delta b^*)^2} \qquad \text{Equation 2-8}$$

$$\Delta E^*_{ab} = \sqrt{(\Delta L^*)^2 + (\Delta C^*_{ab})^2 + (\Delta H^*_{ab})^2}$$

The chroma difference, ΔC^*_{ab}, and hue angle difference, Δh_{ab}, are defined as

$$\Delta C^*_{ab} = C^*_{ab,B} - C^*_{ab,S} \qquad \text{Equation 2-9}$$

$$\Delta h^*_{ab} = h^*_{ab,B} - h^*_{ab,S}$$

Where, the indicate B and S refer to a batch (B) and standard (S) of a pair of samples.
In case of hue difference, the unit of this difference is degree.
Seve(1991) developed the Hue difference formulae with the hue angle difference

$$\Delta H^*_{ab} = 2\sqrt{C^*_{ab,B} \bullet C^*_{ab,S}} \sin\left(\frac{\Delta h_{ab}}{2}\right) \qquad \text{Equation 2-10}$$

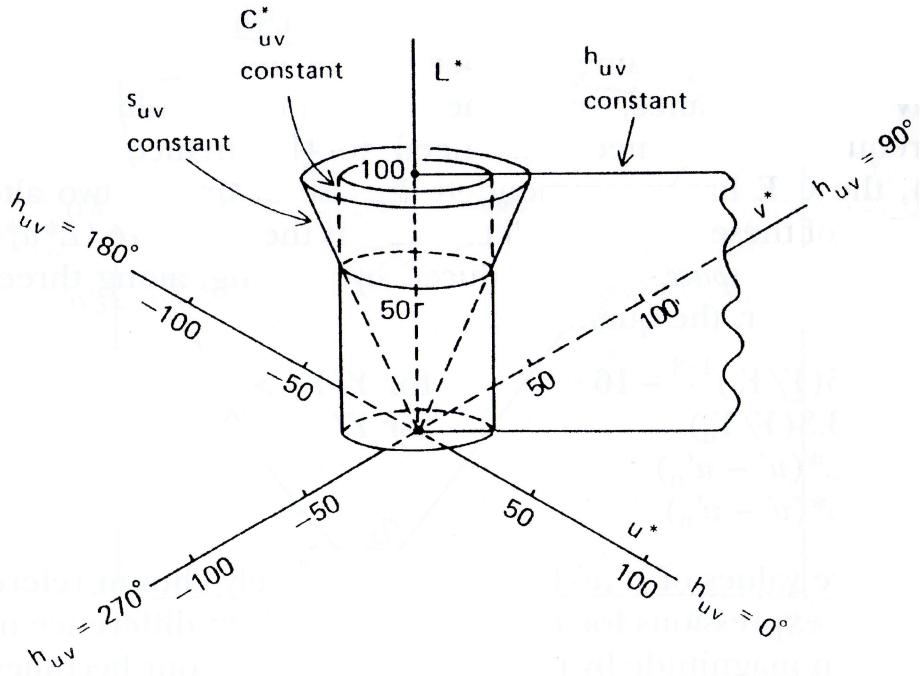

Figure 2-11 A three dimensional representation of the CIELUV (Hunt, 204)

CIELAB and CIELUV have equal merit in correlating with visual color tolerance and both equations can be readily applied to all types of coloured stimuli. It can be sad that the CIELAB and CIELUV are similar, except whether there is no representation of saturation.

2.2.4. Limitations of Colorimetry

Colorimetry is developed to answer one question, 'Does this test colour match this reference colour?' In sections 2.2, the answer is well explained from CIE colorimetric system which is the technology for specifying colours and colour differences. There are, however, constrains in the usage of the CIE colorimetric system in which colours were seen in quite limited viewing condition. The CIELAB and CIELUV colour difference formulae should only be applied to objet colour stimuli of the same size, shape, viewed in white to middle-grey surroundings, by an observer photopically adapted to a field whose chromaticity is not too much different from that of average daylight. It cannot be said that the viewing conditions recommended from CIE is in reality. Colours are viewed under diverse viewing condition and on the various types of image. To overcoming the drawback

of the CIE colorimetric system, CIECAM02 colour appearance model were recommended which is capable of predicting the appearance of colours under a very wide range of viewing conditions. Therefore, following section will explain colour appearance models that specify colous seen under various viewing conditions in terns of colour appearance attribute.

2.3. Appearance

2.3.1. Colour appearance

The colour appearance of an object, or an image, changes according to different viewing conditions such as media, light sources, background colours, and luminance level. Hence, various industrialists related to colour have desired to accurately quantify changes in colour appearance in order to minimize observer dependencies.

2.3.1.1. Colour appearance attributes

The CIE Technical Committee 1-34 defined colour appearance model as follows. “A colour appearance model is any model that includes predictors at least the relative colour appearance attributes of lightness, chroma and hue. Also, Fairchild (1999) proposed “for a model to include reasonable predictors of these attributes, it must include at least some form of a chromatic-adaptation transform. Models must be more complex to include predictors of brightness and colourfulness or to model luminance dependent effects such as the Stevens effect or the Hunt effect”. The colour appearance attributes mentioned above may affect each attribute was defined by CIE (CIE International Lighting Vocabulary, 1987).

Brightness *Attribute of a visual sensation according to which an area appears to exhibit more or less light.*

Lightness *The brightness of an area judged relative to the brightness of a similarly illuminated area that appears to be white or highly transmitting.*

Colourfulness *Attribute of a visual sensation according to which an area appears to exhibit more or less of its hue.*

Chroma *The colourfulness of an area judged in proportion to the brightness of a similarly illuminated area that appears to be white or highly transmitting.*

Saturation *The colourfulness of an area judged in proportion to its brightness.*

Hue *Attribute of a visual sensation according to which an area appears to be similar to one, or to proportion of two, of the perceived colours, red, yellow, green, and blue.*

2.3.1.2.Colour appearance phenomena

The colour appearance phenomena is affected by various viewing conditions including illumination, surround condition, background colour, size, shape texture, viewing geometry. Here are some colour appearance phenomena, which affect to the cross media image reproduction.

At first, it can be categorised by five bigger attributes: change of luminance, change of chromaticity of a light, background, surround and cognitive.

There are three phenomena related to the change of the luminance level. The first one can be described an increase in perceived chromatic contrast (colourfulness) when increasing luminance. This phenomenon called the *Hunt effect* (Hunt, 1952). It supports that a typical outdoor scene appears much more colourful in bright sunlight than it does on a dull day. The second one is the *Stevens effect* (Stevens, 1963). It means that it will be made an increase in brightness or lightness contrast with an increasing luminance. The third phenomenon is the *luminance adaptation* and is responsible for the fact that objects can be recognised with remarkably good consistency over a wide range of illumination levels.

A great deal of research was done about the change of the chromaticity of a light source. The colour of an object can be recognised the difference by the *colour adaptation*. This is achieved by means of the contraction of the pupil, changes in photoreceptor (Cone and Rod) responses, retinal pigment bleaching, changes in cellular activity and cortical changes (Kaiser, 1996). It was assumed that chromatic adaptation could be represented by the cone responses being multiplied by factors that result in reference whites giving rise to the same signals for all states of adaptation by Von Kries (1911) (Von Kries, 1911). Helson (1934) suggested that the visual system regards the averaged colour signals from all over the viewing field as neutral grey and the averaged signals should hence be used as scaling factors instead of using the reference whites. Land (1977) demonstrated that colour appearance is controlled by surface reflectance rather than by the spectral distribution of reflected light. Also, he suggested that the colour of a unit area is determined by a trio of numbers $\left(\overline{R}^{L}, \overline{R}^{M}, \overline{R}^{S}\right)$ each computed on a single waveband (long-, middle-, or short-waveband) to give the relationship for that waveband between the unit area and the rest of the unit areas in the scene (Land, 1986). The concepts of taking the ratio are based on an assumption that human visual system perceives a colour by respecting the luminance ratios from the area to its surroundings rather than its absolute intensity. After these studies about chromatic adaptations, some chromatic adaptation transform (CATs) models based on the above theories were developed. The CIE recommended the CIECAT97 model, which is also used in the CIECAM97s colour appearance model (Luo and Hunt, 1998) for chromatic adaptation transform and a revision of the CAT named CMCCAT2000 (Li et al. 2002) was proposed recently (Luo and Hunt, 1998; Li *et al.*, 2002a).

Colour appearance also changed by the different backgrounds. This colour appearance phenomenon called as the *simultaneous contrast effect*. Figure 2-12 shows one of the general effects, Crispening effect, on simultaneous contrast. Crispening effect is a phenomenon that the apparent contrast between stimuli increases when the stimuli have similar colour against that of background between them. In Figure 2-12, each three small squares arrayed in a line have same colour respectively on three large squares. The lightness difference between two grey stimuli is greater when the stimuli are presented against a background with a lightness value between them.

Figure 2-12 Crispening effect (http://facweb.cs.depaul.edu)

There are the modified effects from simultaneous contrast effect. Spreading effect is one of the illusions when the spatial frequency of the stimuli increases. Simultaneous contrast effect is disregarded and spreading effect causes. Figure 2-13 shows a basic image of this effect. Two set of grey patches have the same space on the pink background. The left patches with low spatial frequency appear slightly greenish due to the effect of simultaneous contrast. However, the right patches with high spatial frequency represent pinkish.

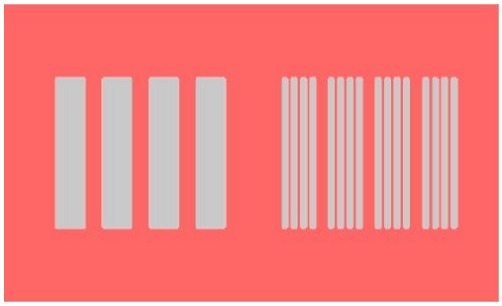

Figure 2-13 Spreading effect (http://www.colorcube.com)

Jameson and Hurvich (1961) showed that the central colour is inversely proportional to the opponent response of the background colour. The effect of simultaneous contrast from complex backgrounds on achromatic attributes also has been investigated (Fairchild, 1999)**;** Lee and Morovic, 2001) and the results reveal that the effect from complex backgrounds is very similar to that of uniform backgrounds when the latter is a linear integration of the former. This is also explains why colour appearance models derived from individual surface colour estimations also perform well for complex images.

Bartleson and Breneman (1967) found that perceived image contrast in colourfulness and brightness is increased with increasing surround luminance level from dark (projection viewing), dim (CRT viewing) and average surround (reflection viewing). It shows the

impact of the surround about the colour appearance phenomenon also. This is an important colour appearance phenomenon to be modelled, especially for the imaging and graphic arts industries, in which it is often required to compare different media under quite different viewing conditions (Luo, 2002).

The last attributes of colour appearance effect are the cognitive attributes. One of these effects, the most important one is the *memory colour*. It can be explained that recognisable objects often have a prototypical colour that is related with them. In other words, most people have a memory colour of green leaf, therefore they can select the proper colour without providing references. Bartleson (1960) investigated the difference between memory colours and actual colours of ten familiar objects. The results showed that saturation and lightness increased in memory and hue shifted in the direction of what is the most impressive chromatic attribute of the object in question. Hunt (1998) also pointed out that as the hues of familiar objects are less variant when light source or lighting geometry change, memory colours are more critical in hue rather than in lightness or colourfulness.

2.3.1.3.CIECAM02 colour appearance model

The colour appearance model, defined by CIE TC1-34 (1998), is a model that includes a chromatic adaptation transform and at least can predict the relative colour appearance attributes of lightness, chroma and hue. Fairchild (2005). summarised that the colour appearance model contains three main parts: a *chromatic adaptation transform* to transform colour stimulus across various viewing conditions; a *dynamic response function* to simulate luminance adaptation; and a *uniform colour space* to predict human perceptual attributes. Various colour appearance models were developed over the years. In 2002, the CIE TC8-01 recommended a new model: CIECAM02. The CIECAM02 is not only a refinement of CIECAM97s, removing many shortcomings, but also an improvement giving equivalent or better predictions of colour appearance data sets (Li *et al.*, 2002b; Li *et al.*, 2005).

2.3.1.3.1. The forward mode

The CIECAM02 model can be divided into three stages: the *chromatic adaptation transform* and *dynamic adaptation*, the derivation of opponent colour signals, and finally the prediction of the colour appearance attributes. The following is the calculation procedure of the CIECAM02 forward mode:

Adopted white in test illuminant: X_W, Y_W, Z_W (Y_W=100)
Background in test conditions: Y_B
Luminance of test adapting field (cd/m2): L_A

Table 2-1 Value of c, N_c and F for different surrounds

Surround	c	N_c	F
Average	0.690	1.0	1.0
Dim	0.590	0.9	0.9
Dark	0.525	0.8	0.8

Step 1: Convert the X,Y,Z of sample to sharpened R,G,B

$$\begin{pmatrix} R \\ G \\ B \end{pmatrix} = M_{CAT02} \begin{pmatrix} X \\ Y \\ Z \end{pmatrix} \quad M_{CAT02} = \begin{pmatrix} 0.7328 & 0.4296\,0 & 0.1624 \\ -0.7036 & 1.6975 & 0.0061 \\ 0.0030 & 0.0136 & 0.9834 \end{pmatrix} \qquad \text{Equation 2-2}$$

Step 2: Calculate the degree of adaptation to white point, the D factor. It ranges from 0 to 1.

$$D = F\left[1 - \left(\frac{1}{3.6}\right) e^{\left(\frac{-(L_A+42)}{92}\right)}\right] \qquad \text{Equation 2-12}$$

Step 3: Compute R_C, G_C, B_C. The subscript *w* and *wr* mean that the values are for the adopted white in the test condition and the reference white respectively.
($Y_{Wr} = R_{Wr} = G_{Wr} = B_{Wr} = 100$)

$$R_C = D_R R \qquad D_R = (Y_W / Y_{WR})(R_{WR} / R_W)D + (1-D)$$
$$G_C = D_G G \qquad D_G = (Y_W / Y_{WR})(G_{WR} / G_W)D + (1-D)$$
$$B_C = D_B B \qquad D_B = (Y_W / Y_{WR})(B_{WR} / B_W)D + (1-D) \qquad \text{Equation 2-3}$$

Step 4: Compute F_L. The subscript b means that the value is for the background

$$F_L = 0.2K^4(5L_A) + 0.1(1-k^4)^2(5LA)^{1/3} \quad \text{Where} \quad k = \frac{1}{5L_A + 1} \qquad \text{Equation 2-4}$$

$$n = \frac{Y_b}{Y_w} \quad , \quad N_{bb} = N_{cb} = 0.725\left(\frac{1}{n}\right)^{0.2} \quad , \quad z = 1.48 + n^{0.5} \qquad \text{Equation 2-15}$$

Step 5: Convert to X,Y,Z corresponding colours

$$\begin{pmatrix} X_C \\ Y_C \\ Z_C \end{pmatrix} = M_{CAT02}^{-1} \begin{pmatrix} R_C \\ G_C \\ B_C \end{pmatrix}, \quad \text{where} \quad M_{CAT02}^{-1} = \begin{pmatrix} 1.096124 & -0.278869 & 0.182745 \\ 0.454369 & 0.473533 & 0.072098 \\ -0.009628 & -0.005698 & 1.015326 \end{pmatrix}$$

Equation 2-16

Step 6: Convert to Hunt-Pointer-Estevez cone responses

$$\begin{pmatrix} R' \\ G' \\ B' \end{pmatrix} = M_{HPE} \begin{pmatrix} X_C \\ Y_C \\ Z_C \end{pmatrix}, \quad \text{where} \quad M_{HPE} = \begin{pmatrix} 0.38971 & 0.68898 & -0.07868 \\ -0.22981 & 1.18340 & 0.04641 \\ 0.00000 & 0.00000 & 0.00000 \end{pmatrix} \qquad \text{Equation 2-17}$$

Step 7: Multiplied *R'G'B* with a luminance-level adaptation factor F_L
(the term '+0.1' accounts for noise)

$$R_a' = \frac{400\left(F_L R'/100\right)^{0.42}}{27.13 + \left(F_L R'/100\right)^{0.42}} + 0.1 \qquad \text{Equation 2-18}$$

$$G_a' = \frac{400\left(F_L G'/100\right)^{0.42}}{27.13 + \left(F_L G'/100\right)^{0.42}} + 0.1 \qquad \text{Equation 2-19}$$

$$B_a' = \frac{400\left(F_L B'/100\right)^{0.42}}{27.13 + \left(F_L B'/100\right)^{0.42}} + 0.1 \qquad \text{Equation 2-20}$$

Step 8: Calculate colour difference signals, and b, and hue angle h_r

$$a = R_a^{'} - 12G_a^{'}/11 + B_a^{'}/11 \quad \text{Equation 2-21}$$

$$b = (1/9)\left(R_a^{'} + G_a^{'} - 2B_a^{'}\right) \quad \text{Equation 2-22}$$

$$h_r = \arctan(b/a) \quad \text{Equation 2-23}$$

Step 9: Hue quadrature, H, is calculated using the following hue data.

Table 2-2 The hue angles and eccentricity factors of the unique hues for computation of hue quadrature, H.

	Red	Yellow	Green	Blue	Red
i	1	2	3	4	5
h_i	20.14	90.00	164.25	237.53	380.14
e_i	0.8	0.7	1.0	1.2	0.8
H_i	0	100.0	200.0	300.0	400.0

$$H = H_i + \frac{100\left(h^{'} - h_i\right)/e_i}{\left(h^{'} - h_i\right)/e + \left(h_{i+1} - h^{'}\right)/e_{i+1}} \quad \text{Equation 2-24}$$

Step 10: Calculate eccentricity factor, e_t

$$e_t = \left(\frac{1}{4}\right)\left(\cos\left(\frac{h^{'}\pi}{280} + 2\right) + 3.8\right) \quad \text{Equation 2-25}$$

Step 11: Calculate the achromatic response, A and A_w

$$A = \left(2R_a^{'} + G_a^{'} + (1/20)B_a^{'} - 0.305\right)N_{bb} \quad \text{Equation 2-26}$$

$$A_w = \left(2R_{aw}^{'} + G_{aw}^{'} + (1/20)B_{aw}^{'} - 0.305\right)N_{bb} \quad \text{Equation 2-27}$$

Step 12: Calculate the correlate of lightness, J

$$J = 100\left(A/A_w\right)^{cz}$$

Step 13: Calculate the correlate of brightness, Q

$$Q = (4/c)(J/100)^{0.5}(A_w + 4)F_L^{0.25}$$

Step 14: Calculate a temporary magnitude quantity, t

$$t = \frac{(50000/13)N_c N_{cb} e_t \sqrt{a^2 + b^2}}{R_a' + G_a' + (21/20)B_a'}$$ Equation 2-28

Step 15: Calculate the correlate of chroma, C

$$C = t^{0.9}\sqrt{J/100}\left(1.64 - 0.29^n\right)^{0.73}$$ Equation 2-29

Step 16: Calculate the correlate of colourfulness, M

$$M = CF_L^{0.25}$$ Equation 2-30

Step 17: Calculate the correlate of saturation, s

$$s = 100\sqrt{M/Q}$$ Equation 2-31

2.3.1.3.2. Uniform colour space based on CIECAM02

The CIECAM02 is an updated version of CIECAM97s in terms of ability of predicting data and some simplifications. Li *et al.*(2002b) explained that the CIECAM02 colour appearance model gives accurate prediction of all the available colour appearance data (Li *et al.*, 2002b). Luo *et al.* (2006) have then extend CIECAM02 for predicting available colour discrimination data sets (Luo *et al.*, 2006). The data set are composed of two types, Large and Small magnitude Colour Differences, designated by LCD and SCD respectively.

Three different colour spaces can be formed the components of CIECAM02 by the combination of lightness (J) and hue angle (h), and three correlates of chromatic content, Chroma (C), Colourfulness (M), and Saturation (s).

a) J, a_c and b_c where, $a_c = C\cos(h)$, $b_c = C\sin(h)$
b) J, a_M and b_M where, $a_M = M\cos(h)$, $b_M = M\sin(h)$
c) J, a_s and b_s where, $a_s = s\cos(h)$, $b_s = s\sin(h)$ Equation 2-32

Li *et al*. (2003) found that the colour space derived using J, a_M and b_M provide the most uniformly minimum error between the experimental and predicted colour-difference data for both LCD and SCD cases (Li *et al.*, 2003). The modified J and M are designated as J' and M' by using below equations respectively. The corresponding colour space can be derived using J, a_M and b_M where $a'_M = M' \cos(h)$, $b'_M = M' \sin(h)$. The colour-difference formula in the new colour space is expressed by Equation 2-35 :

$$\boldsymbol{J' = \frac{(1+100c_1)J}{1+c_1 J}} \qquad \text{Equation 2-33}$$

$$\boldsymbol{M' = (1/c_2)In(1 + c_2 M)} \qquad \text{Equation 2-34}$$

$$\boldsymbol{\Delta E = \sqrt{(\Delta J'/K_L)^2 + \Delta a'^2_M + \Delta b'^2_M}} \qquad \text{Equation 2-35}$$

where, c_1 and c_2 are constants and K_L is a lightness parameter, as given in Table 2-3.
Three sets of optimised c_1, c_2, and K_L values were established for the three types of data, LCD, SCD, and LCD and SCD combined. The corresponding three colour spaces were derived using the three sets of optimised parameters for J', M' and K_L , and were named CAM02-LCD, CAM02-SCD and CAM-UCS.

Table 2-3 The three sets of coefficients for the three corresponding colour

Versions	CAM02-LCD	CAM02-SCD	CAM02-UCS
K_L	0.77	1.24	1.00
c_1	0.007	0.007	0.007
c_2	0.0053	0.0363	0.0228

The performances of new CAM02 were tested by comparing with the best available colour difference formulae such as CIEDE2000, DIN99d, CIEDE94,etc, by Luo *et al* (2006) (Luo *et al.*, 2006). The results showed that CAM02-LCD and CAM02-SCD performed either better or equal to the other colour spaces for LCD and SCD data. In addition, the CAM02-

UCS gave excellent performance for predicting the data sets. Therefore, CAM02-UCS is suitable for evaluation of colour-difference on a uniform colour space.

2.3.2. Object appearance

Appearance was defined by the ASTM E284 (2004) to be "the aspect of visual experience by which things are recognised" and "in psychophysical studies, visual perception in which the spectral and geometric aspects of a visual stimulus are integrated with its illuminating and viewing environment". The study will deal with the optical attributes of various materials with gonio-apparent surface closely related to the latter definition: gloss, sparkle, pearlescent, graininess, texture, and haze. Before summary about the optical properties, most of all, it is necessary to understand about gonio-appearance. The ASTM E284 (2004) defined it as "the phenomenon in which the appearance of a specimen changes with change in illumination or viewing angle".

2.3.2.1.Gloss

Gloss is a visual impression that is caused by a shining surface. The more direct light that is reflected, the more obvious will be the impression of gloss. Hunter and Harold (1987) defined it as the attribute of surfaces that causes them to have a shiny or lustrous appearance. Gloss perception is associated with how an object reflects light, particularly due to the way that light is reflected from the surface of the object at and near the specular direction. The specular direction is the angular direction symmetrically to the incident light with respect to the normal direction to the surface. It may well sometimes coincide with the direction of the greatest intensity of reflected light, but not always. However, specular reflection can vary from one surface to another because of a) the fraction of light reflected in the specular direction, b) the manner and extent to which light is spread to either side of this specular direction and c) the change of specular reflection factor as specular angle changes. Hunter studied many different materials and their “glossiness” rankings during the period of 1934 to 1937. He first defined specular gloss as the ratio of light reflected from a surface at a specified angle to that incident on the surface at the same

angle on the other side of the surface normal. Hunter recognised that the perception of gloss requires more than just consideration of specular reflection. He then proposed six types of gloss as shown in Table 2-4.

Table 2-4 Hunter's six type of gloss with their visual evaluation and examples

Type of gloss	Visual evaluation	Types of example surfaces
Specular gloss	Shininess, brilliance of highlights; Mirror-like reflection.	Medium gloss surfaces of book paper, paint, plastics, etc.
Sheen	Shininess at grazing angles; Brilliancy of low-gloss surface especially when curved.	Low-gloss surfaces of paint, paper, etc.
Contrast gloss or Lustre	Contrast between specularly reflecting areas and other areas.	Low-gloss surfaces of textile fibre, yarn and cloth, newsprint, bond paper, diffuse-finish metals, hair, fur, etc.
Absence-of-bloom gloss	Absence of haze, or milky appearance, adjacent to reflected highlights.	High and semi gloss surfaces in which reflected highlights may be seen.
Distinctness-of-image gloss	Distinctness and sharpness of mirror images.	High gloss surfaces of all types in which mirror images may be seen.
Surface - Uniformity Gloss or surface texture	Surface uniformity, freedom from visible non-uniformities such as texture or “orange peel”.	Medium to high gloss surfaces of all types.

2.3.2.2.Pearlescent

'Pearlescent' was defined as exhibiting various colours depending on the angles of illumination and viewing, as observed in mother-of-pearl by the ASTM E284 (E284, 2004). Pearlescent property is commonly shown in natural pearls and mother-of-pearl. **오류! 참조 원본을 찾을 수 없습니다.** shows the optical characteristics of pearlescent flakes are thin, transparent platelets of high refractive index, which partially reflect and partially transmit. The pearlescent flakes named as interference flakes or interference pigments usually consist of thin metal oxide layers on transparent mica platelets and create colour due to light interference (Berns, 2000). The pearlescent effect is produced by interference which occurs through the interaction of light rays of the upper and lower

surfaces of the transparent. More detail, when a portion of the incident light transmitted from transparent mica platelets meet further surfaces with different refractive indices, the part of the light is reflected. The total reflected light is then made up of portions that have travelled on different paths producing optical interference. For the reason, the perceived chroma, hue, and brightness depend on both the illumination and viewing angles (Maria, 2003).

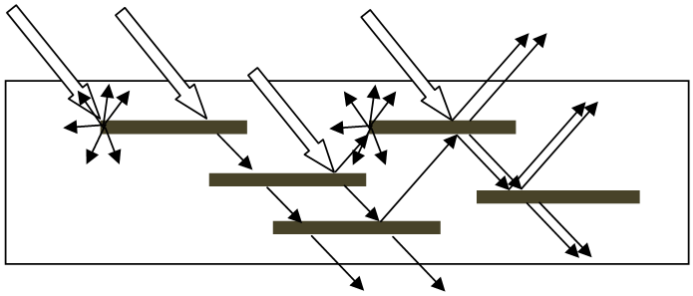

Figure 2-14 Pearlescent flakes both reflect and transmit light.

2.3.2.3.Glint

Akzo-Nobel (2004-2006) explained that glint has been identified as an important attribute of visual texture of metallic coatings. Glint is as an attribute of visual texture and it is categorised as micro appearance, not as macro appearance such as gloss or specular reflection.

Glint is originated mainly in characteristics of aluminium flakes contained in coatings. Akzo-Nobel (2004) proposed three definitions for glint of metallic coatings given. "Point of reflected light of very high intensity that switch on and off while changing panel orientation", "The impression that coatings show bright tiny lights under specific viewing angles only when irradiated by and intense directed light source." and " Tiny spot that is strikingly brighter than its surrounding. It is visible under directional illumination conditions only. The glint may be expected to switch on and off when the observation geometry is changed."

The definition of glint is often mentioned with sparkle and brilliance. They have similar or same appearance properties to glint. There is a definition below which explains glint by taking into account these of them.

"Tiny spot that is strikingly brighter than its surrounding, in other words, bright sparkle. It is visible under directional illumination conditions only. The glint may be expected to switch on and off when the illumination and observation geometry is changed."

2.3.2.4.Coarseness

Kirchner *et al.* (2007) regarded 'Coarseness' as an important aspect of visual texture for metallic coatings and proposed strict definitions taking into account the viewing conditions as " Diffuse Coarseness is the perceived contrast in the light/dark irregular pattern exhibited by effect coatings viewed under diffuse illumination conditions."(Kirchner *et al.*, 2007). Xin and Shen (2005) described it as "related to the spatial repetition period of the local structure"

2.3.2.5.Texture

Texture is a term that refers to the spatial properties representing the surface of an object. ASTM (2001) defined texture; the visible surface structure depending on the size and organization of small constituent parts of a material; typically, surface structure of a woven fabric. Moreover, it was suggested by Pointer (2003) that physical texture and optical texture be differentiated. Physical texture can be associated with physical, topological, variability in a surface and optical texture is texture associated with spatial variation in appearance caused by non-uniformity of colorant. Texture is a widely used term and perhaps intuitively obvious but there are, as yet, no precise methods to describe or measure. It is often described subjectively using terms such as coarse, fine, smooth, granulated and rippled.

2.3.2.6.Pilling

Pilling of fibres on the surface of fabrics is one of big problem in the apparel industry. The pills are formed by the influence of rubbing or friction against the same fabric or another object during wear and/or washing. Cooke (1985) defined pilling as "an undesirable phenomenon that affects the handle and the appearance of sweatshirts" and a pill as "a ball of tangled fibres that is held to the fabric surface by several anchor fibres". Sivakumar and Pillay (1981) defined pills as "bundles of entangled fibres formed on the surface of fabrics during rubbing or wear". According to the ASTM, pills was described as "bunches or balls of tangled fibres which are held to the surface of a fabric by one or more fibres" (Standards, 2002). The definitions from the ISO standard 12945 also states that pilling is the entangling of fibres into balls (pills) which stand proud of the fabric and are of such density that light will not penetrate and will cast a shadow. Pilling is the generation of pills over the surface of the fabric" (Standards B.B., 2000[a]; Standards B.B., 2000[b]).

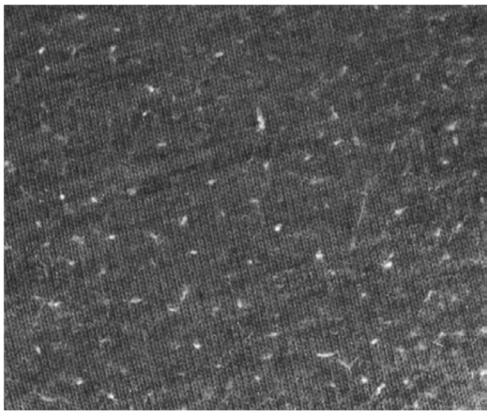

Figure 2-15 An example of pills

2.3.2.7.Haze

ASTM E284 (2004) defined haze as mainly two kinds of attributes in reflection and in transmission: In reflection, (1) scattering of light at the glossy surface of a specimen responsible for the apparent reduction of contrast of objects viewed by reflection at the surface; (2) percent of reflected light scattered by a specimen having a glossy surface so that its direction deviates more than a specified angle from the direction of specular reflection; (3) cloudy appearance attributable to light scattering. In transmission, (1) the

scattering of light by a specimen responsible for the apparent reduction in contrast of objects viewed through it; (2) the percent of transmitted light that is scattered so that its direction deviates more than a specified angle from the direction of the incident beam. The term has been replaced as various words based on situation or industry; (3) *cloudiness* applies to apple juice, *mist* and *fog* to the atmosphere, *clarity* describes wine, *turbidity* relates to water, and *opacity* is used for shower curtains. Haze is caused due to the diffusion of light as it passes through the material. In the extreme case, no light is being transmitted by the material and it is said to be opaque. All concern the scattering and absorption of light occurring in the material.

2.4. Stereoscopic perception

2.4.1. Depth cue in monocular vision

Before a summary about stereoscopic vision, it is necessary to know monocular vision, because it is basis for the perception of depth. Monocular vision means that each eye is used separately. Some monocular depth cues are based on principles of geometry, others are based on conditions of atmosphere and illumination, and still others arise from differential motion (Lipton, 1997).

- Relative size is dependent on the image size of an object projected onto the retina. An object with smaller retinal image is thought further away than the same object with a larger image. Therefore, objects located closer to an observer are judged lager, while same objects positioned farther away are done smaller.
- Light and shade are an important and basic depth cue. The part of an object light reflects from surface of the object is seen brighter according to viewing condition. In other word, they provide cue to their depth relationships.
- Interposition provides the depth ordering of objects.
- Textural gradient appears to a texture of constant size object, such as grassy lawn or the tweed of a jacket. It provides a depth because the texture is judged closer to observer as it is seen larger.
- Aerial perspective is the diminution in visibility of distant objects. Due to

intervening fog, dust or rain in atmosphere, distant prospect becomes a bluish haze. As light travelling long distance it is scattered, hue is shifted towards blue, saturation decrease, and sharp edges are diffused.

- Motion parallax is a depth cue under the condition which an object in the scene or the observer's head moves. An object to be closer from the observer moves past more rapidly than others to be further away.
- Depth cuing is the graphic technique that reduces the intensity of object in proportion to the distance from the viewer.
- Perspective, called geometric, rectilinear or photographic perspective, is the relationship between foreground and background objects. It is method that the image's depth is enhanced using lines receding to a vanishing point.

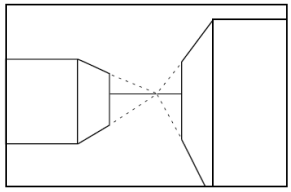

Figure 2-16 Perceptive
(StereoGraphics developer's handbook, 1997)

2.4.2. Retinal disparity

The two eyes are positioned, about 64 millimetres, for adults, and each eye captures a slightly different image from a different point of view even though they focus on a same object. The difference in lateral separation between objects as seen by the left eye and by the right eye is called *retinal disparity*: it provides the information for stereoscopic depth perception. The magnitude of the disparity, expressed in terms of lateral separation on the retina, depends on the distance between objects. If one object is much closer to the observer than the other, the resulting retinal disparity will be large. If one object is only slightly closer to the observer than the other, the disparity will be small. This cue to depth, retinal disparity, arises whenever objects are located in front of or behind the point of fixation. The disparity is processed by brain which combines two different images into a single image. It is called fusion and the resultant sense of depth is stereopsis.

2.4.3. Parallax

Parallax is called the distance between left and right corresponding image points. Parallax has intimate relations with disparity. Parallax produces disparity in the eyes, thus providing the stereoscopic cue. Parallax is seen in the display screen, resulting in the disparity in the retina. Stereoscopic displays for producing parallax information shows two left and right images which are alternated rapidly. Through shuttering eyewear, the left image is seen in only left eye and the right image only the right eye. The eyewear receives the signal and its each shutter is synchronized to transmit the wanted image and to block the unwanted image. As shown in Figure 2-17, parallax can be divided into four basic types. In the first case (a), zero parallax means that the homologous images points of the two images exactly correspond or lie on top of each other. When observer is watching at the display with zero parallax, the eyes are converged at the plane of the screen and the optical axes of the eyes cross at the plane of the screen. Figure 2-17 (b) shows uncrossed or positive parallax. The optical axes of the left and right eyes are parallel. The positive parallax occurs under the conditions. In the visual world, when observers look at great distant objects and for a stereoscopic display, when the distance between the left and right eyes is identical with that of the parallax. Another kind of positive parallax (c) happens when the distance between images points of the two images is further away than that between both eyes and is called as divergent parallax. This divergence does not happen in the visual world and cause discomfort. The drawing (d) illustrates crossed or negative parallax that the optical axes of eyes are crossed. In this case, observer may judge that objects are closer than the surface of the screen.

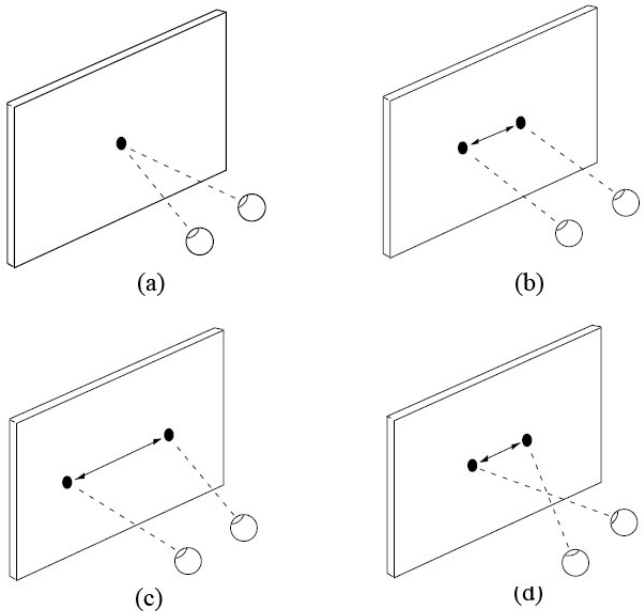

Figure 2-17 Four basic types of parallax
(a) zero (b) positive (c) divergent (d) negative (StereoGraphics developer's handbook, 1997)

2.4.4. Accommodation and convergence relationship

Accommodation means that eyes focus on an object by changing the shape as is pulled by muscles. It is similar with the function that the camera lens focuses by moving closer to or further away from the detector. So it may be seen clearly. Convergence is that eyes rotate toward or away from each other. Even though we look at an object in the visual world, two difference images are projected from different angle due to two eyes are posited with distance. In order for these to be seen singly, the central portion of each retina must see the same object point. When you look behind your finger after focusing the top as one finger, you change the point of convergence and your finger will look blurry or doubled. The muscle responsible for this convergence may provide distance information such as a camera range finder does. Both accommodation and convergence are linked by the necessities of the visual world, because we have grown accustomed or habituated to the linked response for a lifetime of visual experience. Invariably, in looking at objects, accommodation and convergence correspond. However, there is a breakdown of the tied-together responses of two separate mechanisms if the action of the muscles controlling

convergence and the muscles controlling focusing depart from their habitual relationship. In this case, some people may undergo an unpleasant sensation. Especially, the problem is exacerbated for the small screens viewed at close distances. The breakdown of the relationship between accommodation and convergence is one important way in which a plano-stereoscopic display cannot be isomorphic with the visual world and never overcome this artefact. A direct consequence of this is that, as a rule of thumb, one should keep parallax to the minimum required for a satisfactory depth effect.

2.4.5. Benefit of stereoscopic vision

In the real world, it clearly fascinates the majority of people to see a 3D picture. Nick Holliman (2005) explained the benefit of stereoscopic vision below.

- Relative depth judgement. The spatial relationship of objects in depth from the viewer can be judged directly using binocular vision.
- Spatial localisation. The brain is able to concentrate on objects placed at a certain depth and ignore those at other depths using binocular vision.
- Breaking camouflage. The ability to pick out camouflaged objects in a scene is probably one of the key evolutionary reasons for having binocular vision.
- Surface material perception. For example, lustre, sparkling gems and glittering metals are in part seen as such because of the different specular reflections detected by the left and right eyes.
- Judgement of surface curvature. Evidence suggests that curved surfaces can be interpreted more effectively with binocular vision.

2.5. Statistical Methods

2.5.1. Correlation Coefficient and Coefficient of Determination

In many comparisons, the data should be linearly related. Consequently, the correlation coefficient, R is used as a measure of the concordance between the two data sets. The correlation coefficient, R, is a measure of the quality of a least-squares fit between the two original variables as shown in Equation 2-36.

$$\boldsymbol{R} = \frac{\boldsymbol{n}\sum \boldsymbol{xy} - \sum \boldsymbol{x}\sum \boldsymbol{y}}{\sqrt{(\boldsymbol{n}\sum \boldsymbol{x^2} - (\sum \boldsymbol{x})^2)(\boldsymbol{n}\sum \boldsymbol{y^2} - (\sum \boldsymbol{y})^2)}} \qquad \text{Equation 2-36}$$

More commonly, the coefficient of determination, R^2, is used, which is a quantity obtained by squaring the correlation coefficient. It is considered to be more meaningful than R in some situations. The coefficient of determination is the percentage of variance in one variable that is accounted for by the variance in the other variable. For example, when R = 0.8, R^2 = 0.64, they means that 64% of the variance in y can be explained by the regression line between x and y, leaving less than 36% to be explained by other factors.

2.5.2. Coefficient of Variation

Coefficient of Variation, CV, was also used as a statistical measure to investigate the agreement between two sets of data, e.g., x and y. The coefficient of variation is a measure of the distance in the y direction of the points from the 45° line in the plot of y versus x. It expresses the root-mean-squared deviation of the distances of the points from this line as a percentage of the mean value of the data set. This statistic has the advantage of giving results that are independent of the size of the data set. It can be thought of as the relative percentage error and is calculated using the following equations:

$$\boldsymbol{CV} = \frac{\boldsymbol{100}}{\boldsymbol{Yi}} \times \sqrt{\frac{\boldsymbol{1}}{\boldsymbol{N}}\sum_{\boldsymbol{i=1}}^{\boldsymbol{N}} (\boldsymbol{Y_i} - \boldsymbol{f} \times \boldsymbol{X_i})^2} \qquad \text{Equation 2-37}$$

where $f = \frac{\sum_{i=1}^{N}(Y_i \times X_i)}{\sum_{i=1}^{N}(X_i)^2}$ and $Y = \frac{1}{N}\sum_{i=1}^{N} Y_i$ Equation 2-38

when $f = 1$, the resulting *CV* is named as *ObsCV*.

where n is the number of samples in the x and y data sets, and y is the mean value of the y data. A *CV* value equalling zero indicates perfect agreement between the two data sets being compared. The coefficient of variation only has a sensible meaning when it is calculated using similar scales for the x and y data. The values of the coefficient of determination and coefficient of variation were mainly used to indicate the agreement between two data sets (*x and y*) having n data points in each set.

2.6. Psychophysics: Quantitative methods for perceptual responses

2.6.1. Categorical judgement

Categorical judgement is a method in which an observer is asked to assign stimuli into defined categories which represent equal-interval differences in perceptual magnitude. This method is practically useful for scaling large numbers of stimuli. It is desirable to carefully prepare the stimuli by not having them too spread in the distinct categories by different observers, or by the same observer on different occasions. The number of categories is a key factor affecting experimental results. Normally a 9- or 7-point scale is used as the odd number scale helps with the spread of observers' data (Luo *et al.*, 1991). For example, when assessing colour differences, a 9-point scale was used and the categories were defined as follows: 1) no colour difference; 2) just noticeable colour difference; 3) mild colour difference; 4) moderate colour difference; 5) noticeable colour difference; 6) moderate large colour difference; 7) large colour difference; 8) very large colour difference; and 9) largest colour difference. Notice that the perceived colour difference between categories 2 and 3 is the same as that between categories 6 and 7, and so on. Only integers were 1 and 9. Since the categorical judgement method was used in this study, the law of categorical judgement is applicable for data analysis (Torgerson, 1958). Observer results could be analysed using the mean-category-value method. The mean observer value for each sample divided by the total number of observations can be

directly used to represent the perceived categorical boundary for an interval scale. This means observer data represents the central tendency for all the observers participating in the experiment.

2.6.2. Magnitude estimation

Magnitude estimation has been used increasingly in recent years. Here, observers are asked to scale colour appearance attributes such as lightness, colourfulness and hue under fully dapted viewing conditions (Luo *et al.*, 1991). Its only disadvantage is lower precision. Many advantages are associated with this technique, however, such as normal viewing conditions using both eyes, a steady-state of adaptation, results that are described in terms of perceived attributes which can be directly compared with the predictions of colour appearance models, and a shorter training period than for memory matching.

Since the individual data are either logarithmic or power functions of the stimulus, they will each be related to the geometric mean function by a power transform (Bartleson., 1979; Stevens., 1971). This automatically establishes a basis for normalising the results of individual observers.

$$\boldsymbol{log_{10}\bar{s}_i = a log_{10} s_i + b} \qquad \text{Equation 2-5}$$

$$\boldsymbol{\dot{s}_i = 10^{\frac{log_{10}\bar{s}_i - b}{a}}} \qquad \text{Equation 2-40}$$

where S_i and $\bar{S}_i$ are an individual observer's raw data and the geometric mean calculated from all observers. The coefficients "*a*" and "*b*" for each individual observer were obtained using the least-squares fitting method between $\bar{S}$ and the geometric mean values. After applying coefficients "*a*" and "*b*", each observer's data was adjusted to a common scale.

2.6.3. Scale value

The simplest way to analyse these data is to take an arithmetic mean over the results from all observers to obtain a mean scale value for each sample. This is known as the mean-category value method and assumes that the observers are capable of keeping the intervals between category boundaries psychologically equal. However, there is always doubt about an observer's ability to categorise samples into an equal-interval of the categories. Thus, a more sophisticated technique known as the categorical-judgement method is preferred. This transforms scaled data to an equal-interval scale.

1. An *m X n* frequency matrix was constructed regarding *m* samples (stimuli) and *n* categories in a categorical judgement assessment. Each entry shows the frequency for a sample being judged as being in a specific category.
2. An *m X n* cumulative frequency matrix was constructed in which each entry shows the frequency of a sample judged to be below a given category.
3. An *m X n* cumulative probability matrix as obtained by divided each entry in the cumulative frequency matrix by the number of observations.
4. An *m X n* LG matrix (logical function values) is obtained from the cumulative frequency matrix using Equation 2-41. This function can be used to estimate z-scores in Step 5.

$$\mathbf{LG} = \mathbf{In}\left(\frac{\mathbf{CF}+\boldsymbol{\alpha}}{\mathbf{N}-\mathbf{CF}+\boldsymbol{\alpha}}\right) \qquad \text{Equation 2-6}$$

   Where CF represents the cumulative frequency matrix, *N* is the number of the observations and α is an arbitrary additive constant (0.5 was suggested by Bartleson (1984) and was used in this study).
5. Z-scores can be obtained from the cumulative probability matrix as probability is the area (proportion) under the normal distribution curve. According to a property of the normal distribution, for those having probability values of 0 or 1, the z-scores are -∞ or ∞ respectively. Therefore, in both cases, an *m X n* z-score matrix was estimated from the LG values using a scaling coefficient α (and if necessary a coefficient β) as given in Equation 2-42, which was calculated using linear regression between the valid z-scores and corresponding LG value.

$$\text{Z-score} = \boldsymbol{\alpha}LG+\boldsymbol{\beta} \qquad \text{Equation 2-42}$$

6. An *m X (n-1)* difference matrix between adjacent columns was calculated followed by calculation of the mean for each column.
7. Category boundaries were determined by setting the origin to zero and adding adjacent mean values from the different matrix.
8. An *m X (n-1)* scale value matrix was calculated by subtracting each entry of the z-score matrix from the corresponding category boundaries. The mean values of each row represent the coarseness of the samples as their scale value.

2.7. Texture analysis

The following section describes common texture which is important attribute of the total appearance of an object. So far, ASTM standard (ASTM, 2004) defines it as "the visible surface structure depending on the size and organisation of small constituent parts of a material: typically, the surface structure of a woven fabric".

Surface texture could be classified as physical texture and optical texture. The former definition was suggested by Hutchings (1999) that physical texture is the spatial variation of the surface structure from a physical point of view. It is the texture associated with physical, topological variability in a surface. The latter was described by Pointer (2003) that optical texture is the structure visible beneath a surface depending on the size and organisation of small constituent parts of a material. It means that it is texture associated with spatial variation in appearance caused by non-uniformity of colorant. In the human response to texture, the variation was represented as terms such as fine, coarse, smooth and grained.

There are various approaches for surface texture analysis in image processing. One of the relative approaches to this study is that the image analysis gives some psychological meaningful numbers which features of based on digital images captured from surface of some object.

2.7.1. Grey Level Co-occurrence Matrices (GLCM) –spatial grey analysis

The grey level co-occurrence matrices have become one of the most well-known and widely used texture features and also called the grey level dependence method. Haralick suggested the method which concerned with the grey level occurrence and their spatial distribution (Haralick, *et al*., 1973).

The spatial grey level co-occurrence matrix is based on the estimation of the second-order joint conditional probability density functions, *f(i,j,d,a)*, where *a* usually takes an angle of either, 0°,45°, 90°, 135°. Each value of *f(i,j,d,a)* is the probability of going from grey level I, and j. given that the inter-ample spacing is *d* and the direction is defined by angle *a*. If an image has M grey levels, then the size of the density functions is M×M matrices. Each matrix is calculated from a digital image by counting the number of times each pair of grey levels occurs at separation d and in the direction specified by a. In Figure 2-18, an example shows how to compute the co-occurrence matrices. This image has four grey levels (0~3) and 4×4 size of digital image. The second-order grey level co-occurrence matrices for the four principal directions were resulted in Figure 2-18.

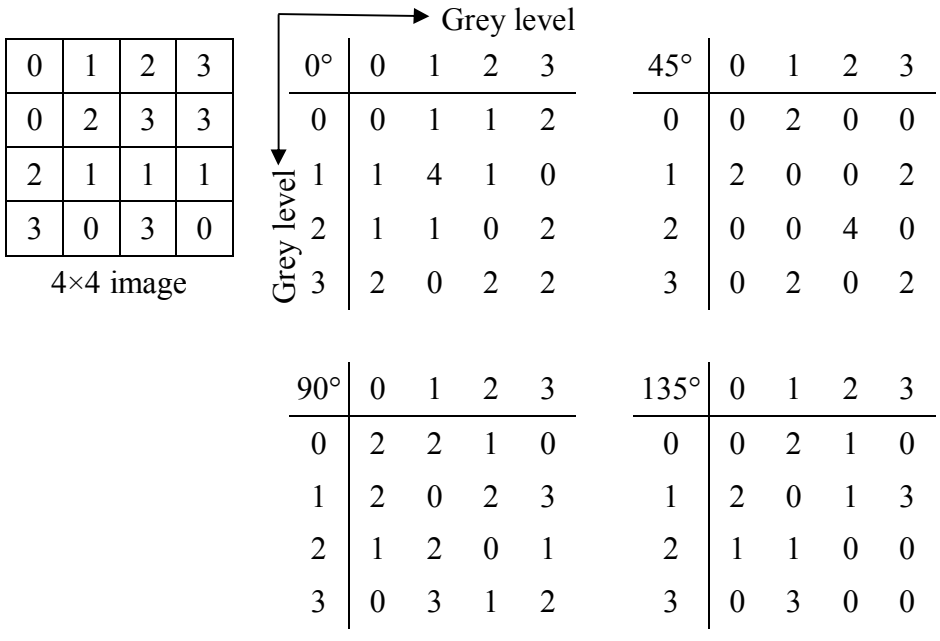

0	1	2	3
0	2	3	3
2	1	1	1
3	0	3	0

0°	0	1	2	3
0	0	1	1	2
1	1	4	1	0
2	1	1	0	2
3	2	0	2	2

45°	0	1	2	3
0	0	2	0	0
1	2	0	0	2
2	0	0	4	0
3	0	2	0	2

90°	0	1	2	3
0	2	2	1	0
1	2	0	2	3
2	1	2	0	1
3	0	3	1	2

135°	0	1	2	3
0	0	2	1	0
1	2	0	1	3
2	1	1	0	0
3	0	3	0	0

Figure 2-18 An example of the spatial co-occurrence calculations.

For texture analysis, a total of fourteen statistical features can be derived from the co-occurrence matrix. Four common features sere listed below.

Energy : $\sum_i \sum_j [\boldsymbol{f}(\boldsymbol{i},\boldsymbol{j},\boldsymbol{d},\boldsymbol{a})]^2$ Equation 2-43

This measures the homogeneity of texture image. The homogeneous image has few dominant grey level transitions and hence few entries of large magnitude. On the contrary to this, the energy feature is small since the matrix has large number of small entries for an image which is not homogeneous.

Entropy: $-\sum_i \sum_j [\boldsymbol{f}(\boldsymbol{i},\boldsymbol{j},\boldsymbol{d},\boldsymbol{a}) \log(\boldsymbol{f}(\boldsymbol{i},\boldsymbol{j},\boldsymbol{d},\boldsymbol{a}))]$ Equation 2-7

The entropy measures the complexity of the image. A simple image tends to have lower entropy value than a complex one.

Contrast: $\sum_i \sum_j [(\boldsymbol{i}-\boldsymbol{j})^2 \boldsymbol{f}(\boldsymbol{i},\boldsymbol{j},\boldsymbol{d},\boldsymbol{a})]$ Equation 2-45

With the entropy, contrast is commonly used as texture feature and also is called as inertia. The contrast is a difference of the second-order grey level statistics and of the amount of local variations shown in one image compared to another then its contrast value will be consistently higher.

Local Homogeneity: $\sum_i \sum_j [\boldsymbol{f}(\boldsymbol{i},\boldsymbol{j},\boldsymbol{d},\boldsymbol{a})/(\boldsymbol{1}+(\boldsymbol{i}-\boldsymbol{j})^2)]$ Equation 2-8

This local homogeneity measures the degree to which similar grey levels tend to be neighbours.

2.7.2. Grey Level Run Length Matrices (GLRLM) –Structural Methods

Galloway (Galloway, 1975) defined that "a grey level run is a set of consecutive, collinear image points having the same grey level value". The length of the run is the

number of image points in the run. When a grey level run length matrix of a given image was computed for runs having any given direction, let *P(i,j,a)* be the number of times that the image contains a run of length j, in the given direction *a*, consisting of points having grey level *i* (or lying in grey level range *i*). For a digital image, runs of adjacent pixels having the same grey levels may take place along a given direction. For example, coarse texture is expected that the long runs would appear often, whereas a fine texture would include a higher proportion of short runs. The following example is expressed in Figure 2-19 presenting the calculation of GLRLM. To obtain texture features from the matrices, four features can be extracted; Short run emphasis, Long run emphasis, Grey level nonuniformity and Run length nonuniformity.

Short run emphasis: $\sum_{i=1}^{N_g} \sum_{j=1}^{N_r} \frac{p(i,j)}{j2}$ Equation 2-47

This function divides each run length value by the length of the run squared. This feature tends to emphasise short runs. The denominator means the total number of runs of the image and act as a normalising factor. Therefore, this feature gives greater weight to short runs of any grey level.

0	1	2	3
0	2	3	3
2	1	1	1
3	0	3	0

4×4 image

Run length

Grey level

0°	1	2	3	4
0	4	0	0	0
1	1	0	1	0
2	3	0	0	0
3	3	1	0	0

45°	1	2	3	4
0	4	0	0	0
1	4	0	0	0
2	0	0	1	0
3	3	1	0	0

90°	1	2	3	4
0	2	1	0	0
1	4	0	0	0
2	3	0	0	0
3	3	1	0	0

135°	1	2	3	4
0	4	0	0	0
1	4	0	0	0
2	3	0	0	0
3	5	0	0	0

Figure 2-19 An example of calculating GLRLM

Long run emphasis: $\sum_{i=1}^{N_g}\sum_{j=1}^{N_r} j^2 p(i,j) / \sum_{i=1}^{N_g}\sum_{j=1}^{N_r} p(i,j)$ Equation 2-48

This function multiplies each run length value by the length of the run squared. This feature emphasizes ling runs and then gives greater weight to long runs of any grey level.

Grey level nonuniformity: $\sum_{i=1}^{N_g}(\sum_{j=1}^{N_r} p(i,j))^2 / \sum_{i=1}^{N_g}\sum_{j=1}^{N_r} p(i,j)$ Equation 2-49

This function squares the number of run lengths for each grey level. When runs are equally distributed throughout the grey levels, the feature takes on its lowest values. High run length values contribute most to this feature.

Run length nonuniformity: $\sum_{i=1}^{N_r}(\sum_{j=1}^{N_g} p(i,j))^2 / \sum_{i=1}^{N_g}\sum_{j=1}^{N_r} p(i,j)$ Equation 2-50

This feature should measure the nonuniformity of the run lengths. If the runs are equally distributed throughout the lengths, the feature has a low value. Large run contributes most to this feature.

2.7.3. Fourier Transform

As known by Cooley and Tukey (Cooley, *et al.*, 1967a, 1967b, 1969, 1965), Fourier transform is one of the most important image processing methods in a wide range of applications. The Fourier Transform has mainly used to do filtering in the frequency domain and then enhance one dimensional signal or two dimensional images.
Let f(u) of a single variable and discrete function, f(x), x=0,1,2,3,..M-1, is defined as (Gonzalez and Woods, 2002)

$$F(u) = \frac{1}{M}\sum_{x=0}^{M-1} f(x) e^{-j2\pi ux/M}$$ Equation 2-51

Where $j=\sqrt{-1}$. Conversely, given *F(u), f(x)* can be derived by applying the inverse Fourier transform defined by the Equation 2-52.

$$f(x) = \sum_{u=0}^{M-1} F(u) e^{j2\pi ux/M}$$ Equation 2-52

Both Equation 2-51 and 2-52 consist of the Fourier transform pair. The concept of the frequency domain start from Equation 2-53

$$e^{j\theta} = \cos\theta + j\sin\theta$$ Equation 2-53

By substituting this expression into Equation 2-52,

$$F(u) = \frac{1}{M}\sum_{x=0}^{M-1} f(x)[\cos 2\pi ux/M - j\sin 2\pi ux/M]$$ Equation 2-54

The Fourier transform can easily be extended to two dimension of digital image. The 2D discrete Fourier transform (DFT) converts a digital image *f(x,y)* of into a two-dimensional complex function of energy, also referred to as magnitude and phase, in the frequency domain (Gonzalez &Woods, 2002). The 2D discrete Fourier transform (DFT) of an image *f(x,y)* of size is given by the equation

$$F(u,v) = \frac{1}{MN}\sum_{x=0}^{M-1}\sum_{y=0}^{N-1} f(x,y) e^{-j2\pi(ux/M+vy/N)}$$ Equation 2-55

Similarly, *F(u,v), f(x,y)* was obtained by applying the inverse transform defined by the Equation 2-56

$$f(x,y) = \frac{1}{MN}\sum_{u=0}^{M-1}\sum_{v=0}^{N-1} F(u,v) e^{j2\pi(ux/M+vy/N)}$$ Equation 2-56

Both Equations 2-55 and 2-56 comprise the 2D discrete Fourier transform (DFT) pair. The component of the Fourier transform is complex quantities. If *F(u,v)* can be simply expressed in polar coordinates

$$F(u,v) = |F(u,v)| e^{-j\varphi(u,v)}$$ Equation 2-57

Where,

$$|F(u,v)| = \sqrt{R^2(u,v) + I^2(u,v)}$$ Equation 2-58

is called the **spectrum** of the Fourier transform.

$$\boldsymbol{\varphi(u,v) = \tan^{-1}[I(u,v)/R(u,v)]} \qquad \text{Equation 2-59}$$

Equation 2-59 shows the *phase angle* of the Fourier transform. *R(u,v)* and *I(u.v)* denote the real and imaginary component of *F(u,v)* respectively.

The Power spectrum *P(u,v)* of an image can be calculated from the Fourier transform function as shown in Equation 2-60. It is useful equation in digital image processing for analysing the intensity of the image.

$$\boldsymbol{P(u,v) = \pi|F(u,v)^2} \qquad \text{Equation 2-60}$$

For analysis, power spectrum may be split into concentric rings and wedges to encode frequency content and orientation content respectively. Because of the two kind of information, various statistical techniques have been applied to find out the meaningful information and extract the correlated features.

2.8. Limitations

So far, several methods, mainly Kitaguchi's study (2008), were reviewed for modelling metallic-coating panels based on visual experiment setup, image acquisition system and digital image processing. The major limitations can be outlined below;

- A vital drawback is that the existing methods for capturing some image of metallic-coating surface were designed not to take into account stereoscopic vison which refers to the human ability to view with both eyes. In particular, the metallic-coating strongly depends on the viewing geometry. Therefore, each of eyes capture slightly different image from a different point of view even though they focus on a same metallic since two eyes are posited with distance, about 6.4. It means that the concept of many image acquisition systems is different to that of real perception of human.

- It is controversial that the GretagMacbeth Sol-source lamp used in Kitaguchi's experiment was employed as light source because of yellowish colour. The coloured light source can affect to reflection of coloured coating samples.

- Illumination uniformity was measured, but there is no information about temporal stability of illumination. The intensity of light source with variable intensity can give rise to the low reliability of result.

- Most of the studies have focus on one dominant perceptual attribute of metallic-coating panel under corresponding illumination geometry. However, they have not considered a visually-complex nature of coatings which may have a various properties of perceptual attributes.

- Glint, gloss or specular reflection are categorised as micro appearance. To obtain reliability result, it is essential to capture metallic coating images with high resolution.

- In computer vision, stereo matching is one of the most difficult research areas. It is aim to find out the corresponding pixels from two or more images and then reconstruct information for each pixel. Especially, in the study dealing with small aluminium flakes, it is extremely challengeable to do stereo matching. It means that applying stereo matching to digital imaging process is difficult.

- It is necessary for observers to take a near visual acuity test

CHAPTER 3.

DIFFERENCE BETWEEN STEREOSCOPIC AND MONOCULAR VISION FOR GONIO-APPARENT SURFACES

3.1. Introduction

This chapter describe the psychophysical experiment to understand how stereoscopic vision quantifies the appearance of gonio-apparent surface features and influences the perception of coloured objects. This experiment was designed mainly to compare and verify the difference between stereoscopic and monocular visions for various types of samples.

The perceptual attribute of various objects were examined which are one dominant attribute of each type of objects. In order to show one attribute of combination of various attributes as predominant one, the viewing condition was controlled depending on the perceptual attribute of each object in visual assessment.

3.2. Psychophysical experiment

In this psychophysical experiment, category judgement for eight properties was made by each observer on each individual sample using a scale from 0 to 9. Here, a scale value of 1 represented *not noticeable*, while 9 represent *largest.* According to each property of gonio-apparent materials, four different experiment setups were designed with various apparatus: two different light sources, pilling assessment viewer, tilling table, chinrest and viewing cabinet.

3.2.1. Samples and observers

3.2.1.1. Sample preparation

The overall appearance of any object consists of a combination of various attributes. One attribute might appear stronger than the others under one viewing condition.

Glint

A set of 10 plastic panels produced by "Silberline" manufacturing company which products the visual appeal of coatings, paints, inks, plastics and textiles. The samples used have different size particles ranged from 11 to 330 microns as shown in Table

3-1. They were silver panels with size of 7×4.5cm and were used as test samples for three properties: glint intensity, glint density and glint size. Reference sample used was a plastic panel which is an exactly same size particle with sample 1 and a slightly different gold plastic between the colour of test samples.

Table 3-1 Size particles

Sample No.	1	2	3	4	5	6	7	8	9	10
Size(microns)	11	30	33	36	70	90	95	165	225	330

Gloss

As shown in Figure 3-1 (b), a set of samples was prepared including 10 grey coloured patches which have with the size of 8×8cm. A reference sample used was low gloss as much as a test sample 1.

Pearlescence

A pearlescence samples was made of a wrapping paper, gift bags and box which was general materials in daily use. As shown in Figure 3-1 (c), 10 samples used have different patterns and texture but grey colour equally. To prevent a distortion and scratch of their surface, they were stuck on a cardboard of 8×6cm size. A reference sample was the same test sample 1 which shows exhibit.

Texture

A set of 10 texture samples were not only chosen in similar colours, khaki, but also the different variations of fabric weave in which sample 1 was woven densely with thin thread; while sample 10 were made roughly by thick thread. The texture with size of about 8×6 cm^2. They are shown in Figure 3-1 (d).

Pilling

As shown in Figure 3-1(e), 10 samples pilled at different grades by "Martindale abrasion tester" were prepared for the pilling experiment. They differed in colour but had the same texture. An unpilled sample was used as a reference sample.

Haze sample

10 variations of haze sample used in the experiment were made by the deionised water being added black colorant. The sample was contained in a highball glass with a uniform shape. Samples 1 and 10 were prepared almost identical to pure water and 100% haze respectively and rest samples have different concentration of the colorant between samples 1 and 10 as shown in Figure 3-1(f). All highball glasses were sealed by translucent plastic cover to prevent contamination. Pure deionised water was used as a reference sample.

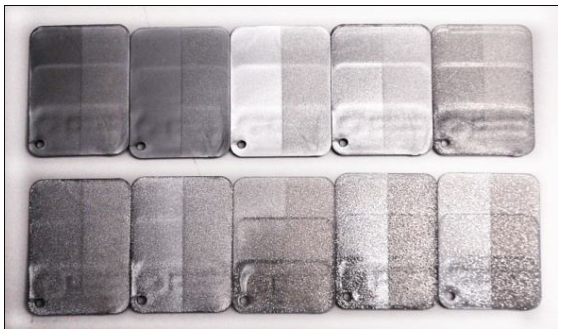

(a) Glint

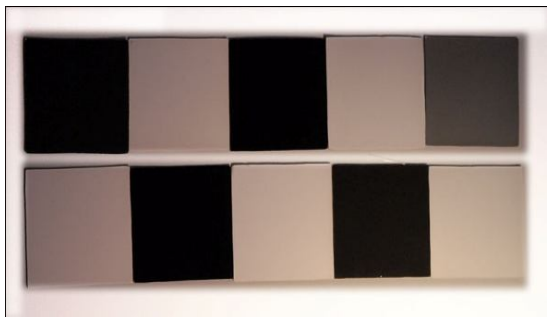

(b) Gloss

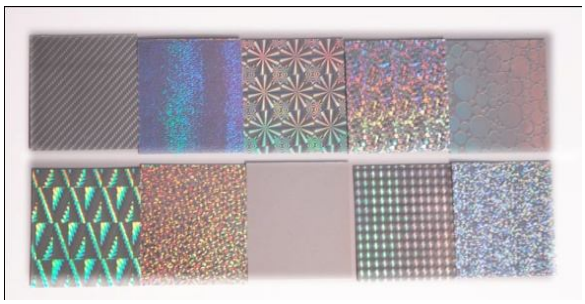

(d) Texture

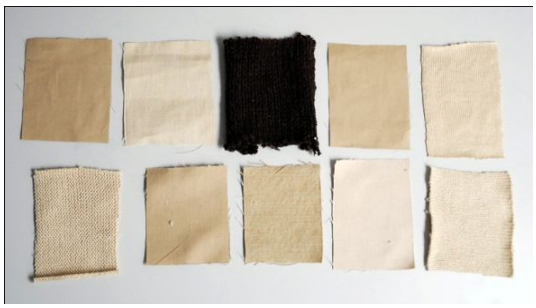

(c) Pearlescence

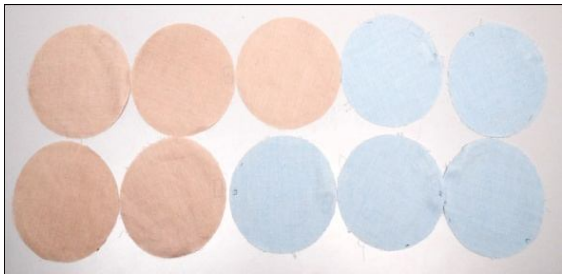

(e) Pilling

(f) Haze

Figure 3-1 Gonio-apparent samples: Plastic (a), Gloss (b), Pearlescence (c), Texture (d), Pilling (e) and Haze (f)

3.2.1.2.Observers

Ten observers participated in the psychophysical experiment. They each performed a normal visual acuity and colour vision test by using a near visual acuity test chart and Ishihara vision test before the assessment. They consisted of seven females and three males: 1 British (female), 3 Korean (female), 1 Chinese (female), 2 Taiwanese (male), 1 Pakistani (male) and 2 Greek (female). Nine of them were research or postgraduate students at the University of Leeds and other interested volunteers. The age range of observers was 24 to 33 years. They performed the assessment twice on different day and each section took approximately 1 hour and 10 minutes and break for 5min in the middle of it. All observers were expected to read small letters that the defined a minimum of 20/15 on binocular vision and of 20/20 on monocular vision (near visual acuity test). When the repetition for monocular vision was performed to dominant eye, eight and two observers used their right eye and rest left respectively.

3.2.2. Viewing conditions and apparatus

Human perception is affected by the viewing conditions such as the distance, light source and angle between observer and the sample. In addition, the overall appearance of any object consists of a combination of various attributes and one attribute might appear stronger than the others under one viewing condition. Therefore, the experiment was

designed as controlled viewing conditions specified, in terms of light source and the angle between light source and observer.

3.2.2.1.Glint

For glint, it is ideal to use a light source having directional illumination which is strong enough to bring out glint appearance and is able to illuminate a viewing field uniformly. A large high-power light would be ideal, as would sunlight. However, because of the limited availability of light sources for this experiment, the GretagMacbeth Sol-source lamp was employed, although it was not possible to illuminate the viewing field uniformly. However, the illuminance at the centre of both a reference and test sample was adjusted to be as close as possible. The glint can be seen on a metallic coating at various geometries as long as it is viewed under directional illumination. However, intensity of the glint changes with viewing geometries. Therefore, the observers adjusted the tilting table to the angle which provides the maximum perceptual the coarseness and glint. The angle was recorded.

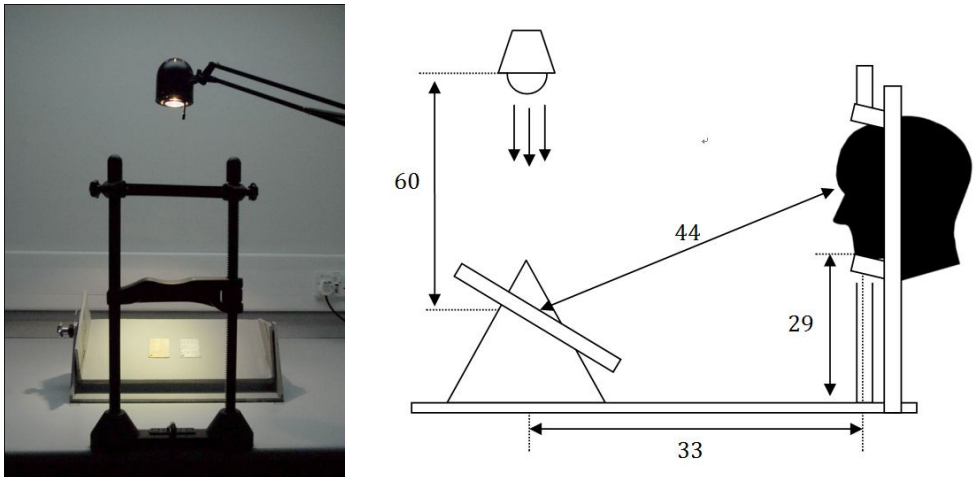

(a) (b)

Figure 3-2 Experimental setup for coarseness and glint
(a) real setup (b) Schematic of viewing condition

As shown in Figure 3-2, the spot light was posited on the tilling table vertically. The distance between observer's eye and the tilting table was approximately 44 cm and that between the light source and the surface of tilting table was 60 cm. The observer's head was fixed by a chin-rest, which guaranteed that the visual direction was in the specular direction.

3.2.2.2.Gloss and pearlescence

The experiment for gloss and pearlescence was designed similar to that for the coarseness and glint properties. As shown in Figure 3-3, there was one difference between both experiment setup which was a light source. A big diffuse light, Verivide VL120 was used instead of a spot light. The light source had the distance of 102 cm from the surface of the tilting table. It could illuminate the viewing field uniformly.

(a) (b)

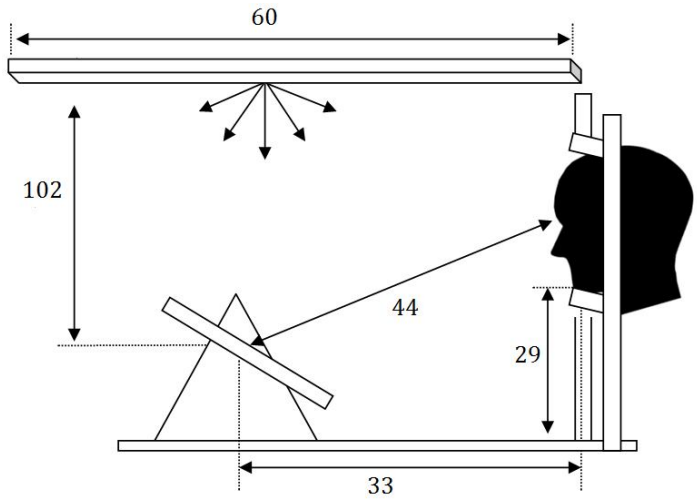

(c)

Figure 3-3 Experimental setting for gloss and pearlescence
(a), (b) real setup and (c) schematic of viewing condition

3.2.2.3. Texture and pilling

For texture and pilling assessment, the experiment was carried out on the illumination and observation geometries as shown in Figure 3-4. The observer is placed directly above the specimens and a high intensity light source, a white fluorescent tube, is used to illuminate the sample at an oblique angle. A viewing cabinet satisfying this condition is shown in Figure 3-5.

Dissimilar to previous two experiment setting, chinrest was not used in this experiment. Although the tool could generally play an important role in the visual geometry, there is no meaning in the pilling and texture assessments. The reason is that observers could rotate the fabric sample during assessment in order to perceive the maximum degree of texture and pilling properties. These geometries and observer instruction were designed based on ASTM and British standard (Standards, 2002; Standards B.B., 2000[a]).

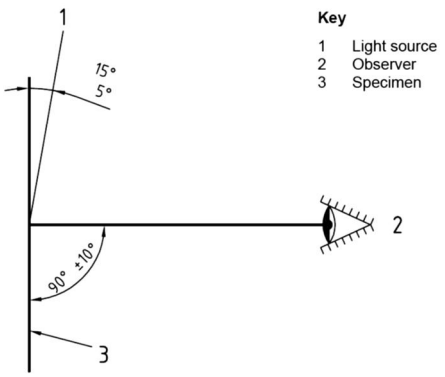

Figure 3-4 Illumination of geometry specified for pilling visual assessment

Figure 3-5 Pilling assessment viewer.

3.2.2.4.Haze

The experiment for assessing haze was designed as shown in Figure 3-6. The test sample, highball glass, was placed against the background of viewing cabinet which is half black and half white backing. It was illuminated under diffuse light in viewing cabinet. Both a reference and test samples were located side-by-side.

(a) (b)

Figure 3-6 Experiment setup for haze; (a) VeriVide viewing cabinet, (b) schematic of viewing condition

3.2.3. Experiment setup

3.2.3.1.Monocular viewing

As explained in the Section 2.4.1, monocular vision means that each eye is used separately. In repetition using monocular vision, observers performed using their dominant eye. Two eye patches were prepared: one blocks only right eye and another cover right eye. According to the result of a visual acuity test, they could choose a suitable eye patch for their dominant eye.

As shown in Figure 3-7, the eye patch was a modified safety goggle that the part for one lens was cut and another part was pained matt black. It was useful for observers to perform the assessment not only with wearing glasses for good eyesight but also without inconvenience which can cause visual fatigue.

Figure 3-7 Eye patches for each eye

3.2.3.2.Observer screening and training

Before beginning the visual experiment, observers underwent in both a visual acuity test and a training session. To check whether observers were able to distinguish small particles clearly on various materials, all were first asked to carry out a visual acuity test. This test was conducted under the same geometric and illumination conditions as were used during the actual coarseness and glint assessment. A near-vision acuity test chart comprising modified ETDRS with SKOAN letters was adopted and this was placed on the

tilting table which exhibit maximum. All observers were expected to read small letters that defined a minimum of 20/15 and 20/20 on binocular and monocular vision respectively. Experimental instructions were provided before commencing the assessment session. To help observers to understand each definition and the process of the assessment, verbal instructions were also provided. In these instructions, the definitions and grading scheme were explained. The description of scale to perception used in the visual assessment was slightly modified based on a 9-point category scale (Luo *et al.*, 1991) and half grading was not allowed.

3.2.3.3. Experimental procedure

Psychophysical experiments were conducted following the procedure below.

A. Observers were asked to sit comfortably in dark room until adaptation was completed. They were screened using the Ishihara colour vision test and wore gloves to prevent contamination of the samples. Instructions for this experiment were provided and explained.

B. Observers were asked to place their chin on the chinrest and adjust the angle of a tilting table to produce the largest specular reflection. In these viewing conditions, they performed an additional test in which a near-vision acuity performance chart was positioned on the tilting table. The tilting angle and visual acuity performance for each observer were recorded.

C. Two reference samples were provided to observers before commencing the main experiment. There were the very similar to samples for the minimum and maximum categories. In this step, observers were able to appreciate the approximate range of each property. One relative sample of minimum category was provided on the left as reference when comparing a test sample on the right.

D. According to the scale of the perceptions shown in Table 3-2, observer assessed three properties: glint intensity, glint density and glint size. These properties were judged using stereoscopic vision.

Table 3-2 The scale perceptions

1	2	3	4	5	6	7	8	9
Not noticeable	Just noticeable	Weak	Moderately small	**Moderate**	Moderately large	Large	Very large	**Largest**

E. Once again, observers conducted visual assessments using monocular vision for the same three properties. Repetition was performed using the dominant eye for each observer.

F. After assessing three properties on two viewing modes for same material named "plastic", the light source was changed from a spot light source to a diffuse D65 simulator.

G. After light adapting for five minutes, gloss was assigned using stereoscopic vision under the same geometric conditions, but with the changed light source. Pearlescence was then evaluated using the same viewing conditions as gloss. The repetition with monocular vision was also conducted for two properties.

H. Observers were asked to sit in front of a pilling assessment viewer and to maintain the specified geometry of illumination, specimen and observer as explained above. Texture and pilling were assessed. Observers could rotate the fabric sample during assessment in order to perceive the maximum degree of texture and pilling properties. After that, the two properties were judged using monocular vision again.

I. Observers were asked to move to viewing cabinet. There they scaled test samples for haze by comparing with pure water. As mentioned in Section 2.3.2.7, haze causes the apparent reduction in contrast of objects viewed through it. Therefore, it can be presented that high haze has the low contrast against white and black background, while lower haze shows the larger contrast.

J. After assessment using stereoscopic vision was done, a repetition was performed using dominant eye of each observer using a modified eye patch. The process of

assessment on both viewing modes for all eight properties was classed as one session. The session was repeated twice in different random order on a different day.

3.3. Results

3.3.1. Observer Variability

Uncertainty in the experimental results is determined by observer variability. Observer variability was investigated for two aspects: repeatability and accuracy (sometimes called intra-observer agreement and inter-observer agreement respectively). Observer repeatability indicates how well the experimental results agree with results reproduced by the same observer. Observer accuracy investigates how well individual observers agree with the mean experimental results. Thus, for the repeatability investigation, the raw data in the first session of various properties for the 160 observations (80 samples $\times$ 2 viewing modes $\times$ 2 repeat $\times$ 10 observers) was compared with that in the second session for individual observers. The two methods used in this section for analysis were explained in section 2.5.

Repeatability

Observer repeatability was quantified by calculating values of the coefficient of determination, R^2, and the coefficient of variation, CV, between two set of row data for each individual observer. The raw data signify the category data assigned by observers in psychophysical experiment. The results of the observer repeatability for seven properties under stereoscopic and monocular vision are shown in Table 3-3 and Table 3-4 respectively. In terms of statistic values for all observers, mean and median of the coefficient of determination, R^2, and the coefficient of variation, CV for stereoscopic vision were similar to these values for monocular vision respectively. The results of an R^2 mean 0.75 and median 0.77 for stereoscopic vision were similar with these of 0.76 and

0.81 for monocular vision. The results of a *CV* mean 30 and median 28 were almost same with these of 31 and 28. Observer repeatability is high when R^2 is closer to 1 and *CV* is lower. On that basis, it was found that the result of haze repeatability with high R^2 and low *CV* was excellent; while glint intensity, with relatively low R^2 (0.67 and 0.70) high *CV* (39 and 40) was relatively poor for both stereoscopic and monocular vision respectively is poor.

Accuracy

Observer accuracy was investigated by calculating values of the coefficient of determination, R^2, and the coefficient of variation, *CV*, between the raw data for each individual observer and the mean observer data of all the observers. The results for accuracy of two viewing modes from all the observers are shown in Table 3-5 and Table 3-6. In comparison with repeatability, observer accuracy of both viewing modes was found to be relatively higher: the mean and median values of stereoscopic vision R^2 were 0.81 and 0.82, and mean and median values of *CV* were 26 and 25 respectively. For monocular vision, mean and median R^2 were 0.79 and 0.81, and mean and median values of *CV* were 28 and 26 respectively. For all the observers, the mean and median values of R^2 for accuracy were closer to 1 and the values of *CV* of these attributes were lower than these values of R^2 and *CV* of repeatability. For the eight properties, observer accuracy for haze with the highest of correlation determination R^2 and the lowest coefficient variation *CV* was excellent regardless of viewing mode. On the other hand, the worst result for perceptual properties was found in glint-intensity because correlation determination R^2 was slightly low and the coefficient variation *CV* was the highest. This indicates that the values of the perceptual haze were more reliable than those of glint-intensity. Most properties have similar or identical R^2 and *CV* between stereoscopic and monocular vision, however the coefficient of variation for pearlescence properties shows a big difference. It can be explained as being due to a lack of significant difference in the accuracy between stereoscopic and monocular vision, except for one property (pearlescence).

Table 3-3 Observer repeatability for stereoscopic vision

	R^2									CV								
Stereo		Task 1			Task 2	Task 3	Task 4	Task 5	Task 6		Task 1			Task 2	Task 3	Task 4	Task 5	Task 6
		Glint									Glint							
	All	Intensity	Density	Size	Gloss	Pearlescence	Texture	Pilling	Haze	All	Intensity	Density	Size	Gloss	Pearlescence	Texture	Pilling	Haze
Obs 1	0.82	0.67	0.72	0.76	0.90	0.71	0.97	0.83	0.96	24	37	32	32	18	25	10	27	14
Obs 2	0.81	0.69	0.79	0.82	0.83	0.88	0.87	0.78	0.83	21	24	14	22	25	13	26	32	13
Obs 3	0.82	0.76	0.72	0.92	0.90	0.74	0.79	0.75	0.97	23	29	13	24	22	23	35	27	10
Obs 4	0.77	0.87	0.71	0.62	0.82	0.98	0.63	0.62	0.90	31	27	18	50	37	7	46	44	20
Obs 5	0.79	0.76	0.76	0.73	0.78	0.63	0.97	0.70	1.00	22	31	20	38	31	23	10	25	0
Obs 6	0.59	0.61	0.12	0.73	0.91	0.03	0.84	0.52	0.94	39	37	53	55	19	65	30	38	12
Obs 7	0.76	0.97	0.90	0.92	0.80	0.61	0.82	0.13	0.93	27	10	13	21	31	51	29	46	12
Obs 8	0.72	0.78	0.64	0.81	0.84	0.82	0.84	0.11	0.90	28	34	14	24	29	18	29	55	17
Obs 9	0.77	0.69	0.64	0.66	0.84	0.46	0.97	0.92	0.97	32	52	34	59	32	39	15	14	9
Obs 10	0.94	0.95	0.93	0.98	0.92	0.89	0.93	0.97	0.98	15	16	14	17	21	14	19	9	6
Mean	0.78	0.78	0.69	0.80	0.85	0.68	0.86	0.63	0.94	26	30	22	34	27	28	25	32	11
Median	0.80	0.76	0.72	0.79	0.84	0.73	0.86	0.72	0.95	24	30	16	28	27	23	27	30	12
Max	0.97	0.97	0.93	0.98	0.92	0.98	0.97	0.97	1.00	48	52	53	59	37	65	46	55	20
Min	0.47	0.61	0.12	0.62	0.78	0.03	0.63	0.11	0.83	11	10	13	17	18	7	10	9	0

Table 3-4 Observer repeatability for monocular vision

	R^2									CV								
Mono		Task 1			Task 2	Task 3	Task 4	Task 5	Task 6		Task 1			Task 2	Task 3	Task 4	Task 5	Task 6
		Glint									Glint							
	All	Intensity	Density	Size	Gloss	Pearlescence	Texture	Pilling	Haze	All	Intensity	Density	Size	Gloss	Pearlescence	Texture	Pilling	Haze
Obs 1	0.88	0.89	0.90	0.70	0.95	0.83	0.91	0.97	0.90	20	24	15	36	16	20	18	9	19
Obs 2	0.81	0.90	0.94	0.63	0.87	0.42	0.95	0.87	0.91	22	21	17	30	24	39	15	17	12
Obs 3	0.75	0.82	0.63	0.80	0.85	0.54	0.83	0.65	0.91	29	30	17	28	37	44	28	32	16
Obs 4	0.80	0.71	0.90	0.94	0.97	0.75	0.77	0.48	0.89	28	51	13	21	19	23	33	43	19
Obs 5	0.78	0.93	0.79	0.85	0.66	0.66	0.96	0.37	1.00	23	20	19	28	36	27	13	40	0
Obs 6	0.63	0.35	0.48	0.76	0.95	0.59	0.47	0.50	0.92	39	60	27	35	16	63	53	41	13
Obs 7	0.86	0.92	0.88	0.94	0.71	0.88	0.96	0.59	0.96	22	23	16	18	42	23	12	30	9
Obs 8	0.75	0.72	0.43	0.59	0.91	0.90	0.92	0.70	0.86	24	24	14	41	21	15	20	37	22
Obs 9	0.70	0.26	0.69	0.69	0.70	0.48	0.97	0.83	0.99	41	104	23	68	48	39	16	21	6
Obs 10	0.92	0.97	0.89	0.96	0.98	0.86	0.80	0.95	0.98	16	17	15	21	11	15	30	11	6
Mean	0.79	0.75	0.75	0.79	0.86	0.69	0.85	0.69	0.93	26	37	18	33	27	31	24	28	12
Median	0.82	0.85	0.83	0.78	0.89	0.71	0.91	0.67	0.91	22	24	16	29	22	25	19	31	12
Max	0.96	0.97	0.94	0.96	0.98	0.90	0.97	0.97	1.00	54	104	27	68	48	63	53	43	22
Min	0.51	0.26	0.43	0.59	0.66	0.42	0.47	0.37	0.86	12	17	13	18	11	15	12	9	0

Table 3-5 Observer accuracy for stereoscopic vision

	R^2									CV								
Stereo		Task 1			Task 2	Task 3	Task 4	Task 5	Task 6		Task 1			Task 2	Task 3	Task 4	Task 5	Task 6
		Glint									Glint							
	All	Intensity	Density	Size	Gloss	Pearlescence	Texture	Pilling	Haze	All	Intensity	Density	Size	Gloss	Pearlescence	Texture	Pilling	Haze
Obs 1	0.90	0.85	0.92	0.93	0.94	0.74	0.97	0.92	0.94	17	28	15	22	17	22	11	14	10
	0.91	0.86	0.90	0.86	0.91	0.98	0.98	0.88	0.91	20	26	19	29	29	8	10	25	14
Obs 2	0.88	0.87	0.88	0.95	0.92	0.88	0.96	0.85	0.75	20	21	12	15	19	15	16	28	31
	0.90	0.86	0.91	0.93	0.97	0.92	0.91	0.95	0.78	18	27	12	20	14	14	18	9	28
Obs 3	0.91	0.88	0.92	0.94	0.97	0.84	0.86	0.95	0.92	17	20	12	13	15	19	26	15	15
	0.89	0.91	0.76	0.89	0.91	0.89	0.95	0.86	0.94	19	18	20	23	23	17	18	21	15
Obs 4	0.83	0.96	0.94	0.80	0.61	0.90	0.90	0.64	0.88	21	10	9	27	44	16	18	27	15
	0.83	0.93	0.84	0.84	0.73	0.95	0.57	0.78	0.97	20	11	15	20	34	11	34	24	13
Obs 5	0.89	0.88	0.91	0.91	0.79	0.88	0.98	0.83	0.92	18	22	13	24	29	13	7	20	14
	0.86	0.89	0.88	0.81	0.86	0.58	0.99	0.94	0.92	18	18	11	27	27	26	7	12	14
Obs 6	0.81	0.65	0.86	0.90	0.94	0.78	0.88	0.55	0.95	23	46	15	23	17	22	23	30	11
	0.68	0.50	0.20	0.79	0.98	0.12	0.95	0.89	0.98	26	60	37	20	10	46	16	11	7
Obs 7	0.83	0.95	0.93	0.96	0.92	0.85	0.80	0.41	0.84	19	14	15	15	19	14	26	31	16
	0.87	0.97	0.97	0.96	0.93	0.54	0.91	0.76	0.90	15	11	14	16	18	16	15	18	13
Obs 8	0.87	0.93	0.81	0.85	0.97	0.95	0.96	0.52	0.93	17	16	17	21	13	10	16	30	14
	0.87	0.93	0.77	0.81	0.93	0.91	0.89	0.75	0.97	16	12	20	22	17	14	18	18	9
Obs 9	0.94	0.95	0.93	0.91	0.96	0.85	0.96	0.98	0.96	20	20	25	34	18	20	18	10	12
	0.86	0.73	0.77	0.86	0.93	0.71	0.98	0.94	0.93	18	25	17	22	18	28	11	13	13
Obs 10	0.90	0.82	0.89	0.93	0.96	0.80	0.94	0.89	0.94	21	33	17	33	20	18	17	17	12
	0.91	0.86	0.85	0.91	0.89	0.92	0.91	0.94	0.96	20	29	20	27	28	11	23	14	11
Mean	0.86	0.86	0.84	0.89	0.90	0.79	0.91	0.81	0.91	19	20	14	21	24	15	19	21	18
Median	0.90	0.88	0.89	0.90	0.93	0.85	0.95	0.86	0.93	18	20	14	21	21	15	18	23	15
Max	0.98	0.97	0.97	0.96	0.98	0.98	0.99	0.98	0.98	30	28	20	29	44	22	34	28	31
Min	0.49	0.50	0.20	0.79	0.61	0.12	0.57	0.41	0.75	10	10	9	13	14	8	10	9	10

Table 3-6 Observer accuracy for Monocular vision

	R^2									CV								
Mono		Task 1			Task 2	Task 3	Task 4	Task 5	Task 6		Task 1			Task 2	Task 3	Task 4	Task 5	Task 6
		Glint									Glint							
	All	Intensity	Density	Size	Gloss	Pearlescence	Texture	Pilling	Haze	All	Intensity	Density	Size	Gloss	Pearlescence	Texture	Pilling	Haze
Obs 1	0.93	0.94	0.99	0.94	0.96	0.82	0.95	0.94	0.88	17	19	13	19	17	21	14	17	15
	0.87	0.93	0.85	0.65	0.85	0.96	0.96	0.88	0.87	22	18	15	38	39	11	14	24	16
Obs 2	0.87	0.98	0.95	0.84	0.99	0.65	0.92	0.91	0.75	20	14	7	23	10	31	20	18	33
	0.89	0.90	0.94	0.87	0.91	0.74	0.95	0.93	0.86	22	31	13	25	24	25	16	16	23
Obs 3	0.82	0.85	0.50	0.77	0.92	0.87	0.95	0.87	0.86	23	31	24	30	25	18	16	19	20
	0.90	0.96	0.93	0.97	0.97	0.67	0.91	0.84	0.95	17	14	10	17	13	28	21	20	13
Obs 4	0.82	0.84	0.94	0.95	0.70	0.73	0.91	0.57	0.90	23	28	9	13	42	29	18	32	13
	0.87	0.79	0.93	0.98	0.80	0.93	0.69	0.89	0.96	18	18	12	6	32	14	30	16	13
Obs 5	0.86	0.96	0.92	0.90	0.85	0.86	0.98	0.43	0.95	18	13	13	22	25	17	8	34	12
	0.90	0.98	0.91	0.95	0.89	0.68	0.95	0.87	0.95	17	15	13	21	25	23	13	15	12
Obs 6	0.83	0.66	0.84	0.89	0.86	0.91	0.87	0.68	0.95	23	51	14	16	28	15	24	26	12
	0.71	0.43	0.54	0.80	0.86	0.54	0.59	0.91	0.97	27	59	22	20	28	27	38	11	9
Obs 7	0.89	0.90	0.93	0.94	0.91	0.80	0.90	0.79	0.92	19	22	17	26	22	14	17	19	13
	0.91	0.98	0.96	0.99	0.92	0.63	0.89	0.92	0.95	16	21	15	21	18	15	18	11	10
Obs 8	0.84	0.75	0.37	0.86	0.95	0.96	0.96	0.96	0.94	17	19	26	24	16	10	14	10	15
	0.91	0.90	0.94	0.83	0.96	0.87	0.96	0.83	0.97	14	12	14	20	15	16	13	13	12
Obs 9	0.90	0.83	0.87	0.91	0.92	0.82	0.98	0.94	0.96	20	28	15	28	25	23	14	16	10
	0.77	0.26	0.84	0.74	0.84	0.64	0.96	0.94	0.97	21	27	16	21	28	33	19	13	8
Obs 10	0.91	0.92	0.92	0.95	0.90	0.81	0.92	0.90	0.95	21	30	15	25	28	17	20	19	11
	0.93	0.93	0.93	0.99	0.91	0.89	0.88	0.92	0.97	17	21	14	8	26	13	27	15	9
Mean	0.86	0.83	0.85	0.88	0.89	0.78	0.90	0.84	0.92	20	24	15	22	24	21	18	18	15
Median	0.90	0.90	0.92	0.90	0.91	0.81	0.95	0.89	0.95	18	20	14	21	25	20	16	17	13
Max	0.98	0.98	0.99	0.99	0.99	0.96	0.98	0.96	0.97	38	59	26	38	42	33	38	34	33
Min	0.54	0.26	0.37	0.65	0.70	0.54	0.59	0.43	0.75	9	12	7	6	10	10	8	10	8

3.3.2. Data Analysis

The raw experimental data were analysed using the two methods; the mean-category value method and the categorical-judgement method. These methods were compared by plotting two sets of results as shown in Figure 3-8 and Figure 3-9 where the mean-category value method is plotted on the horizontal axis and the categorical-judgement method on the vertical axis. As can be seen in Figure 3-8 and Figure 3-9, most of properties have the coefficient of the determination value (R^2) of over 0.95 except for two properties: gloss and pearlescence. The properties with high determination value indicate that the results from both methods are well correlated. Frequently, it is found that a simple mean-category value method yields scale values that are very similar to those determined by a categorical-judgement method (Bartleson, 1984; Han, 2006). This high level of correlation indicates that the observers could follow the instructions with the respect to the equal-interval properties of the category scales with a high degree of precision. On the other hand, two properties with relative low coefficient of the determination value have opposite meaning. Therefore, the scale values derived from the simple mean-category value method was not useful for representing the perceptual properties of overall gonio-apparent properties scaled by the observers. In addition, as shown in Figure 3-10, there was lack of significant difference between stereoscopic and monocular vision.

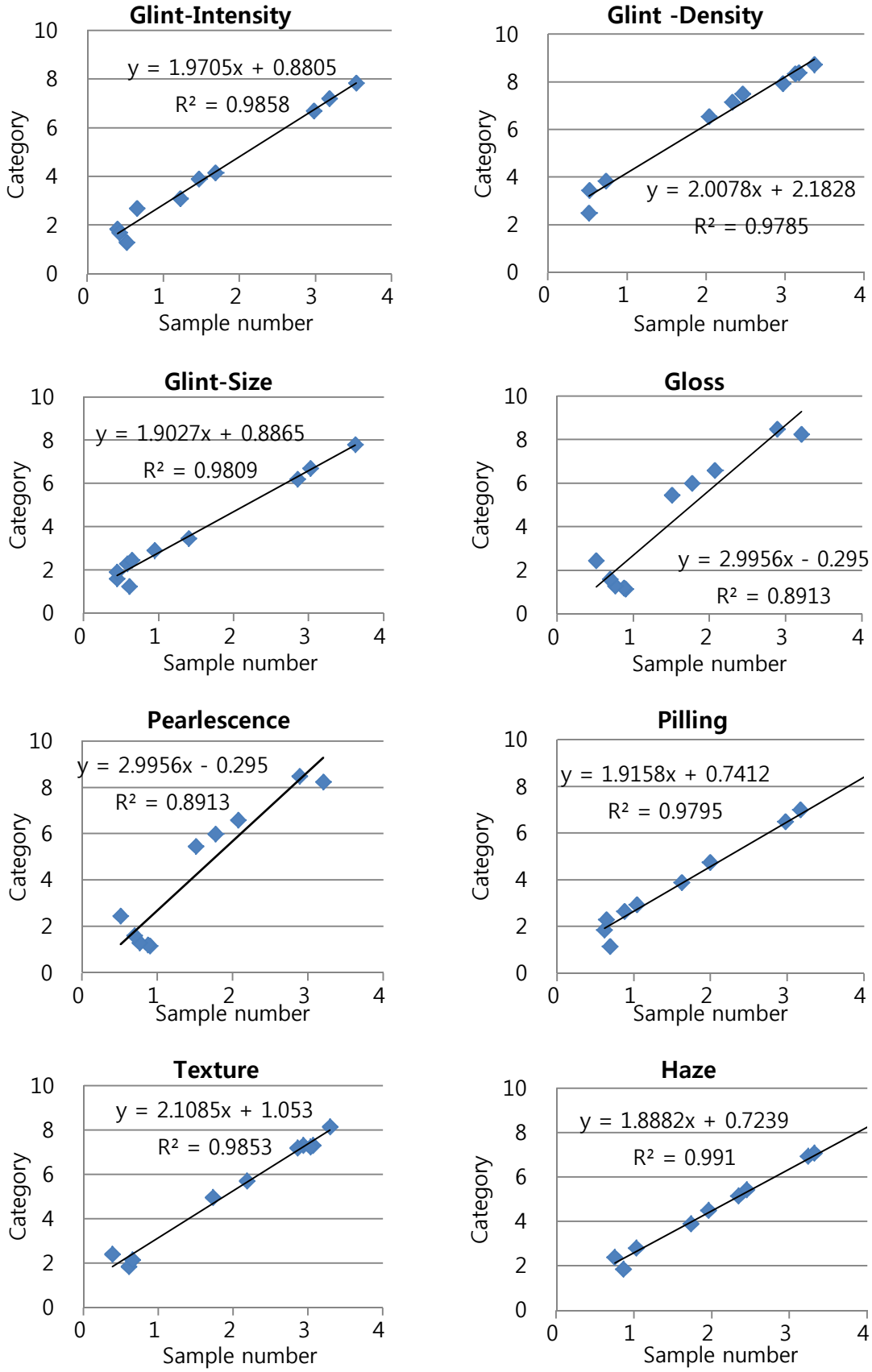

Figure 3-8 For stereoscopic vision comparison of the scale values derived from the mean-category value method and the categorical-judgement method for all samples.

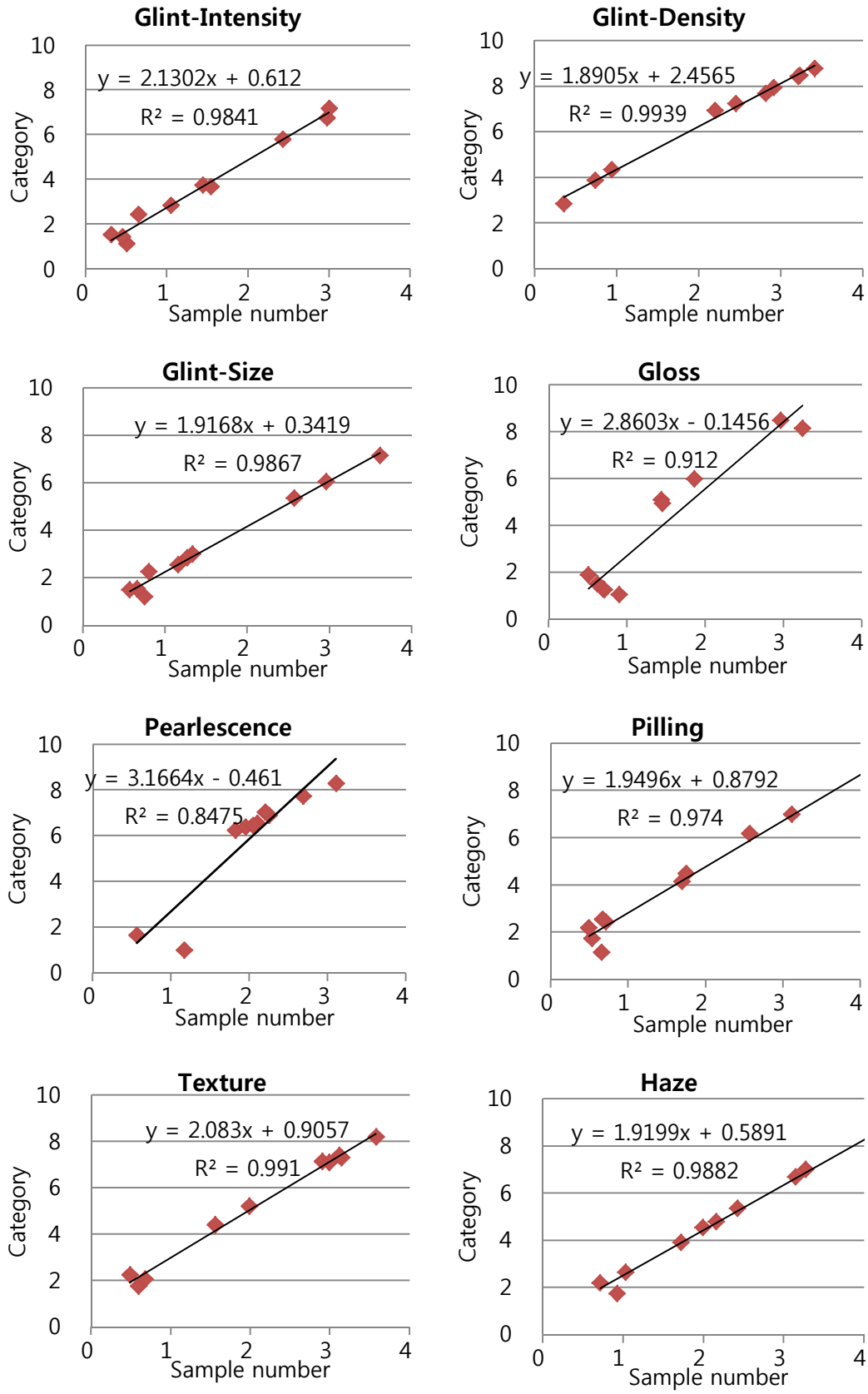

Figure 3-9 For monocular vision comparison of the scale values derived from the mean-category value method and the categorical-judgement method for all samples.

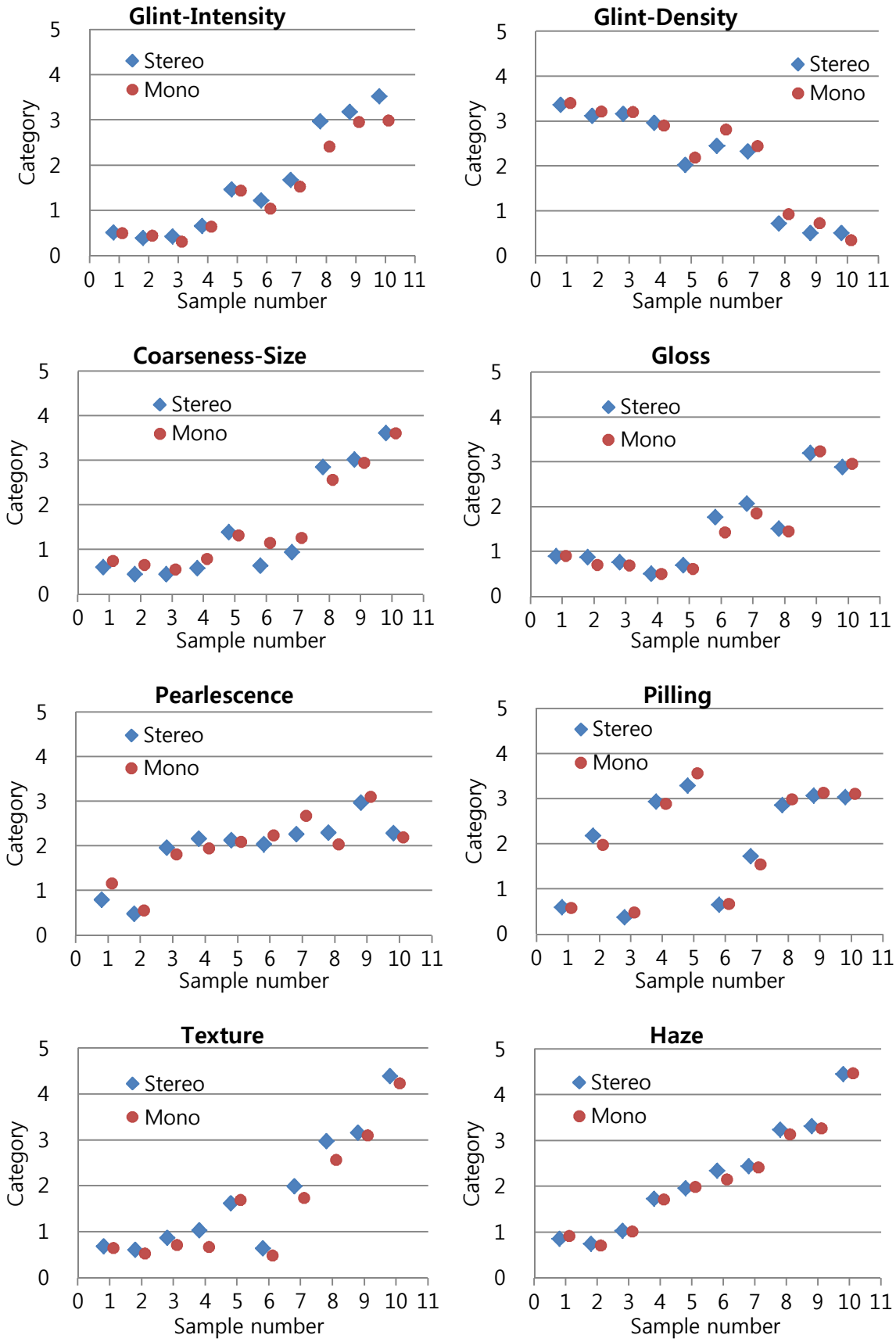

Figure 3-10 Comparison of scale value between stereoscopic (stereo) and monocular (mono) vision.

3.3.3. Comparisons between Stereoscopic and Monocular Vision

The objective of this section is to compare the difference between stereoscopic and monocular vision for perceptual properties of various gonio-apparent materials. Two viewing modes were compared by plotting two sets of results as shown in Figure 3-11 where sample number is plotted on the horizontal axis and category number on the vertical axis. For each sample, there are two points with standard error where blue and red points indicate a median category of twenty observations for stereoscopic and monocular vision respectively. The median is the middle of a distribution: half the scores are above the median and half are below. The median is less sensitive to extreme scores than the mean and this makes it a better measure for highly skewed distributions. In the results with skewed distributions for several properties, median is more useful and meaningful than mean. Most of the properties for stereoscopic vision have category points higher than or equal to those for monocular vision except glint density. In particular, the most obvious difference between two viewing modes was for glint intensity. Glint intensity, glint density and pearlescence have relatively bigger standard error bars, while the error bars for both texture and haze properties manifest the smallest standard error. These tendencies for standard error were shown regardless of viewing mode. These can be seen in all subfigures of Figure 3-11, that the two median sets of two viewing modes using samples 1 and 10 have same value or a half grade difference between each other.

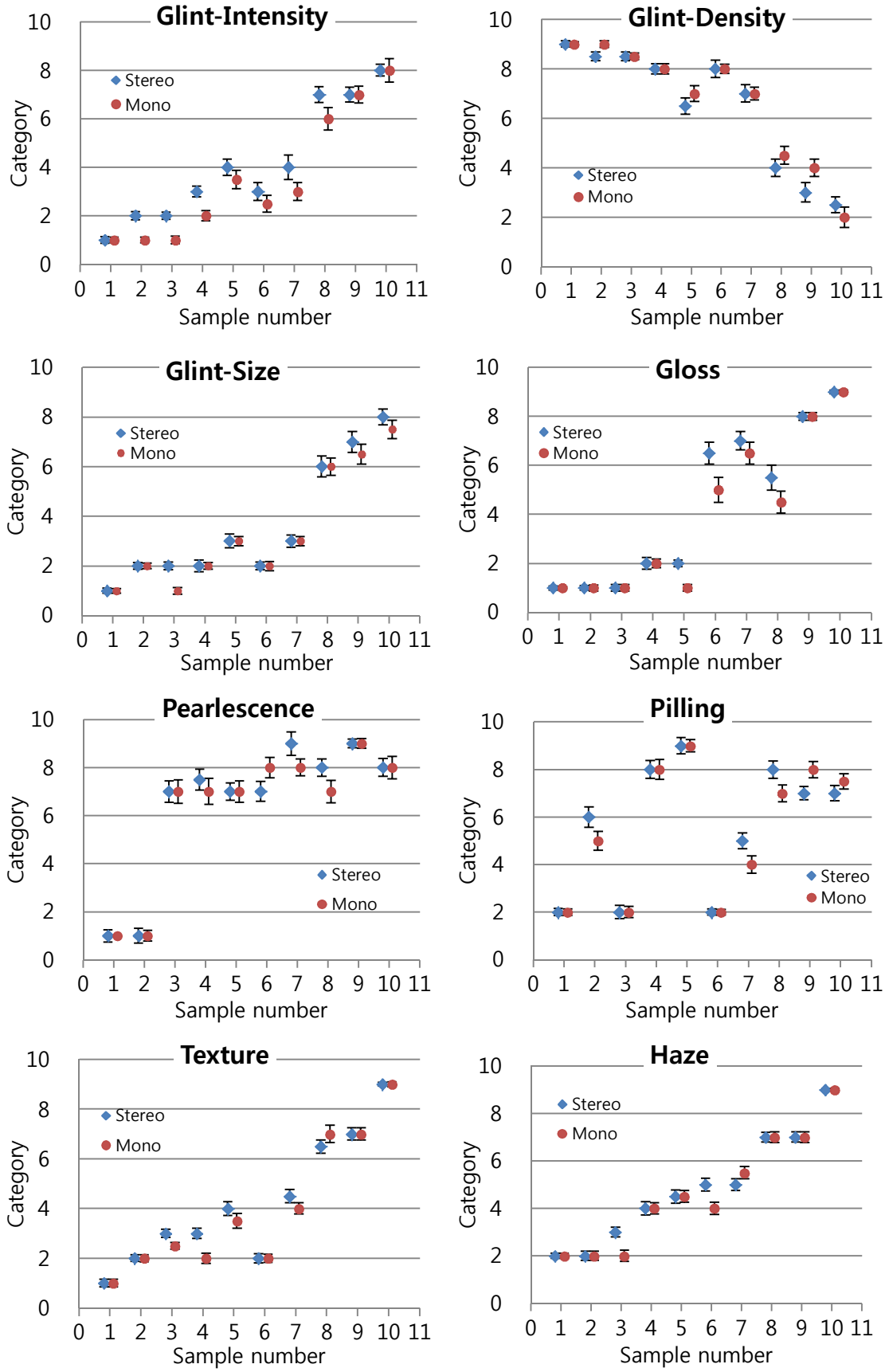

Figure 3-11 Comparison between stereoscopic and monocular vision and the associated median and standard error.

3.4. Discussion

Observer variability indicates the uncertainty in the experiment. Table 3-7 and Table 3-8 show the observer repeatability for eight properties under stereoscopic and monocular vision respectively. In terms of four statistical values for all observers, the repeatability of the two viewing modes are similar to each other. The mean and median R^2 of 0.78 and 0.80 for stereoscopic vision were similar to those of 0.79 and 0.82 for monocular vision. In addition, the results of a *CV* mean 26 and median 24 were almost same as those of 26 and 22. It is difficult to evaluate these results robustly. However, the observer repeatability obtained in a separate study to scale colourfulness (Luo *et al.*, 1991) or gloss (Wei, 2006) had *CV* values of around 19. According to the results of these previous experiments, although R^2 values does not indicate poor agreement between two set of observations from each observer, the repeatability taking account both R^2 and *CV* values seems to be slightly low. In comparison with repeatability, observer accuracy was found to be relatively higher. Along with repeatability, observer accuracy for haze and glint intensity was high and low respectively. However, there is no significant difference between stereoscopic and monocular vision in terms of accuracy and repeatability.

In Figure 3-120, the results were illustrated by plotting the values of median and standard error. For standard error, it can be explained that, as the error bar is longer, the raw categories obtained from observers were distributed widely and the agreement of observations is low. In other words, big error bars mean that observers find it relatively more difficult to judge the relevant property, e.g. glint-intensity, glint-density and pearlescence. However, the variation was still within one grade unit. On the other hand, texture samples typically have not only small error bars but also big differences between the results from stereoscopic and monocular vision for the same sample. It means that it is easier for observers to judge texture and this property can lead big different perception between two viewing modes. Therefore, it can be concluded that the texture is the best type of sample for verification of the difference between two modes of viewing. Table 3-7 shows how many categories had a big difference between two viewing modes for each type of sample. Along with texture, glint intensity is also a good property because, although error bars for several samples were not small, the two modes of viewing had big differences for 7 out of 10 samples. In addition, pilling property having 5 differences is good for comparing between both viewing modes. The error bars of pilling can be

evaluated that the distribution is not big spread. However, in comparison with other result shown in Figure 3-12, The pilling error bar is longer. The reason can be explained by visual fatigue. The effort from long experiment time and using monocular vision influences the accuracy of assessment.

Table 3-7 The number of different samples between stereoscopic and monocular vision.

	Task 1 (Plastic)			*Task 2 Gloss*	*Task 3 Pearl-escence*	*Task 4 Texture*	*Task 5 Pilling*	*Task 6 Haze*
	Glint							
	Intensity	*Density*	*Size*					
Number	*7*	*5*	*3*	*4*	*4*	*5*	*5*	*3*

In Figure 3-11, error bars of middle categories for most properties have relatively large than those of minimum and maximum categories. Observers had difficulty to grade relevant samples with middle categories regardless of any properties and any vision. The reason can be caused in by low-grade reference such as category 1 or 2 for each property. In addition, there was another factor, observer's memory in which they recognised the category ranges of each property, especially maximum and minimum properties, in training section. Observers can, therefore, assess low and high grade samples of each property relatively easier using two reasons. Figure 3-12 show a similar tendency to have relatively big error bars of middle categories due to a low-grade reference in the same categorical judgement experiment of pilling assessment (Jung, 2010). The result could help to design new psychophysical experiment.

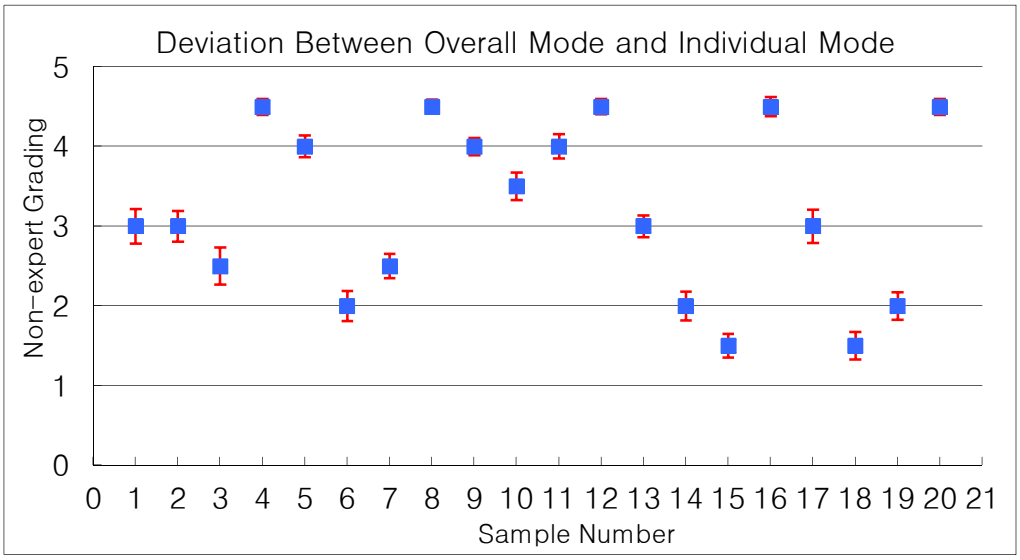

Figure 3-12 Results of pilling assessment (Jung, 2010).

Table 3-8 shows the angle of a tilting table which was adjusted by each observer for specular reflection. The difference of range from 47 to 56 is mainly depends on their face length in which means that the position of the eyes of observers is different even though a chin rest was used in the experiment. It report that illumination geometry was adjusted to suit individual condition, viewing positon.

Table 3-8 Degree of tilting table for each observer

(degree)	Obs 1	Obs 2	Obs 3	Obs 4	Obs 5	Obs 6	Obs 7	Obs 8	Obs 9	Obs 10
1 st	50	50	52	58	52	48	52	48	48	46
2 nd	52	50	52	54	48	52	48	50	46	50
Mean	51	50	52	56	50	50	50	49	47	48

3.5. Summary

Psychophysical experiments were performed to understand how stereoscopic vision quantifies the appearance of gonio-apparent surface features and influences the perception of coloured objects. The overall appearance of any object consists of a combination of various attributes, but one attribute might appear stronger than the others under one

viewing condition. Therefore, the experiment was designed to control viewing conditions specified, in terms of light source and the angle between light source and observer.

Glint was judged under a spot light lamp; gloss, pearlescence and haze under diffuse light; and texture and pilling under directional light. To control the angle, glint, gloss and pearlescence were placed on a tilting table at a specific angle which exhibits specular reflection. Texture and pilling used a pilling-assessment viewer having directional low angle of incidence light (less than15º).

The results of the experiment revealed that observers found it relatively difficult to judge certain properties regardless of mode of viewing. There was pearlescence where the variation for all was significant. Texture and glint intensity were the best properties for differential between stereo and mono viewing since they present an obvious difference between the two viewing modes and are relatively easy to assess. In the experiment, visual fatigue caused lower accuracy comparing with parallel study.

CHAPTER 4.

VISUAL ASSESSMENTS OF TOTAL APPEARANCE

4.1. Introduction

As described in chapter 3, glint intensity of the properties of various gonio-apparent objects has relatively big differences in the visual perception of human between stereoscopic and monocular vision. This property has a characteristic of object which be significantly influenced by viewing mode of observers. This is dominantly visible under directional illumination conditions. Glint is one of visual properties which come from metallic flake pigment in textured metallic coatings. However, it is not enough in itself to explain textured metallic-coatings because the overall appearance of any object consists of a combination of various attributes even though one attribute might appear stronger than the others according to viewing condition. In this study, the main question is how the visual texture properties of metallic-coating can be visually assessed under specific viewing geometry, in which 'glint' is represented as dominant texture property.

Over recent decades, the textured coating provided by metallic surfaces has been an important factor in attracting customers of the automobiles industry. VINCENTZ Network (Vincentz, 2006) argued that 'texture' can be used to effectively distinguish different effect coatings shades as the two properties, glint impression and the diffuse coarseness. Eric Kirchner (Kirchner et al., 2007) also evaluated that the visual texture properties of effect coatings can be visually assessed in terms of two attributes; glint impression and the diffuse coarseness. With these studies, many researches (Lans *et al*., 2012, Huang *et al*., 2010, Kirchner *et al*., 2009) have developed their projects based on same concept. Therefore, it is seen that visual texture property 'coarseness' is one of major properties with glint impression in the appearance of metallic-coatings.

With regard to another visual attribute of texture metallic-coating, 'Brightness' was taken account into in this study according to several definitions, "glint" by researchers in Akzo Nobel (2004).

- Points of reflected light of very high intensity that switch on and off while changing panel orientation.
- The impression that coatings show bright tiny lights under specific viewing angles only when irradiated by an intense directed light source.

- Tiny spot that is strikingly brighter than its surrounding. It is visible under directional illumination conditions only. The glint may be expected to switch on and off when the observation geometry is changed.

From definitions, these terms, 'high intensity', 'bight tiny lights' and 'brighter', seen to relate to "brightness" which are one of the colour attributes.

Finally, this chapter was to investigate the interaction between three parameters affecting the total appearance of metallic-coating surfaces; glint, coarseness, and brightness under specific viewing condition, in which 'glint' is represented as dominant texture property.

4.2. Samples and observers

This section explains a method of visual assessment to qualify glint and others of metallic-coating panels. Viewing condition for psychophysical experiment and the results were discussed.

4.2.1. Samples preparation

An experiment was designed in which a number of observers would visually scale the apparent 'total appearance' of a series of samples in a set of defined viewing condition. A set of samples were 54 metallic-coating panels which consist of 10 red colour panels, 10 green colour panels, 10 blue colour panels, 10 brown colour panels, 9 yellow colour panels and 6 grey colour panels. The surface of these metallic-coating panels was composed of combination solid-colour pigments with aluminium flakes in different proportions. In order to investigate the effect of perceptual glint and others, the panels of each colour group had different amount of aluminium flakes while the proportion of solid-colour pigments was equal. They were produced by Akzo Nobel and one of grey panels was used as a reference. The spectral reflectance of them was measured by Minolta CS1000 tele-spectroradiometer.

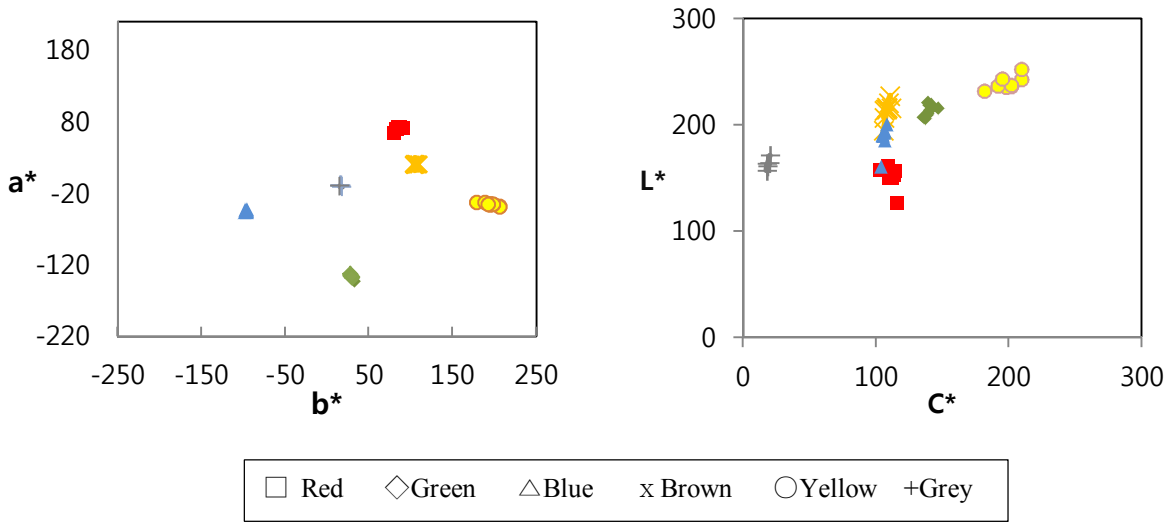

Figure 4-1 Sample selection represented in the chromaticity diagram

4.2.2. Observers and Task

Ten observers with normal (or corrected to normal) visual acuity and colour vision participated in the visual assessments for grading total appearance of the metallic-coating panels. The session was carried out twice, each on a different day, in order to test repeatability. Each session lasted around 35 minutes, but was limited to 45 minutes so as to avoid visual fatigue. All observers were students at the University of Leeds.

Similar to visual assessment in section 3.2.3, observer was asked to sit in front of the experiment table in dark room. For adapting viewing environment for 5 minutes, observers were asked to place their chin and the chinrest and adjust the angle of a tilting table to produce the largest specular reflection. They then had the Ishihara colour vision test and near visual acuity test. They judged three perceptual attributes of 54 metallic panels under directional illumination by comparison with a reference sample. The position of test sample and reference sample were randomly changed on either the left or right hand and all samples were presented in random order. At each section of visual assessment, three scaled values, the angle of the tilting table were recorded. Observer judged a number that best describes the perception of glint, coarseness and brightness of the test sample comparing with the reference grey sample having the value 50 of three visual properties.

Magnitude estimation method was conducted in visual assessment. Before the start of assessment, the experiment instruction was given to observer and the three properties had the following definitions.

- *Glint: tiny spot that is strikingly brighter than its surrounding.*
- *Coarseness: the perceived contrast in the light/dark irregular pattern exhibited by effect coatings*
- *Brightness: visual sensation according to which an area appears to exhibit more or less light (adjectives: bright and dim)*

4.3. Experimental settings

A schematic diagram of the experimental setting is shown in Figure 4-2. The visual assessment was carried out in dark room. As the viewing geometry, observers' viewing geometry was kept constant using a chin-rest after adjusting the tilting table which presents maximum glint perception. A LED spot light was used as the light source and it was located closely above the observer's head to minimise the angle between light source and observer. Both the use of directional light and the minimizing angle of the incident ray enable the visual texture property, glint, to be presented most strongly from the coating sample on tilting table adjusted by observers. Actually, Kirchner (Kirchner, et al., 2012) testified that the higher degree between incident light and surface (closer to normal), the visual accuracy of assessing glint is higher.

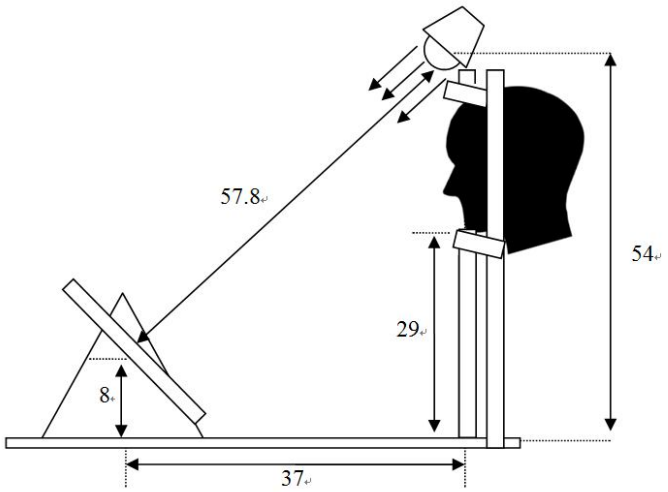

Figure 4-2 Experimental settings

4.3.1. Viewing conditions and apparatus

Table 4-1 shows the specification of LED light source provided by manufacturer. In Figure 4-3, a graph (a) is SPD of the LED light source and (b) indicates temporal stability, in which the luminance line tends to decrease and stabilised after 40 minutes. Spatial uniformity evaluation was introduced in Figure 4-4.

Table 4-1 specification of LED light

Colour Temperature	6500K
Intensity	650 cd
Lumens	500 lm
Angle	35°
Operating Hours	25000
Dimensions	57 x 50 (length x dia)
Watts	7 W

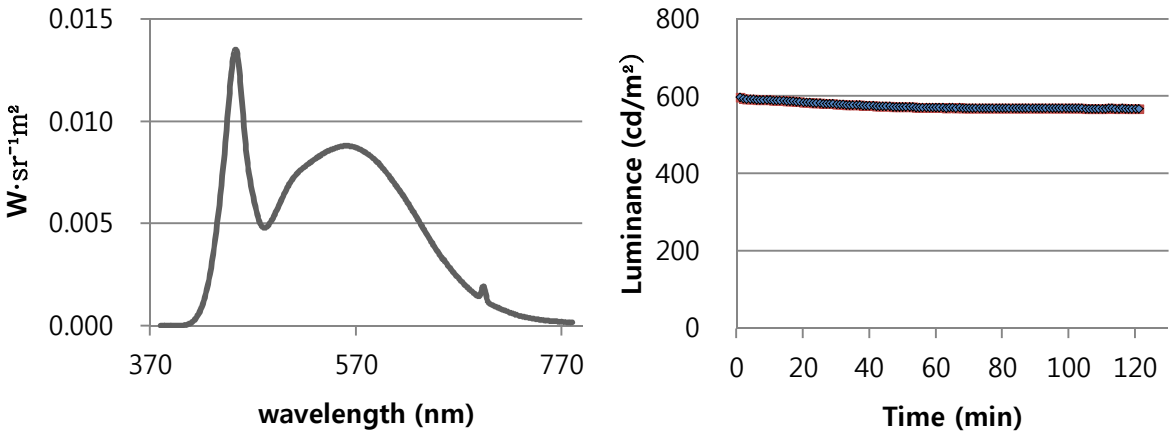

(a) (b)

Figure 4-3 Illumionation condition (a) SPD of the LED light source and (b) Temporal stability

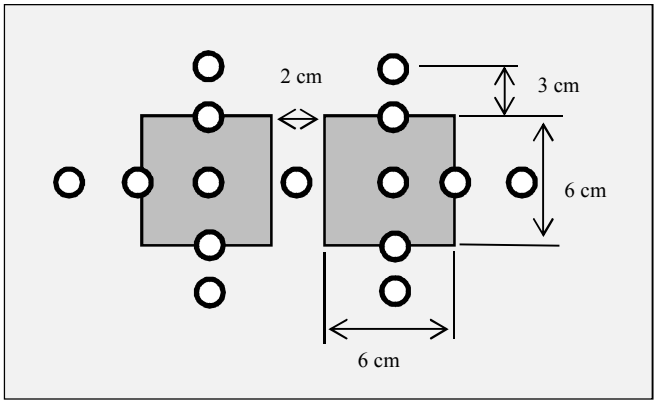

(a)

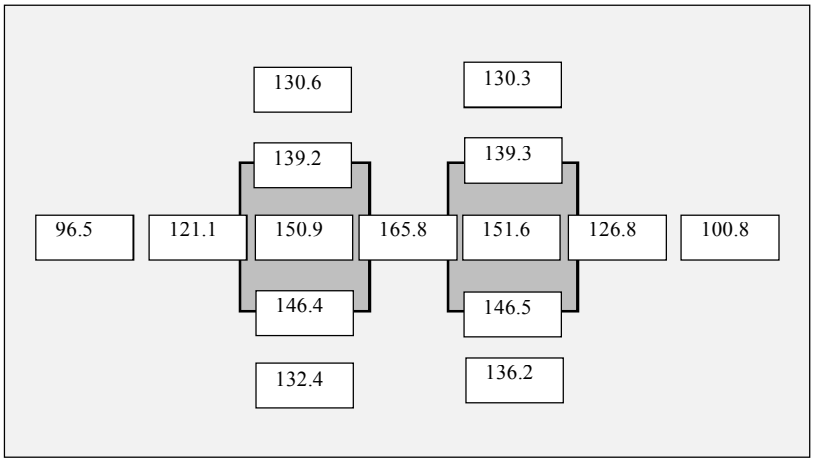

(b)

Figure 4-4 Spatial uniformity evaluation of the illumination
(a) Position of measurements in uniformity evaluation. (b) Illuminance variation

4.4. Results

In this section, reliability of the psychophysical experiments was examined by analysing observer variability. Observer variability of glint, coarseness and brightness was quantified using observer accuracy and repeatability respectively. The statistical methods used for data analysis were the coefficient of determination, R^2, and coefficient of variation, *CV,* as described in chapter 2.5. The higher the agreement between two set of data is, the closer values of R^2 and *CV* are to 1 and 0 respectively. Observer accuracy and repeatability for glint, coarseness and brightness measures in terms of mean, median, max and min of all the sessions from all the samples

4.4.1. Glint

Table 4-2 summarise observer accuracy measures from all the samples and the samples in each red, green, blue, brown, yellow and grey sample group. The result shows that the coefficient of determination, R^2, of the logarithmic scale for all the samples is 0.90 on average with a range from 0.75 to 0.96. The correlation of the raw observer data is 0.85 on average with a range from 0.68 to 0.94. Since the correlations of a log-log scale are higher than these of raw scale, logarithms of the data may be useful to evaluate observer accuracy and repeatability. Table 4-3 shows a summary of observer repeatability measures from all the samples and the samples in each colour sample group. Similarly, the correlations of logarithms for observer repeatability measures were higher. Table 4-4 and Table 4-5 present the accuracy and repeatability measures of each observer from all samples respectively.

Table 4-2 A summary of observer accuracy measures from all the samples and the samples in each red, green, blue, brown, yellow and grey sample group.

	Sample	All Samples	Red samples	Green samples	Blue Samples	Brown samples	Yellow samples	Grey Samples
	Logarithmic Scale							
R^2	Mean	0.90	0.94	0.91	0.94	0.92	0.93	0.91
	Median	0.91	0.94	0.96	0.96	0.93	0.94	0.97
	Max	0.96	0.99	0.99	0.99	0.98	0.98	1.00
	Min	0.75	0.86	0.55	0.85	0.76	0.86	0.67
CV	Mean	13.67	12.54	12.53	12.19	12.73	12.84	15.58
	Median	12.49	12.26	11.79	9.91	11.47	11.27	16.20
	Max	22.95	22.98	24.12	28.02	21.70	20.19	27.34
	Min	8.19	4.04	5.76	3.24	4.18	6.62	2.47
	Raw Scale							
R^2	Mean	0.85	0.88	0.89	0.87	0.88	0.84	0.94
	Median	0.87	0.93	0.91	0.91	0.90	0.87	0.95
	Max	0.94	0.97	0.96	0.99	0.97	0.96	0.99
	Min	0.68	0.57	0.72	0.55	0.64	0.61	0.79
CV	Mean	30.09	26.73	24.54	26.61	25.87	29.41	21.25
	Median	24.94	25.41	21.69	20.86	24.76	25.72	17.20
	Max	54.22	51.75	53.28	60.50	46.39	67.47	46.66
	Min	15.67	10.79	11.38	10.37	8.33	10.42	4.86

Table 4-3 A summary of observer repeatability measures from all the samples and the samples in each red, green, blue, brown, yellow and grey sample group.

	Sample	All Samples	Red samples	Green samples	Blue Samples	Brown samples	Yellow samples	Grey Samples
	Logarithmic Scale							
R^2	Mean	0.90	0.89	0.89	0.94	0.93	0.93	0.92
	Median	0.90	0.92	0.92	0.95	0.93	0.94	0.99
	Max	0.96	0.98	0.97	0.99	0.97	0.99	1.00
	Min	0.82	0.67	0.72	0.89	0.88	0.83	0.66
CV	Mean	10.42	11.81	10.03	8.48	9.33	9.62	7.34
	Median	10.89	11.59	8.56	8.14	9.75	9.18	4.65
	Max	16.06	20.74	19.49	13.13	15.47	20.17	22.47
	Min	5.41	1.90	4.86	4.45	2.94	3.70	2.22
	Raw Scale							
R^2	Mean	0.82	0.85	0.86	0.86	0.83	0.76	0.93
	Median	0.85	0.89	0.88	0.85	0.89	0.84	0.97
	Max	0.93	0.97	0.94	0.99	0.96	0.97	1.00
	Min	0.57	0.62	0.76	0.72	0.40	0.24	0.71
CV	Mean	25.29	25.98	20.04	21.35	23.86	28.21	12.90
	Median	23.74	25.63	19.09	19.99	22.76	20.77	10.10
	Max	42.23	38.45	29.84	34.62	53.06	73.13	32.80
	Min	13.45	10.16	13.03	7.28	9.54	14.23	6.77

Table 4-4 Observer accuracy measures for each session from all samples.

Observer	Session	Logarithmic Scale		Raw Scale	
		R^2	CV	R^2	CV
1	1	0.96	11.33	0.82	44.53
	2	0.95	15.37	0.89	48.15
2	1	0.86	11.89	0.94	18.03
	2	0.91	8.19	0.92	16.48
3	1	0.91	14.28	0.92	48.40
	2	0.93	12.16	0.93	36.65
4	1	0.87	10.98	0.86	21.31
	2	0.88	9.01	0.82	23.38
5	1	0.92	11.21	0.89	19.15
	2	0.94	9.37	0.87	20.92
6	1	0.89	17.00	0.90	15.67
	2	0.88	20.27	0.89	18.23
7	1	0.90	10.14	0.80	24.24
	2	0.90	12.82	0.74	25.55
8	1	0.96	12.14	0.91	24.33
	2	0.92	15.44	0.86	30.87
9	1	0.79	22.95	0.68	29.95
	2	0.75	22.49	0.69	27.87
10	1	0.92	12.84	0.79	53.94
	2	0.89	13.52	0.83	54.22

Table 4-5 Observer repeatability measures of each observer from all samples.

Observer	Logarithmic Scale		Raw Scale	
	R^2	CV	R^2	CV
1	0.89	13.96	0.70	32.40
2	0.90	11.11	0.92	19.10
3	0.94	10.10	0.93	23.13
4	0.89	10.67	0.85	24.34
5	0.96	7.26	0.90	18.31
6	0.91	5.55	0.90	13.45
7	0.82	16.06	0.57	42.23
8	0.93	11.94	0.84	31.91
9	0.84	5.41	0.81	16.28
10	0.91	12.16	0.79	31.71

4.4.2. Coarseness

Table 4.6 shows that observer accuracy for coarseness measures in terms of mean, median, max and min of from all the samples and the samples in each red, green, blue, brown, yellow and grey sample group. The result shows that the coefficient of determination, R^2, of the logarithmic scale for all the samples is 0.71 on average with a range from 0.62 to 0.85. The correlation of the raw observer data is 0.74 on average with a range from 0.46 to 0.89. It seems that raw scale is useful to evaluate observer accuracy due to the better correlation of it than that of a log-log scale. However, the minimum of raw scale is not only very low, 0.46 but also low lower CV. Therefore, for coarseness, logarithms of the data may be appropriate to investigate observer accuracy and repeatability. Table 4.7 shows that a summary of observer repeatability measures from all the samples and the samples in each colour sample group. Similarly, the correlations of logarithms for observer repeatability measures were higher. Table 4-8 and Table 4-9 observer present the accuracy and repeatability measures of each observer from all samples respectively. The result of observer accuracy and repeatability for coarseness was totally lower than that of glint.

Table 4-6 A summary of observer accuracy measures from all the samples and the samples in each red, green, blue, brown, yellow and grey sample group.

	Sample	All Samples	Red samples	Green samples	Blue Samples	Brown samples	Yellow samples	Grey Samples
	Logarithmic Scale							
R^2	Mean	0.71	0.80	0.67	0.83	0.79	0.73	0.84
	Median	0.71	0.85	0.73	0.85	0.78	0.80	0.88
	Max	0.85	0.98	0.92	0.98	0.97	0.96	1.00
	Min	0.62	0.29	0.16	0.40	0.56	0.30	0.51
CV	Mean	12.15	11.30	9.79	10.19	11.86	10.48	10.70
	Median	10.33	8.78	10.03	8.48	9.10	9.85	6.61
	Max	25.11	25.00	14.73	25.11	32.34	26.58	36.28
	Min	6.79	5.98	4.10	3.82	3.93	2.84	1.54
	Raw Scale							
R^2	Mean	0.74	0.83	0.78	0.80	0.80	0.75	0.92
	Median	0.76	0.85	0.84	0.85	0.86	0.74	0.95
	Max	0.89	0.97	0.94	0.93	0.95	0.98	1.00
	Min	0.46	0.59	0.29	0.46	0.32	0.56	0.82
CV	Mean	29.75	25.69	24.37	22.94	23.05	25.68	20.02
	Median	26.19	21.65	24.48	19.31	19.70	25.03	19.19
	Max	56.62	50.29	44.62	55.12	46.17	56.07	43.38
	Min	16.10	11.13	7.46	6.50	8.27	5.52	7.10

Table 4-7 A summary of observer repeatability measures from all the samples and the samples in each red, green, blue, brown, yellow and grey sample group.

	Sample	All Samples	Red samples	Green samples	Blue Samples	Brown samples	Yellow samples	Grey Samples
	Logarithmic Scale							
R^2	Mean	0.75	0.81	0.74	0.83	0.80	0.68	0.92
	Median	0.75	0.80	0.75	0.88	0.82	0.72	0.94
	Max	0.90	0.96	0.98	0.97	0.96	0.98	1.00
	Min	0.58	0.58	0.42	0.44	0.56	0.23	0.73
CV	Mean	11.76	11.07	9.20	9.70	13.17	13.02	7.34
	Median	10.09	10.52	9.89	10.16	10.15	10.64	4.59
	Max	20.93	18.02	16.44	17.97	31.34	23.99	19.35
	Min	7.59	5.52	3.49	4.79	4.77	3.64	1.33
	Raw Scale							
R^2	Mean	0.75	0.77	0.70	0.80	0.72	0.64	0.91
	Median	0.77	0.82	0.70	0.79	0.86	0.64	0.92
	Max	0.92	0.90	0.96	0.96	0.95	0.92	0.99
	Min	0.59	0.42	0.43	0.67	0.11	0.46	0.82
CV	Mean	25.90	23.36	23.39	19.96	25.02	27.93	13.73
	Median	23.95	22.71	25.50	18.27	18.22	27.85	14.98
	Max	41.89	38.46	39.49	37.74	55.22	40.99	21.07
	Min	15.85	15.64	9.69	11.37	11.46	14.57	6.64

Table 4-8 Observer accuracy measures for each session from all samples.

	Logarithmic Scale		Raw Scale	
Session	R^2	CV	R^2	CV
1	0.72	6.98	0.79	35.25
2	0.69	10.72	0.73	51.70
1	0.66	8.31	0.75	20.31
2	0.63	10.93	0.76	23.74
1	0.66	15.50	0.46	24.69
2	0.75	20.08	0.54	31.85
1	0.76	7.01	0.83	26.04
2	0.70	7.19	0.83	21.82
1	0.75	17.68	0.75	31.43
2	0.79	16.30	0.76	30.79
1	0.64	8.46	0.72	20.11
2	0.72	6.79	0.75	20.05
1	0.69	15.16	0.76	26.34
2	0.69	8.70	0.78	23.61
1	0.71	6.84	0.89	16.10
2	0.65	9.02	0.79	21.23
1	0.71	9.95	0.63	28.88
2	0.62	10.81	0.60	28.96
1	0.82	21.46	0.83	56.62
2	0.85	25.11	0.85	55.44

Table 4-9 Observer repeatability measures of each observer from all samples.

	Logarithmic Scale		Raw Scale	
Observer	R^2	CV	R^2	CV
1	0.79	10.35	0.76	24.71
2	0.74	8.45	0.72	19.56
3	0.75	20.93	0.74	41.89
4	0.79	8.25	0.78	26.95
5	0.90	10.01	0.92	15.85
6	0.71	9.11	0.85	16.62
7	0.58	15.51	0.59	32.40
8	0.74	10.17	0.77	22.75
9	0.62	7.59	0.61	23.19
10	0.84	17.25	0.80	35.08

4.4.3. Brightness

Table 4-10 shows that observer accuracy for brightness measures in terms of mean, median, max and min of from all the samples and the samples in each red, green, blue, brown, yellow and grey sample group. The result shows that the coefficient of determination, R^2, of the logarithmic scale for all the samples is close to 0 on average. The correlation of the raw observer data also is 0.58 on average. Both result means that accuracy is low and thus not meaning. In Table 4-11, observer repeatability for brightness measures also is much low.

Table 4-10 A summary of observer accuracy measures from all the samples and the samples in each red, green, blue, brown, yellow and grey sample group.

	Sample	All Samples	Red samples	Green samples	Blue Samples	Brown samples	Yellow samples	Grey Samples
	Logarithmic Scale							
R^2	Mean	0.09	0.20	0.16	0.32	0.22	0.14	0.33
	Median	0.08	0.14	0.13	0.28	0.15	0.11	0.31
	Max	0.26	0.70	0.54	0.78	1.00	0.65	0.76
	Min	0.01	0.00	0.00	0.00	0.00	0.00	0.03
CV	Mean	4.26	3.60	2.68	2.67	3.19	2.74	4.47
	Median	3.50	2.75	2.01	2.39	2.56	2.13	4.58
	Max	8.84	16.64	9.14	7.19	8.79	14.25	8.33
	Min	2.30	1.53	1.02	1.11	1.25	1.26	1.67
	Raw Scale							
R^2	Mean	0.58	0.38	0.33	0.46	0.49	0.15	0.53
	Median	0.59	0.36	0.34	0.52	0.61	0.10	0.60
	Max	0.85	0.82	0.76	0.89	0.95	0.46	0.97
	Min	0.30	0.02	0.00	0.01	0.01	0.00	0.00
CV	Mean	19.72	13.27	14.78	13.12	18.17	13.04	18.05
	Median	14.04	10.99	9.79	8.61	11.53	10.05	16.36
	Max	68.99	29.74	77.46	48.51	85.22	37.71	47.76
	Min	7.15	5.01	3.60	5.26	4.46	4.85	6.94

Table 4-11 A summary of observer repeatability measures from all the samples and the samples in each red, green, blue, brown, yellow and grey sample group.

	Sample	All Samples	Red samples	Green samples	Blue Samples	Brown samples	Yellow samples	Grey Samples
	Logarithmic Scale							
R^2	Mean	0.52	0.24	0.21	0.32	0.26	0.16	0.46
	Median	0.52	0.21	0.16	0.26	0.18	0.09	0.40
	Max	0.77	0.74	0.46	0.90	0.73	0.58	0.82
	Min	0.24	0.01	0.00	0.00	0.00	0.00	0.09
CV	Mean	4.64	5.12	3.35	2.93	3.48	3.76	4.43
	Median	3.49	3.55	2.73	2.58	3.20	2.39	4.37
	Max	8.98	19.73	6.93	6.10	7.63	16.40	7.09
	Min	2.49	2.09	1.51	1.18	1.17	1.08	1.95
	Raw Scale							
R^2	Mean	0.52	0.27	0.20	0.32	0.26	0.15	0.42
	Median	0.47	0.24	0.14	0.22	0.16	0.09	0.39
	Max	0.79	0.81	0.44	0.86	0.73	0.58	0.82
	Min	0.25	0.02	0.00	0.01	0.00	0.00	0.07
CV	Mean	17.75	16.49	14.67	13.07	16.73	14.47	18.61
	Median	14.49	13.67	12.25	10.91	14.69	10.68	16.06
	Max	35.13	31.66	26.50	28.25	43.74	48.35	31.68
	Min	8.78	9.67	5.94	5.00	4.83	4.43	8.14

Table 4-12 Observer accuracy measures for each session from all samples.

	Logarithmic Scale		Raw Scale	
Session	R^2	CV	R^2	CV
1	0.17	4.71	0.59	29.70
2	0.19	8.84	0.45	36.84
1	0.03	3.31	0.55	12.34
2	0.05	4.17	0.64	12.49
1	0.15	2.30	0.85	7.15
2	0.26	2.51	0.77	7.77
1	0.06	4.01	0.39	14.37
2	0.07	3.12	0.61	10.64
1	0.10	2.79	0.78	19.67
2	0.15	3.47	0.72	25.37
1	0.01	8.60	0.64	12.99
2	0.05	3.94	0.60	11.09
1	0.03	2.65	0.46	10.30
2	0.01	3.80	0.30	14.98
1	0.05	2.53	0.64	11.74
2	0.09	3.25	0.44	14.57
1	0.12	3.22	0.42	13.72
2	0.12	3.54	0.55	15.54
1	0.05	6.02	0.63	44.15
2	0.09	8.46	0.49	68.99

Table 4-13 Observer repeatability measures of each observer from all samples.

	Logarithmic Scale		Raw Scale	
Observer	R^2	CV	R^2	CV
1	0.28	8.98	0.38	34.00
2	0.72	3.40	0.67	13.10
3	0.77	2.49	0.79	8.78
4	0.56	3.58	0.50	15.41
5	0.75	2.58	0.71	12.29
6	0.43	8.12	0.75	12.88
7	0.24	3.40	0.25	14.22
8	0.49	3.32	0.44	14.76
9	0.46	3.93	0.33	16.96
10	0.54	6.57	0.40	35.13

4.5. Angle

Illumination and viewing geometry are most important to texture appearance; especially for gonio-apparent materials. In this visual assessment, the experiment was designed to show glint most strongly. Observers adjusted the angle of a tilting table to produce the largest specular reflection and the fourteen angles of the tilting table were recorded for each observer. Table 4-14 shows the result of angles adjusted by observers in terms of mean, minimum and maximum.

Table 4-14 Angle of tilting table adjusted by observers (θ_{Obs})

θ_{Obs}	Obs1	Obs2	Obs3	Obs4	Obs5	Obs6	Obs7	Obs8	Obs9	Obs10
Average	44	43	43	46	45	47	47	48	47	49
Min	41	40	40	43	43	45	46	47	46	48
Max	48	45	45	48	47	48	48	49	49	50

The angle of tilting table is not enough to explain the actual geometry of this experiment. To identify whether the experiment setting is well designed, it is necessary that the actual angle between a light and observer is examined.

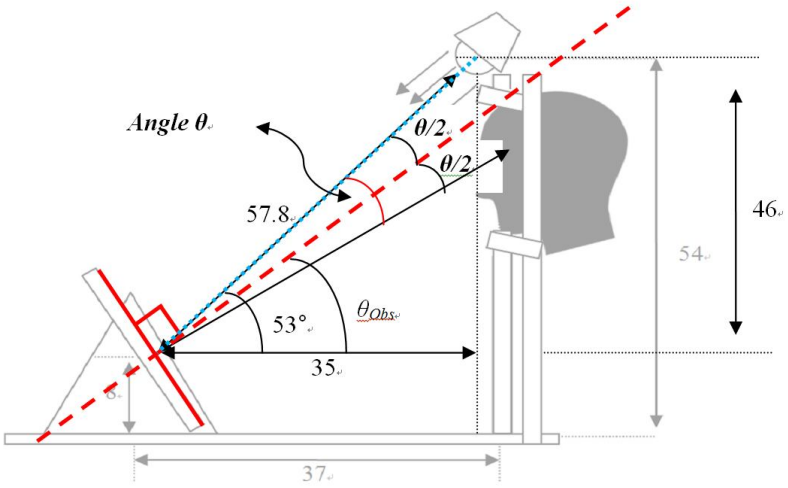

Figure 4-5 The actual angle used by observers

Using the fixed location of the LED light, the actual angle between light source and eye can be calculated from the angle of tilting table adjusted. The actual angle selected by observers was calculated from Equation 4-1.

$$Angle\ \theta = (53° - obs\ \theta) \times 2 \qquad \textbf{Equation 4-1}$$

The results of the actual angles of observers are shown in Figure 4-6. A mean value of selected angle for all observers was 14° in their measurement with minimum and maximum angle of 8° and 20° respectively. It is verified that the experiment of this visual assessment was well designed to minimise the distance between light source and the eye of observer. The disagreement between the observers is depended on the difference of length and of their faces.

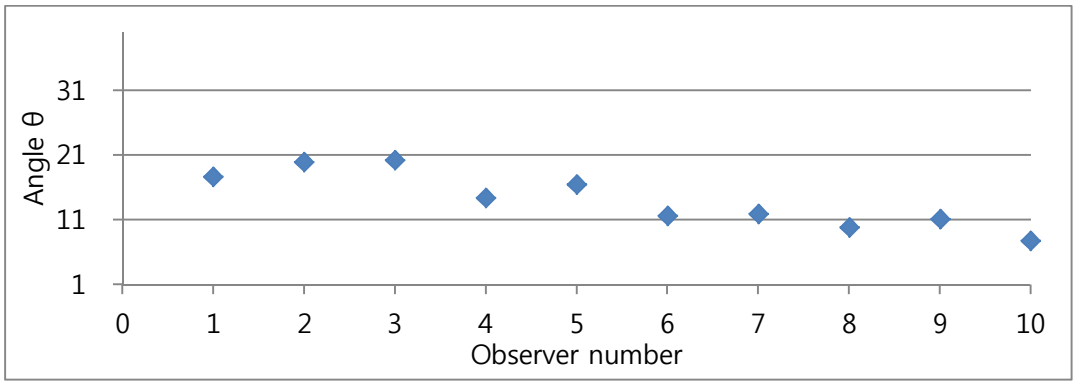

Figure 4-6 The indication of the actual angle measurement of observers

4.6. Conclusions and discussions

Uncertainty of the visual assessment results were examined in terms of the observer accuracy and repeatability. The results of glint, coarseness and brightness can be found in Tables 4.2-4.5, Tables 4.6-4.9 and Tables 4.10-4.13 respectively.

For glint, the mean accuracy of R^2 was 0.92 0.94, 0.91, 0.94, 0.92 0.93 and 0.91 for the all the samples, red, green, blue, brown, yellow and grey samples respectively. The R^2 of mean accuracy values for all colour groups were close to 1. These imply that individual observer data is linearly correlated with the mean observer data. The CV of mean accuracy values was 13.67 for all the samples with a range from 8.19 to 22.95. The CV mean accuracy values for each colour sample group were close to that for all the samples. That

means about 13% disagreement between or 13% variation in individual observer data and mean observer data. The result of observer repeatability was presented in Table 4-3 and the each observer repeatability details in Table 4-5. Similar with the accuracy value, the mean repeatability for all the samples and all colour groups was 0.90, 0.89, 0.89, 0.94, 0.93, 0.93 and 0.92. The CV of mean repeatability value for all the samples was 10.42.

Figure 4-7 shows the median bar and error bar of each coloured panel from visual assessment where sample numbers is plotted on the horizontal axis and perceptual scales of observers on the vertical axis. As shown in the median bars of this graph, the perceptual scale of each coloured group tends to increase as the sample number increases. It means that samples having higher numbers were judged as higher glint by observers. Similarly, error bar has the same tendency which the higher the sample number in each coloured group is, the bigger their distribution is. This result can be come from grading condition; open-end scale. Most error bar of samples having bigger scaling value than 50 become bigger in which the value 50 is the reference. Therefore, it can be said that observer has difficult to judge higher glint samples.

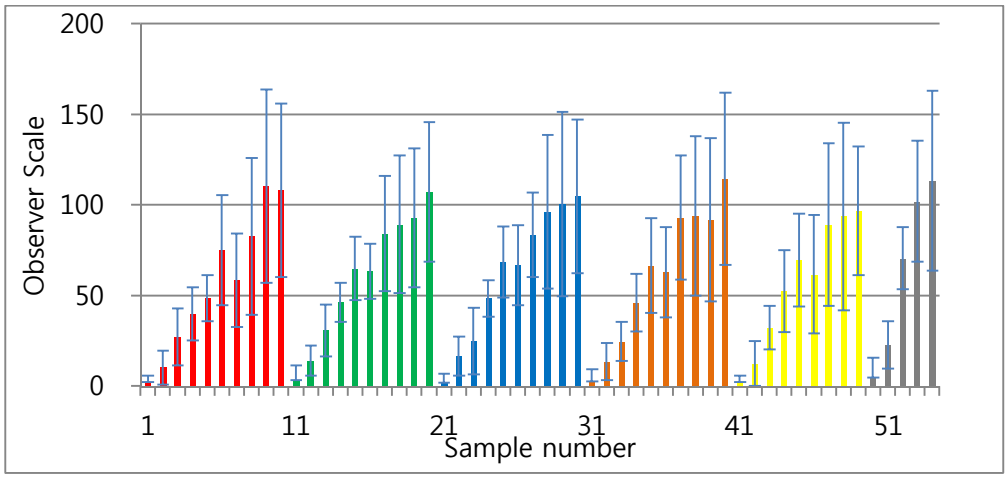

Figure 4-7 Median and error bar of visual assessment

Figure 4-8 simplified the result of visual assessment in order to investigate the clear tendency of scaled glint from observers. Five reversed points drawn by red circles were presented in each coloured sample group respectively. They are placed just above the value of reference sample, 50 in common.

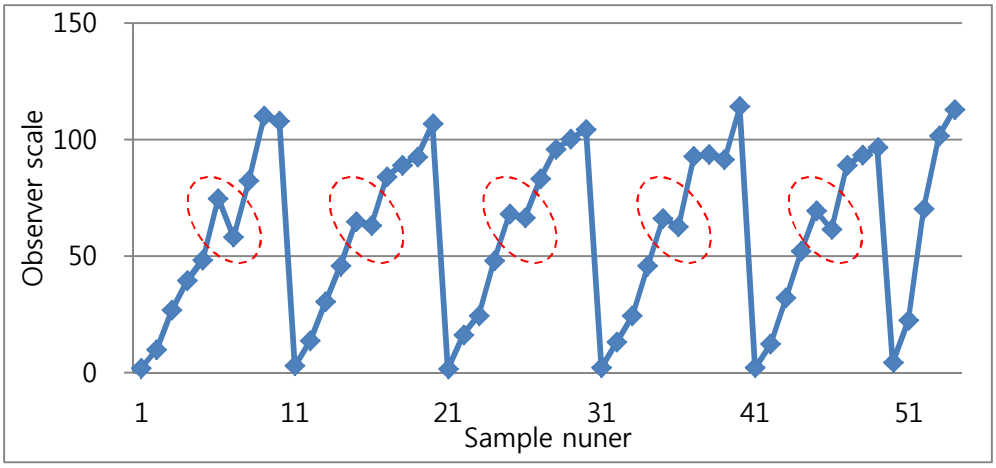

Figure 4-8 Median of visual assessment

This result is partly similar with crispening effect that the contrast between two stimuli increases when the stimuli are presented against a background with a stimuli value between them as described in section 2.3.1.2. The stimulus of crispening effect is related with lightness. Whereas this result of visual assessment comes from the different stimulus, glint that one of the properties of various gonio-apparent objects is. Two stimuli were defined as different names and represent different properties. Even though the higher glint level is, the brighter panel exhibits in each group.

This similar tendency also appeared in Kitaguchi's result. Figure 4-9 shows three reversed points circled by red dot line. The tendency didn't occur in all coloured group. However, it is certain that there was similar phenomenon in previous research.

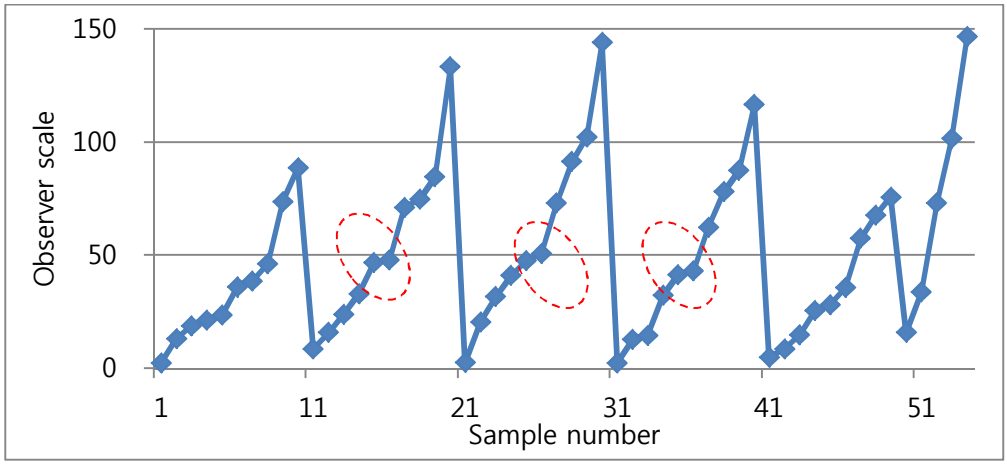

Figure 4-9 Median of visual assessment for glint (Kitaguchi, 2008)

For coarseness, the mean accuracy of R^2 was 0.71 from all the samples with arrange from 0.62 to 0.85. The mean R^2 values of 0.80, 0.67, 0.83, 0.79 0.73 and 0.84 were calculated from the red, green, blue, brown, yellow and grey samples respectively. The R^2 of mean accuracy values of coarseness for all colour groups were lower than that of glint. The CV of mean accuracy values was 12.15 for all the samples with a range from 6.79 to 25.11. The result of observer repeatability was shown in Table 4-7 and the each observer repeatability details in Table 4.9. The mean repeatability for all the samples and all colour groups was 0.75, 0.81, 0.74, 0.83, 0.80, 0.68 and 0.92. The CV of mean repeatability value was 11.76.

Figure 4-10 show the median of visual assessment for coarseness. The tendency is similar with that of glint in which reversed points were placed around the value of reference, 50.

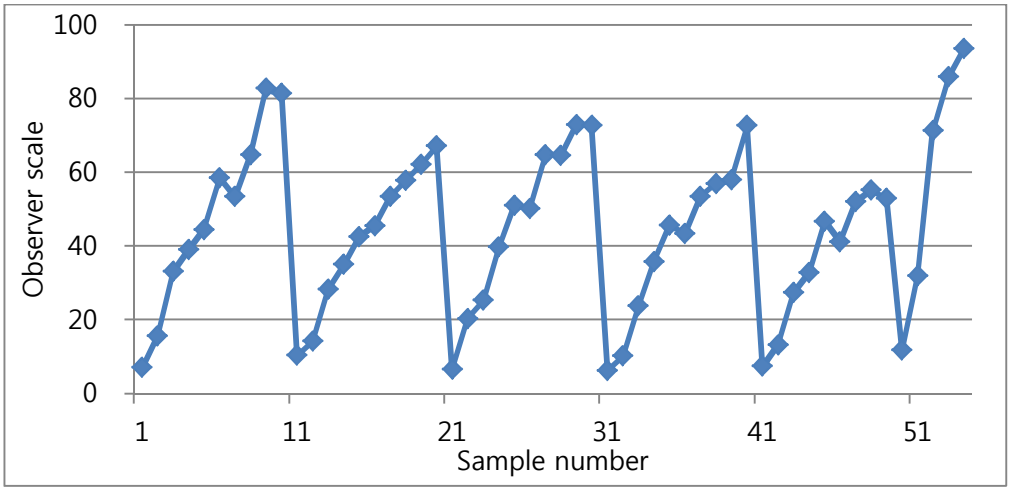

Figure 4-10 Median of visual assessment for coarseness

Figure 4-11 shows the result of visual assessment for brightness. It appears some particular tendency that the higher level of glint assessed as brighter in few coloured groups. However, the median line of visual assessment for brightness appears randomly on the whole. It verifies that brightness is not sufficient for the total appearance.

As mentioned in section 4.4.3, both the accuracy and repeatability of brightness were low regardless of the logarithmic or raw scales. It can be thought that brightness is not one of visual texture properties of metallic-coating under specific viewing condition. Therefore, Brightness property is excluded from the total appearance.

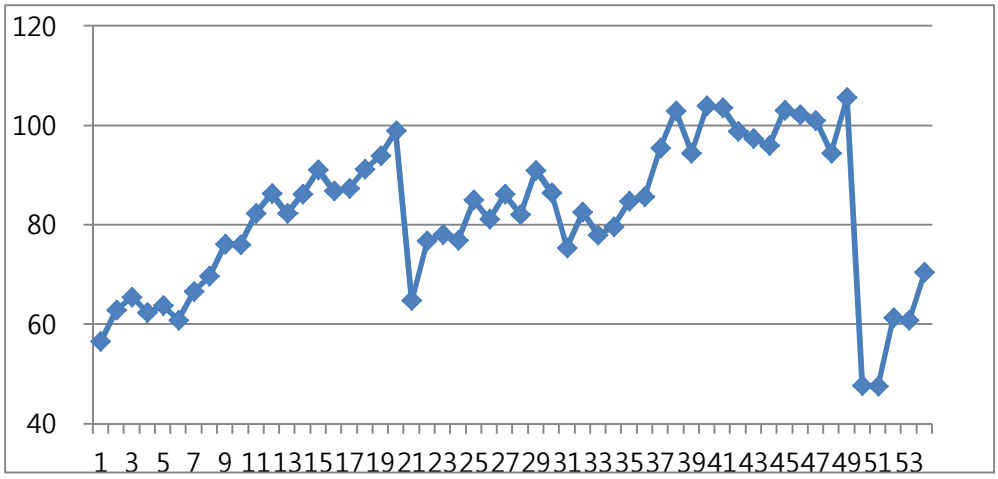

Figure 4-11 Median of visual assessment

CHAPTER 5

DIGITAL IMAGE PREPARATION

5.1. Introduction

Image acquisition is the first step for every digital imaging system. As well as human vision introduced in Chapter 3 and 4, the process can be defined as the combination of primary three elements of vision. They are illumination, objects and the eyes as detectors. Those components can change according to what is target to be 'seen' in digital image acquisition system. For the total appearance in present study, metallic-coating samples are the targets to be 'seen' by a digital camera. Since the metallic images captured by the digital camera can be extremely affected by viewing condition, we attempt to design an optimum system to digitise complex reflection of visual texture of metallic sample surfaces. The 'optimum' here is to produce consistent and meaningful digital images close to real perception of human vison.

5.2. Stereo image acquisition system

In the following section, the hardware is introduced as the image acquisition system. A stereo illumination setup is proposed for the real image capture of the metallic-coating panels. This novel configuration was applied to outperform the conventional illumination systems in several ways. The stereo image acquisition system is comprised of a digital camera and two light sources. The design of the novel image acquisition system stated from several definitions for glint of metallic coatings proposed from Researchers in Akzo-Nobel (2004) below.

- Points of reflected light of very high intensity that switch on and off while changing panel orientation.
- The impression that coatings show bright tiny lights under specific viewing angles only when irradiated by an intense directed light source.
- Tiny spot that is strikingly brighter than its surrounding. It is visible under directional illumination conditions only. The glint may be expected to switch on and off when the observation geometry is changed.

An LED spot was selected as the light source in order to match the conditions outlined in Akzo Nobel (2004), i.e. “irradiated by an intense directed light source” and “directional illumination conditions only”. A digital camera was used as measurement device. This is because like tiny lights, the visual texture of metallic coatings cannot be measured by spectrophotometers (McCamy, 1998) because it measures the average colour over a certain area of the metallic coatings. In comparison, a digital camera can measure the real scene in a similar was to which it is perceived by human vision. Illumination geometry will be explained in detail in Section 5.2.2.

5.2.1. Digital camera Nikon D7100

Digital cameras capture real scenes, producing image data. They can be classified from low-end to high-end according to their specifications. Generally, low-end digital cameras produce images with limited resolution and poor quality. On the other hand, cameras at higher end usually have sensor sizes reaching up to more than thirty-six million pixels. From a technical point of view, the quality of the camera output is influenced by the lens and number of pixels that the camera can record. The quality of a digital image may be evaluated in terms of colour accuracy, dynamic range, geometrical accuracy and noise.

Nikon 7100 is a single-lens reflex type of digital camera (DSLR). The principal technical specifications of this camera were listed in Table 5-1. This camera is classed as middle grade between the high-end consumer and professional digital camera; however image sensor size of this camera is in the high class, having 24.1 million effective pixels. In the stereo image acquisition system developed here, the resolution of this camera is sufficient to capture real reflection of metallic-coating panels. The metallic-coating panels have several attributes of visual texture such as glint, coarseness, etc. They are categorised as micro appearance because aluminium flakes were involved in the coatings. In fact, the physical diameter ranges between 5 and 50 μm (Kirchner *et al.*, 2006). The image capture system was designed so that one pixel of this camera can detect the smallest particle possible. However, the real cover size of one pixel is 20×20 μm which means that an aluminium flake ranging from 5 to 20 μm diameter is represented by the same pixel size. Therefore, if possible, the size of one camera pixel should be smaller or equal to the real

minimum flake size of metallic-coating panel. However, this study focuses on what can be observed on the metallic-coating surface, not physical components. With regards to the visual nature of reflecting flakes, Ďurikovič (2003) mentioned that the bright sparkles observed on metallic coatings looked much larger than the physical size of flakes. Therefore, it can be said that the system setting for cover size of one pixel, middle of physical size of flake, is appropriate. Furthermore, taking into account image processing, there is a compromise between digital data size and details to achieve reasonable results in a practical time-consuming.

Table 5-1 Technical specifications for Nikon D7100

Image sensor	23.5 x 15.6 mm CMOS sensor (24.71 million)
Sensitivity	Auto (100 – 6400) – enabled via custom function
Image Size	DX (24×16) image area: 6000 × 4000 [L], 4496 × 3000 [M], 2992 × 2000 [S]
Storage	SD/SDHC/SDXC (two slots)
Image Format	NEF (RAW): 12 or 14 bit, lossless compressed or compressed JPEG: JPEG-Baseline compliant
Colour Mode	sRGB, Adobe RGB
Autofocus	Nikon Advanced Multi-CAM3500 autofocus sensor module with TTL phase detection, 51 focus points, and AF-assist illuminator
AF Area Mode	Single Area AF 9-,21-,or 51-point dynamic-area AF, 3D-tracking, auto-area AF
Metering	3D Matrix Metering II, Centre-Weighted Average, Spot
Exposure Mode	Multiple exposure mode Number of shots
Shutter Speed	1/8000 to 30 s in steps of 1/3 or 1/2 EV, bulb, time, X250
White Balance	Auto (2 types), incandescent, fluorescent (7 types), direct sunlight, flash, cloudy, shade, preset manual (up to 6 values can be stored, Spot White Balance measurement available during live view), choose colour temperature (2500-10000 K), all with fine-tuning

As seen from Table 5-1, the Nikon 7100 digital camera can work automatically or manually when capturing. The manufacturer has applied a number of technologies into this camera to automatically examine what is measured in order to produce the best

images with correct settings. Through the lens (TTL) phase detection is a representative function which enables autofocus by metering what is seen. On the other hand, manual shooting mode has lots of flexibility to set various combinations of digital camera functions, such as ISO sensitivity, shutter speed, aperture, etc. This optional setting of digital camera enables metallic-coating samples to be captured under controlled condition by only user, not software included in digital camera. In this experiment, the camera setting used manual shooting mode to acquire digital image data for 54 metallic-coating samples captured under the consistent conditions. Further explanation for the illumination conditions will be given in Section 5.2.2.

Table 5-2 Camera configurations

Lens	AF18-250mm / F3.5-6.3
Focal Length	250mm
Shooting Mode	Manual (Release controlled)
Shutter Speed	30s
Aperture	f/6.3
Sensitivity	ISO 200
White Balance	Fluorescent
Focus Mode	MF – Manual Focus
Image Size	6000×4000
Colour Mode	sRGB
Image BPP	14-bit (Tiff 16-bit)
Compression Level	None

The camera configurations are shown in Table 5-2. The quality of image output depends not only on the number of photodetectors in the camera's image sensor but also the lens. Focal length was stated as 250 mm. The focal length of the image system refers to the distance between the lens and the camera image sensor when the object is in focus. The longer the focal length, the smaller the viewing angle of camera and the larger the object appears to be. To obtain meaningful image data with regard to the cover size of one pixel (20×20 μm), the maximum resolution (6000×4000 pixels) of this camera was chosen with

a zoom lens that offered a maximum focal length of 250 mm. There is no need to use a lens with a long focal length if the camera can be positioned close to the sample. Nevertheless, the combination of the sensor size of camera and the viewing angle of lens since the camera should have sufficient distance from a sample not to block out the light irradiated from the illumination of the stereo image acquisition system. The most important task for the system is to capture two images having identical position for the same sample. That means that camera stability is vital to achieving a sharp image due to micro appearance of perceptual attributes of metallic-coating samples. In the experiment, a camera remote shutter release was used as trigger to activate the camera's shutter remotely without touching the shutter release button. The final image data produced by this camera was non-compressed 16-bit RGB. With regard to shutter speed, the exposure time was 30s; however the dynamic range of the real scene is greater than that of an image of some coatings.

5.2.2. Illumination setup

As explained, the aim of the image acquisition system is to produce consistent and meaningful digital images close to the real perception of human vison. In a similar way to determining the light source and measurement device, this design of illumination setup started from "glint" definitions by Akzo Nobel (2004).

From "very high intensity that switch on and off while changing panel orientation" and "switch on and off when the observation geometry is changed", it is known that the appearance of these coated products strongly depends on the viewing geometry. In visual assessment in Chapter 4, viewing geometry was fixed in terms of the position of light source and eyes and the angle of tilting table after each observer adjust. This meant that observers could see the high intensity spots that switch on and off without changing panel orientation. The reason for this is derived from the principle of stereoscopic vision. In human vision, the distance between two eyes cause different viewing angle in which each eye captures its own view. Two different images are sent simultaneously to the brain and united into one picture. As an application of this process to visual assessment, the small differences between two images captured at different angles enable observers see points of

reflected light of very high intensity that switch on and off without any change in viewing geometry. From that, it can be hypothesised that two cameras are needed to mimic the two-eyes corresponding to the real perception by human vision. In various industrial fields, the principle of human vision was implemented. However, those common methods using two cameras are not appropriate for this study dealing with small aluminum flakes. Figure 5-1 shows two images which were captured of a slightly scratched solid-coating using two cameras positioned at a distance. It is not easy to detect a difference between the two images. On the other hand, in Figure 5-2, the two images of metallic-coating panel show big differences between both left and right, even though the same coating sample and area were captured. This means that it is extremely challenging to do stereo matching (image registration). Furthermore, applying stereo matching to digital imaging process is difficult.

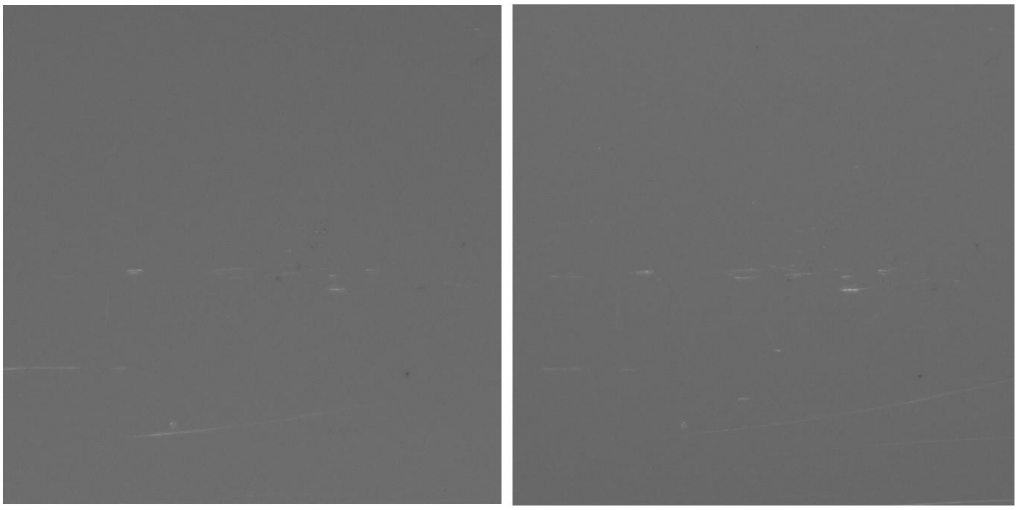

Figure 5-1 Left and right image of solid-colour coatings

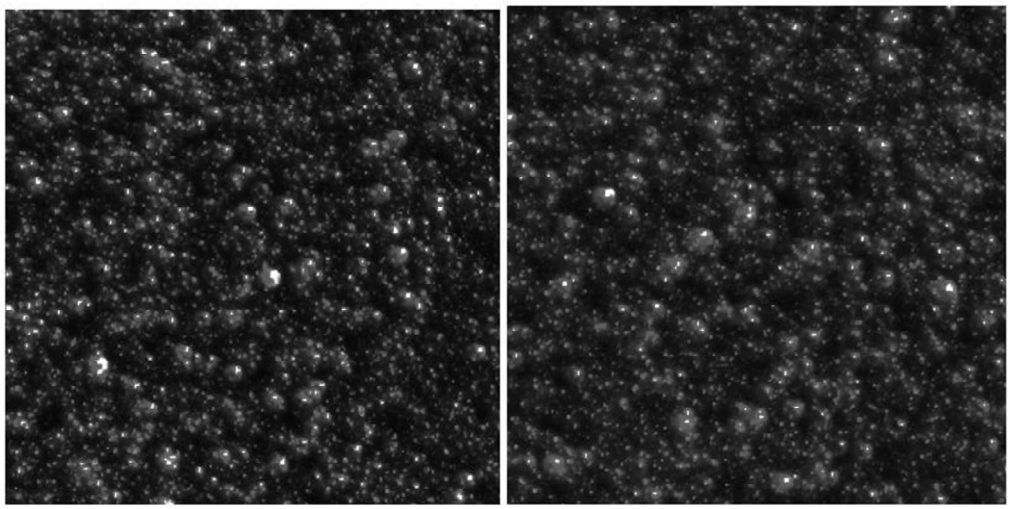

Figure 5-2 Left and right images of metallic-coatings with aluminium flakes

In this section, a novel illumination setup of stereo image system was proposed. The aim is to obtain consistent and meaningful digital images close to real perception of stereo human vison and available to apply stereo matching to digital imaging process. As seen in Figure 5-3, the illumination setup includes two LED directional lights which are located at different lateral positions and each LED source plays a role as each eye of human vision. The scenes illuminated by two different lights differ because of the illumination angle. The angle between camera and light source was the same as that of the viewing geometry used for visual assessment. In practice, two slightly different images for one sample were captured under two different lighting conditions: each image with a single light on.

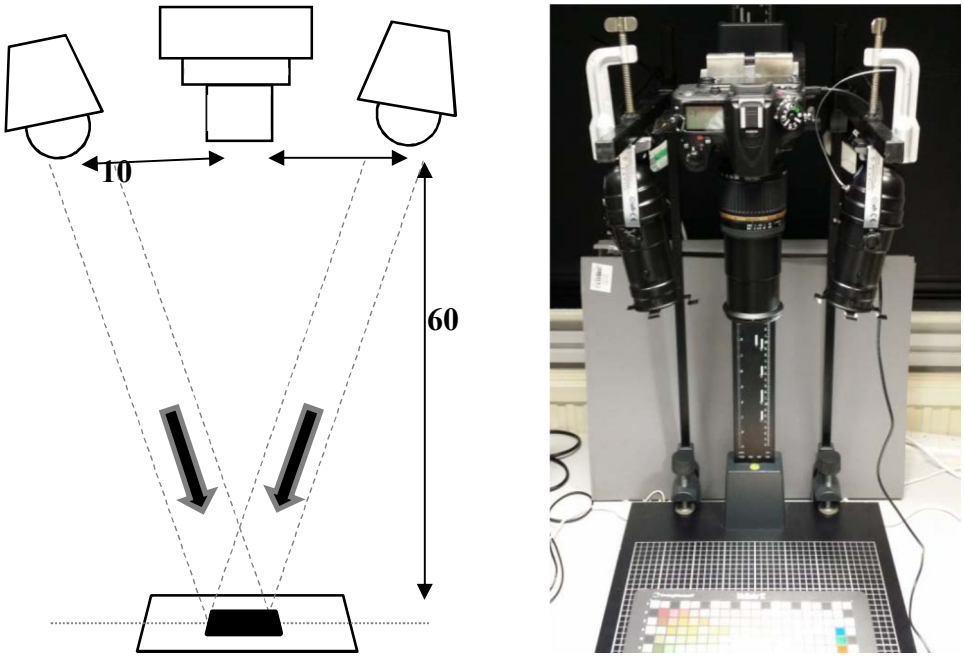

Figure 5-3 Illustration of the stereo image acquisition system

The system consists of a digital camera and two LED spot lights, as shown in Figure 5-3. It was designed to mimic human stereo vision. In the system, one digital camera was used as an image detector in contrast to other types of stereo capture system having two or more lenses and separate image sensors. Nevertheless, the system can reproduce effective images of stereo perception without the complexity of stereo matching. This advantage comes from the illumination set up. Using the stereo image acquisition system, two images were obtained for each metallic-coating sample. They have to be captured in exactly the same position, and thus left and right lights were switched on alternatively. These images are useful for applying stereo matching to digital imaging process. In Figure 5-4, the temporal stability of two light sources is shown. The left and right lights were alternately measured at 1-minute intervals to investigate the real lighting condition when capturing images of metallic-coating samples. The luminance line shown tends to increase until 20 minutes. Therefore, all the samples were captured after a 20-minute warm-up time.

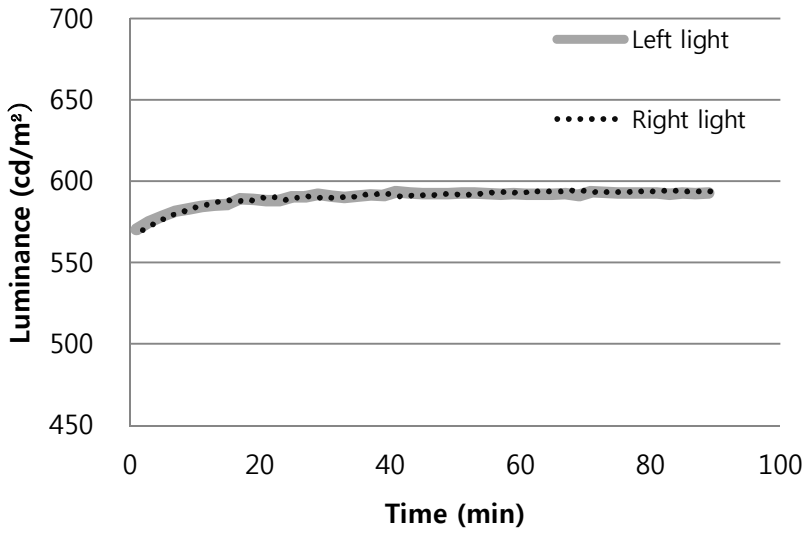

Figure 5-4 Temporal stability of two LED spot lights

5.3. Digital camera characterisation

A digital camera captures two images of metallic-coating samples by saving the digital image data generated from a CMOS sensor. To use a digital camera as a measuring instrument, it is necessary to relate the *RGB* output data of the camera to device-dependent tristimulus values based on CIE colour-matching functions.

A GretagMacbeth ColorChecker DC was used as standard reference chart for characterisation. The chart was intended to cover a broad colour gamut, having colours equally spaced throughout the gamut and with a variation between colours ranging from 5 to 15 ΔE^*_{ab}. The patches represent a number of colours in natural scenes such as skin tones, various shades of green for foliage and blue for sky or water (GretagMacbeth). In the calculation, 12 high-gloss patches were omitted and the majority of 228 patches having matt surfaces were employed since surface material differences give rise to increased error in camera characterisation (Cheung, 2004).

Various terms of polynomial regression model with least-squares fitting were applied and the appropriate terms of the model were then selected to convert RGB to XYZ values resulting in the least colour difference. They can be represented by

$$\boldsymbol{H = MC} \qquad \text{Equation 5-1}$$

where C is a matrix of $N \times 3$ terms according to the complexity of camera RGB characterisation.

Table 5-3 Sizes of the RGB matrices for polynomial regression model

M × 3	Augmented RGB Matrices (C)
3 × 3	R G B
4 × 3	R G B RGB
5 × 3	R G B RGB 1
6 × 3	R G B RG GB BR
8 × 3	R G B RG GB BR RGB 1
9 × 3	R G B RG GB BR R^2 G^2 B^2
11 × 3	R G B RG GB BR R^2 G^2 B^2 RGB 1
20 × 3	R G B RG GB BR R^2 G^2 B^2 R^2G G^2B B^2R G^2B B^2R B^2G R^3 G^3 B^3 RGB 1
35 × 3	R G B RG GB BR R^2 G^2 B^2 RGB R^2G G^2B B^2R G^2B B^2R B^2G R^3 G^3 B^3 R^3G G^3B B^3R R^3B G^3R B^3G R^2GB RG^2B RGB^2 R^2G^2 R^2B^2 G^2B^2 R^4 G^4 B^4 1

The performance of various terms of the polynomial regression model was evaluated in terms of CIELAB ΔE_{00} between the predicted and measured data sets.

Table 5-4 Performance of the camera characterisation model

	Left lighting					Right lighting				
Size × M	Median ΔE_{00}	Mean ΔE_{00}	Max ΔE_{00}	Min ΔE_{00}	95% percentile ΔE_{00}	Median ΔE_{00}	Mean ΔE_{00}	Max ΔE_{00}	Min ΔE_{00}	95% percentile ΔE_{00}
3× 3	0.92	1.03	4.30	0.24	2.13	0.92	1.02	3.99	0.09	2.02
4× 3	1.09	1.31	3.94	0.28	3.25	1.05	1.33	3.72	0.31	3.33
5× 3	1.03	1.15	3.98	0.24	1.99	1.07	1.13	3.67	0.25	1.91
6× 3	1.01	1.07	4.32	0.25	2.07	0.96	1.06	4.04	0.19	1.94
8× 3	0.90	1.01	4.24	0.15	2.05	0.87	0.99	4.07	0.14	1.98
9× 3	0.84	0.85	3.79	0.10	1.66	0.82	0.80	3.60	0.25	1.59
11× 3	0.79	0.87	3.51	0.13	1.65	0.78	0.85	3.39	0.18	1.48
20× 3	0.74	0.77	2.46	0.10	1.32	0.70	0.76	2.70	0.10	1.38
35× 3	0.65	0.68	1.90	0.03	1.32	0.64	0.67	2.51	0.06	1.29

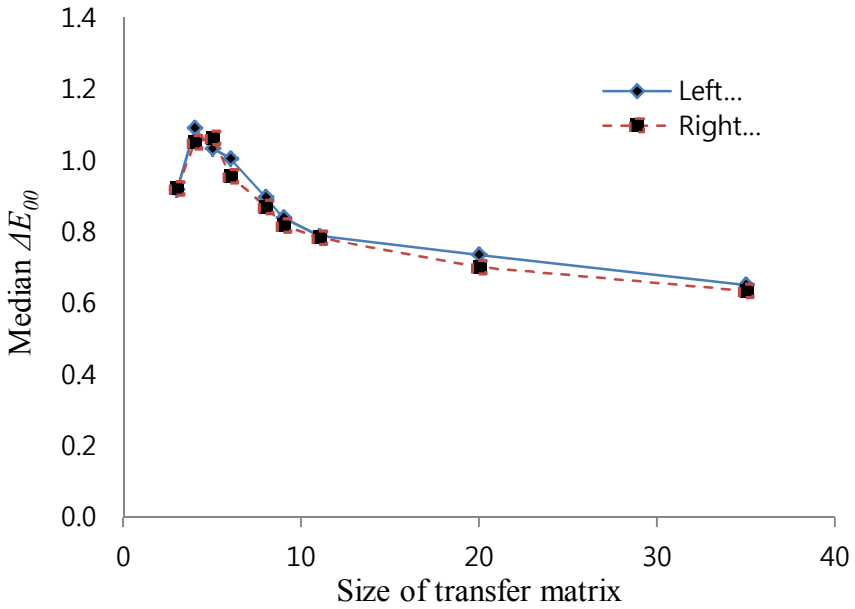

Figure 5-5 Effect of various terms used in the polynomial regression model

As shown in Table 5-4 and Figure 5-5, the colour difference ΔE_{00} between predicted and measured values tends to decrease as the size of matrices is increased. This indicates that the bigger matrices tend to produce the smallest error in the polynomial regression model.

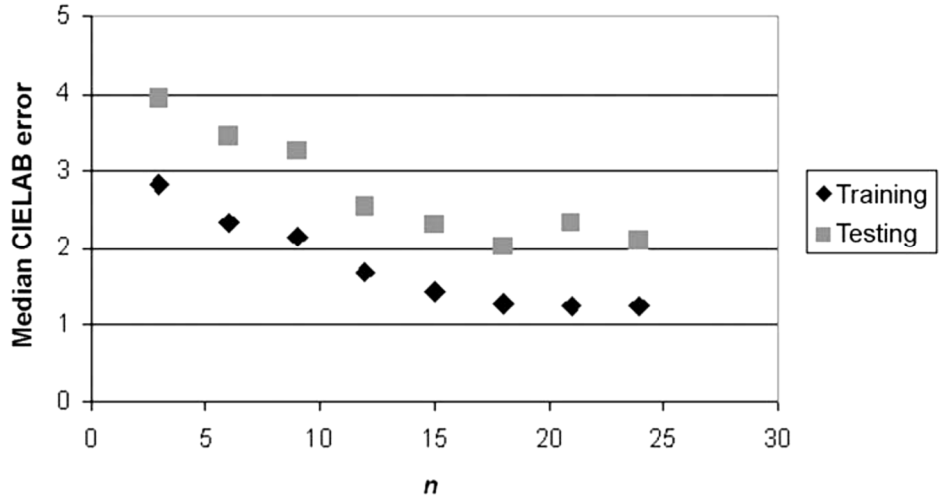

Figure 5-6 Effect of number of terms on training and testing performance (Cheung and Westland, 2001; Cheung, 2004)

As seen in Figure 5-6, it reported that the error of predicting testing data slightly increased after the number of 20, unlike the tendency for the training data (Cheung and Westland, 2001; Cheung, 2004). This phenomenon can be found in Kim's (2004) study. In other words, the testing error of the term of 20 is the smallest. In addition, the numeric improvement found here between 20 and 35 terms is not visually significant despite requiring more effort. Therefore, 20× 3 was selected as an optimisation matrix.

5.4. Illumination uniformity correction

Illumination uniformity correction was applied to reduce to the effect of intensity variation due to lighting. The intensity of the LED spot light used was not equally distributed and thus the large variation was found over the capturing field of metallic-coating panels. These variations in captured images are not attributed to the actual properties of the coating panels. Therefore, the effect of non-uniformity needs to be physically avoided or minimised as much as possible. To evaluate the non-uniformity of the coating images caused by the spot light, an experiment was carried out using a piece of metallic-grey coating panel. The sample was captured under the proposed illumination. The captured image was then evenly divided into 8 regions along the vertical and horizontal directions as seen in Figure 5-7.

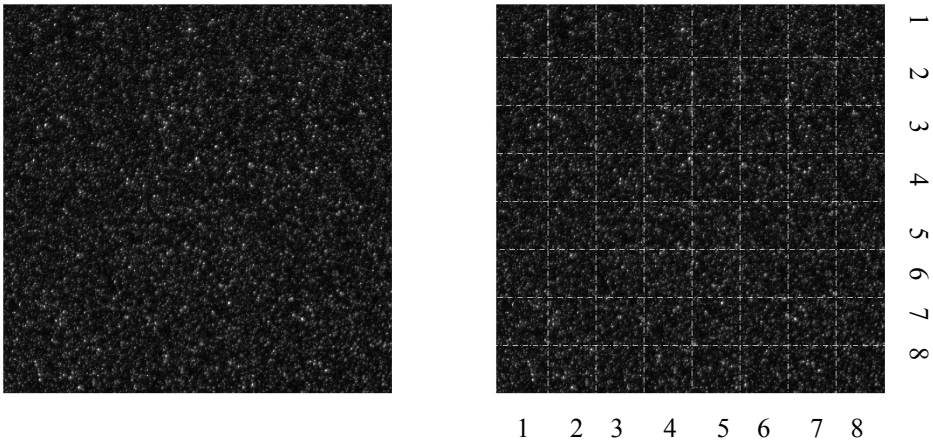

Figure 5-7 Metallic-coating image captured under the proposed illumination (left) divided into 8 equal-sized regions vertically and horizontally (right).

The mean intensity value *m* can be calculated for each region using:

$$\boldsymbol{m} = \frac{\mathbf{1}}{\boldsymbol{N}} \sum_{(\boldsymbol{x},\boldsymbol{y}) \in \boldsymbol{A}} \boldsymbol{f}(\boldsymbol{x},\boldsymbol{y}) \qquad \text{Equation 5-2}$$

where *f(x, y)* indicates the pixel intensity value at image coordinate *(x, y)*, *A* is the area boundary and *N* is the total number of pixels within *A*. It is obvious that the mean intensity values for the 8 areas should ideally be similar if the illumination is uniform.

Table 5-5 Mean intensity values and standard deviation (**σ**) for the 8 vertical and horizontal regions used in the uniformity test

	1	2	3	4	5	6	7	8	σ
vertical	8239	8885	9231	9387	9600	9433	9010	8672	451
Horizontal	11275	12256	13333	14345	15843	17083	18073	19667	2939

The results from this experiment are given in Table 5-5, where the standard deviation describes the variance within the vertical and horizontal 8 regions. It is evident that the standard deviation of mean intensity values from the horizontal regions is much higher than that from the vertical regions.

Illumination compensation was implemented to reduce the effect of non-uniform illumination.

$$Uniformity\_image = coating\_image \times \frac{\sigma}{x} \qquad \text{Equation 5-3}$$

where x is the value to be corrected and σ is the mean of image data. Each pixel in the image was multiplied by a new value (weight) which was calculated by Equation 5-3

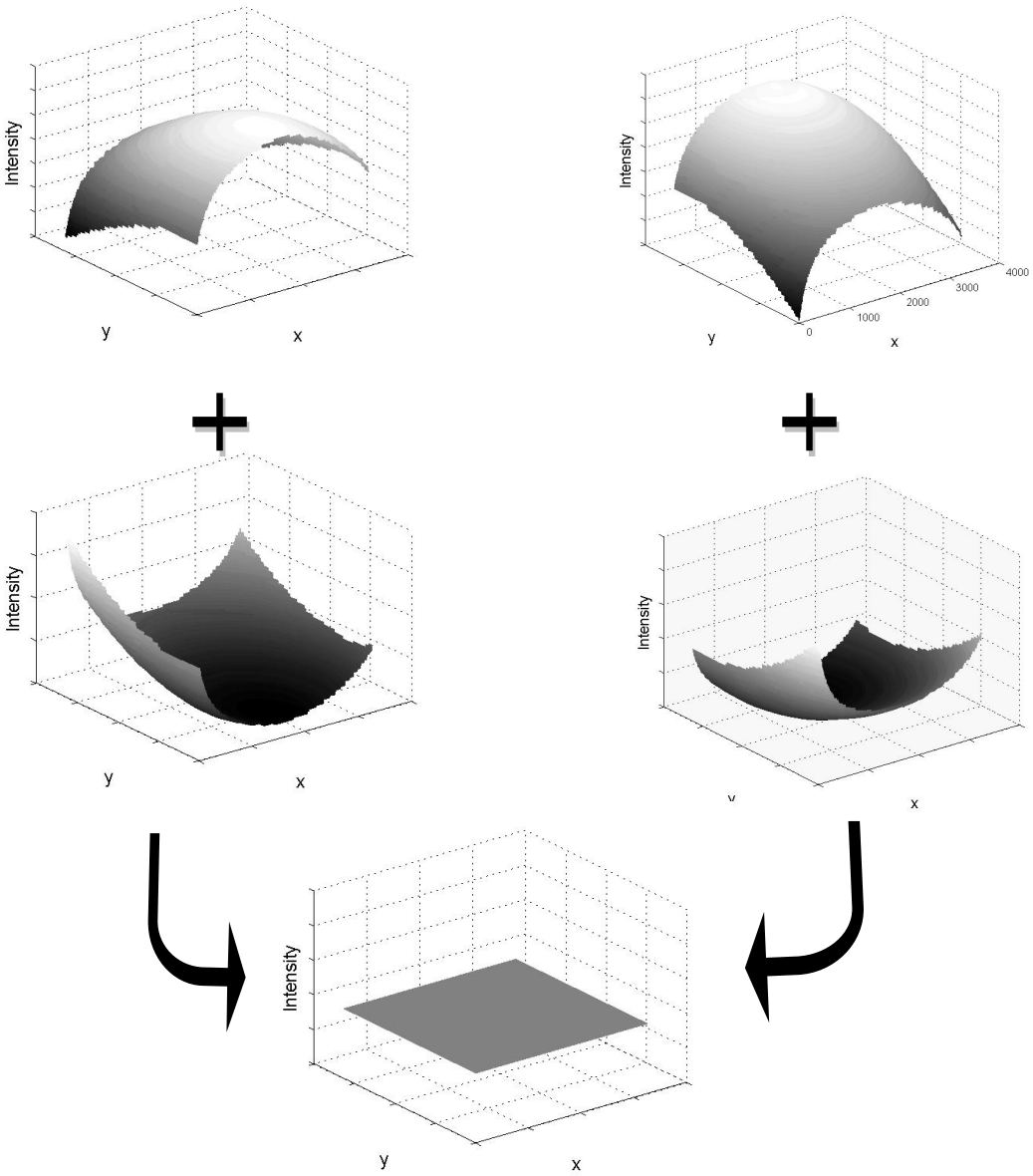

Figure 5-8 Illumination uniformity correction.

5.5. Normalisation

The techniques

Before applying normalisation, a top-hat transform (Gonzalez, 2004) was performed on the image in order to remove small scratches on metallic-coating panels. In practice, it is not easy for metallic-coating samples to be produced and stored without any scratches or chips. To reduce the external effect of those unwanted properties, top-hat transform was applied to the image. The top-hat transform of an image *f* is defined as

$$\boldsymbol{f_{top-hat} = f - (f \circ s)} \qquad \text{Equation 5-4}$$

In statistics, the z-score is often used to standardise data from different population to make them comparable (Lewis and Traill, 1999). The standardised z-score is calculated as:

$$Z = \frac{X - \mu}{\sigma} \qquad \text{Equation 5-5}$$

where *x* is the variable to be standardised, μ is the arithmetic mean and σ is standard deviation of the data set. Based on this concept, each pixel value in the image was standardised according to regional statistics. For this process, a $W \times W$ square window (where W was set to 100) was used which is sufficient to include bright spots of metallic coatings. The window convolved the image from left to right and from top to bottom before computing the local mean and the local standard deviation for each pixel. The standardised z-score was then calculated. At the end of this procedure, each pixel was examined $W \times W$ times in total, and the final score for each pixel was achieved by taking the average score value. Finally, a standardised image was reconstructed from the z-score of each pixel according to Equation 5-6.

$$f_{norm}(x,y) = \frac{1}{W^2} \sum_{s=-\frac{1}{2}W}^{\frac{1}{2}W} \sum_{t=-\frac{1}{2}W}^{\frac{1}{2}W} \frac{f(x,y) - \mu(x-s, y-t)}{\sigma(x-s, y-t)} \qquad \text{Equation 5-6}$$

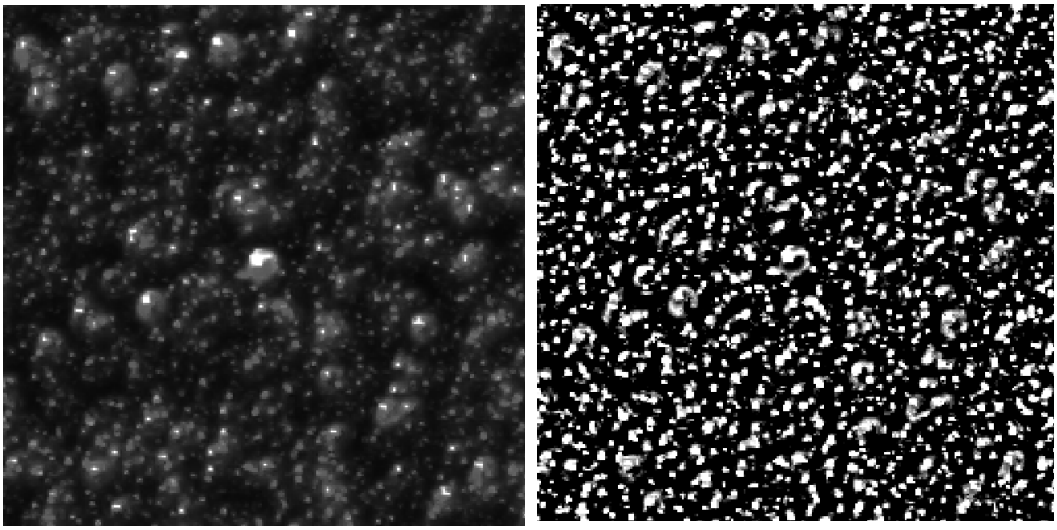

Figure 5-9 Before (left) and after (right) images of applying local z-score standardisation

The result of the local z-score standardisation procedure is presented in Figure 5-9. The effectiveness of the proposed procedure was evident from this resultant image, as the mottled background was removed while bright spots were preserved. Most importantly, bright spots were normalised so that they appear uniformly throughout the whole metallic coating surface rather than according to individual region.

5.6. Stereo image merger

The image-scalar operation was employed to the combination of two images, IM_1 and IM_2, having the same resolution. Instead of simple combining a scalar with each pixel, two pixels with the same coordinates in different images are used. This process can be described in Equation 5-7.

$$\boldsymbol{f = IM_1 \otimes IM_2} \qquad \text{Equation 5-7}$$

This way of combining two digital images is application specific. For example, when generating a blended version of two intensity images of identical resolution, Equation 5-8 represents the process in which *k* was determined according to the mixing proportion. k-

blending is a simple method of morphing and has often been used to dissolve between two scenes in the movie and television industry (Haskell and Netravali, 1997).

$$\boldsymbol{f = floor(k \times IM_1 + (1 - k) \times IM_2)} \qquad \text{Equation 5-8}$$

Figure 5-10 shows a comparison of two images; image (a) reconstructed by stereo image technic and image (b) captured by general image system with single camera. Two images represent not only the same metallic-coating panel but also exactly same area of the sample. Nevertheless, two images show different scene each other. Image (a) is similar to perception of human being with two eyes and gives more visual information than image (b). Intensity histogram of stereo image (a) testifies their difference in detail.

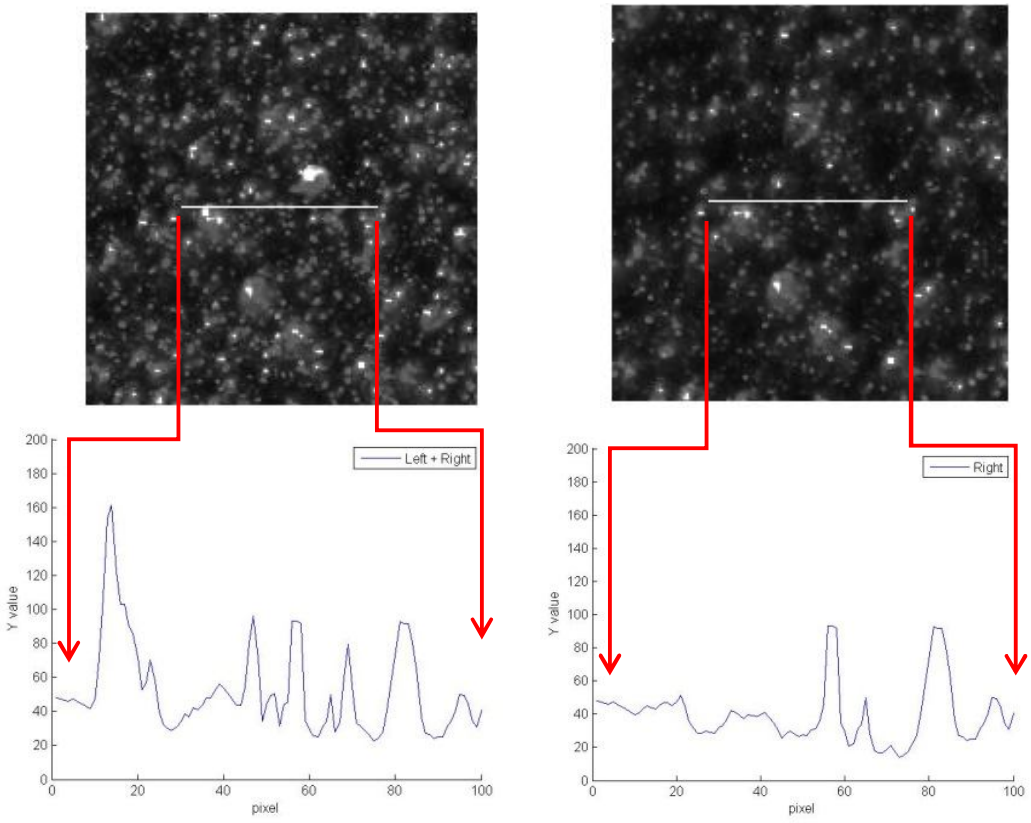

(a) (b)

Figure 5-10 The intensity comparison of two images captured from general acquisition and stereo capture system.

5.7. Summary

This Chapter 5 accomplished to design an optimum system to digitise complex reflection of visual texture of metallic sample surfaces. In order to achieve consistent and meaningful digital images close to real perception of human vison, stereo image acquisition system was proposed for image capture of the metallic-coating panels. This novel system is consisted of a digital camera and two light sources. For preparing image processing, digital camera characterisation, illumination uniformity correction, normalisation and stereo image merger were applied to images. The achievement of this Chapter was summarised below.

With regard to light sources, it is controversial that coloured light source such as yellowish is appropriate for visual and capturing experiment. To this, researchers have generally used some filter of light to reduce the effect of coloured light source. In this experiment, LED white spot light were used. Also, temporal stability of illumination was measured and considered in the experiment to reduce the effect of intensity variation of lighting.

A vital drawback is that the existing methods for capturing some image of metallic-coating surface were designed not to take into account stereoscopic vison which refers to the human ability to view with both eyes. In particular, the metallic-coating strongly depends on the viewing geometry. Therefore, each of eyes capture slightly different image from a different point of view even though they focus on a same metallic since two eyes are posited with distance, about 64 mm. It means that the concept of many image acquisition systems is different to that of real perception of human. In this study, novel image acquisition system was designed to mimic stereo human vision.

For stereoscopic vision, most studies have used two cameras which play role as two eyes. However those common methods using two cameras are not appropriate for this study dealing with small aluminum flakes because it is extremely challenging to do stereo matching (image registration). In the novel image acquisition system, one camera with particularly designed illumination setup reproduce stereo image of metallic-coating panel.

From this point of view, it can be said that HDR progress is similar to stereo matching in terms of the combine of two or three images. In the study dealing with coatings including aluminium flakes, physical diameter ranges between 5 and 50 μm, camera stability is vital to achieving a sharp image due to micro appearance of perceptual attributes of metallic-coating samples. There were not any mentions for camera stability on capturing in most studies. In this experiment, a camera remote shutter release was used as trigger to activate the camera's shutter remotely without touching the shutter release button.

The illumination setup is core of the novel image acquisition because it enables not only one camera paly role as two eyes of human vision but also two images register correctly. Two LED spot lights are located at different lateral positions and Each LED source function as each eye of human vision. Two scenes illuminated by two different lights are different due to illumination angle. The angle between a digital camera and light source was fixed as that of viewing geometry in visual assessment. In practice, two slightly different images for one sample were captured under two different lighting conditions: each image with single light on.

Some researchers have used the compressed format images captured form digital camera. However, in this capturing, a "raw" data which is uncompressed image format was obtained from the camera and converted to "tiff" file. It is indicate that the used images data were lossless in this experiment.

CHAPTER 6

FEATURE EXTRACTION

6.1. Introduction

In Chapter 5, some defects of captured images that are unwanted or irrelevant effects were removed in order to facilitate the subsequent feature extraction step. In this chapter, two main features of metallic-coating panels under this specific illumination, glint and coarseness, were extracted in order to able to sufficiently characterise the total appearance of coatings.

6.2. Glint feature extraction

In Chapter 5, observers carried out visual assessment to grade the glint of the metallic-coating samples according to glint definition, in which there was contrast between the bright spot and its surrounding. Based on the process for visual assessment, images were analysed and the pixels relevant to bright spots were identified as glint features. These were extracted as agglomerates of pixels and then calculated to sub-parameters such as the number of pixels, the sum of those pixel values, the number of particles, etc. Finally they were compared with the visual assessment data to find out what parameters relate to the perceptual attribute, glint, in human vision.

6.2.1. Glint feature extraction

Glint segmentation was attempted to extract meaningful features. This section aims to develop method which can adaptively segment glint from the reconstructed image at this stage. Glint segmentation is conduct in the spatial domain.

In section 5.5, normalisation was applied to all the metallic coating images. A side effect of the normalisation is that histogram of any fabric image is transformed to a single mode function. The shape of the histogram of an image usually provides important information about nature of the image (Umbaugh, 1998). The images of most natural scenes with similar backgrounds tend to a normal distribution (single mode) histogram. A

histogram with multiple modes indicates that multiple regions or objects in the image are in contrast with each other, and the modes tell us something about the general brightness of these regions. Since metallic coating panels usually have different regions with different backgrounds, they tend to have multiple mode histograms. Therefore, it can be concluded that the difference between a single-mode and a multiple-mode histogram presents the difference between solid coating and a metallic coating panel. From Equation 5-6 (section 5.5), the local z-score standardisation method was employed to each pixel in the captured image according to its variance around local regional mean value. The effect on the histogram of a metallic-coating image is likely to shift the multiple peaks together and convert it into a normal distribution, thus bringing different regions towards a similar brightness level. During the process, the bright points were still preserved in the histogram of the reconstructed metallic coating image.

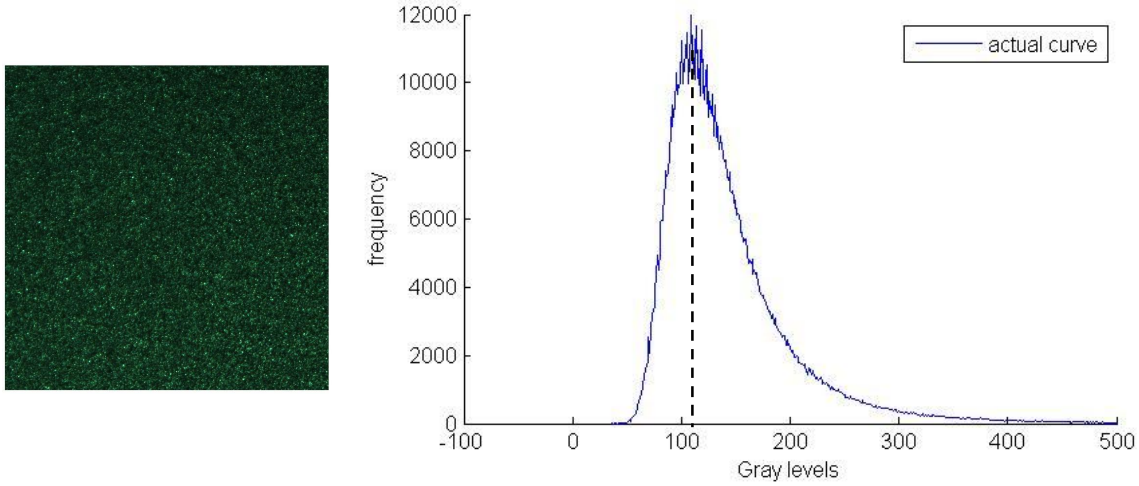

Figure 6-1 A reconstructed metallic coating image (left) and the corresponding histogram (right)

The single mode shaped histogram can be exploited to extract glint features from the base background. In Figure 6-1, a reconstructed metallic coating image is shown together with the corresponding probability density function of an image, denoting the histogram of the image. According to the assumption of normal distribution of the background, the probability density function of an image models by a Gaussian function expressed as

$$\boldsymbol{h(x) = Ae^{-\frac{(x-m)^2}{2\sigma^2}}} \qquad \text{Equation 6-1}$$

where A is the amplitude, σ is the standard deviation and x is the mean.

$$\boldsymbol{in\big(h(x)\big) = \left[\ln(A) - \frac{m^2}{2\sigma^2}\right] + \frac{m}{\sigma^2}x + \frac{-1}{2\sigma^2}x^2} \qquad \text{Equation 6-2}$$

This equation can be simplified as

$$\mathrm{f(x)} = c_1 + c_2 x + c_3 x^2$$

therefore, letting

$$c_1 = \ln(A) - \frac{m^2}{2\sigma^2} \qquad c_2 = \frac{m}{\sigma^2} \qquad c_3 = \frac{-1}{2\sigma^2}$$

Similarly,

$$\begin{bmatrix} \boldsymbol{f(x_0)} \\ \boldsymbol{f(x_1)} \\ \cdots \\ \boldsymbol{f(x_{n-1})} \end{bmatrix} = \begin{bmatrix} \boldsymbol{1} & \boldsymbol{x_0} & \boldsymbol{x_0^2} \\ \boldsymbol{1} & \boldsymbol{x_1} & \boldsymbol{x_1^2} \\ \cdots & \cdots & \cdots \\ \boldsymbol{1} & \boldsymbol{x_{n-1}} & \boldsymbol{x_{n-1}^2} \end{bmatrix} \begin{bmatrix} \boldsymbol{c_1} \\ \boldsymbol{c_2} \\ \boldsymbol{c_3} \end{bmatrix} \qquad \text{Equation 6-3}$$

$$\mathbf{F} = \boldsymbol{MC} \qquad \text{Equation 6-4}$$

$$\boldsymbol{M^T}\mathbf{F} = \boldsymbol{M^T MC}$$

$$(M^T M)^{-1} M^T \mathrm{F} = (M^T M)^{-1}(M^T M)C$$

$$\boldsymbol{C = (M^T M)^{-1} M^T}\mathbf{F} \qquad \text{Equation 6-5}$$

Thus, the three parameters can be recovered from C by

$$\mathbf{A} = \boldsymbol{e^{c_1 + \frac{m^2}{2\sigma^2}}} \qquad \mathbf{m} = \boldsymbol{\sigma^2 c_2} \qquad \boldsymbol{\sigma^2 = -\frac{1}{2c_3}} \qquad \text{Equation 6-6}$$

The three parameters were calculated from Equation 6-6. A Gaussian function generated using Equation 6-1 was used to simulate the background of the metallic-coating samples, where the black curve presents the fitted Gaussian function.

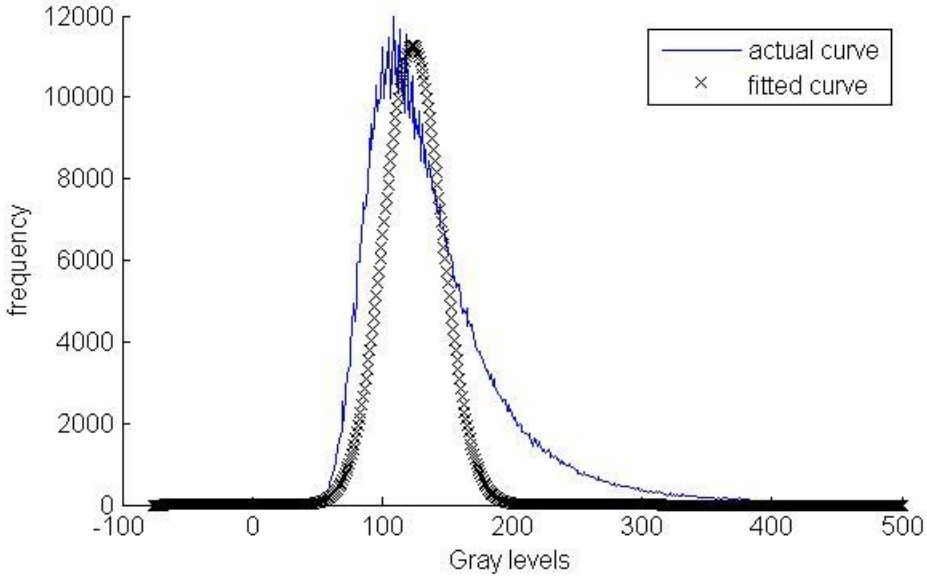

Figure 6-2 The fitted Gaussian function with original PDF

As seen in Figure 6-2, it is clear that the distribution could not be well fitted by the Gaussian curve due to the asymmetrical nature of the original probability density function (PDF). If the probability density function curve in Figure 6-1 is divided into two parts along its mode indicated by the vertical dashed line in the figure, it is immediately clear that the area covered by the right portion is bigger than the left portion. In fact, the bias can be predicted by noticing that values of pixels resulting from glint feature of metallic coating will most likely to be higher than the mode. This is because glint spots of metallic coating tend to be brighter than the background under the proposed illumination model in this study. In other words, the existence of glint feature constitutes the differential portion between the left and the right parts of the histogram and thus disturbs the symmetry. It is this fact that can be exploited to distinguish glint from their normal distributed background.

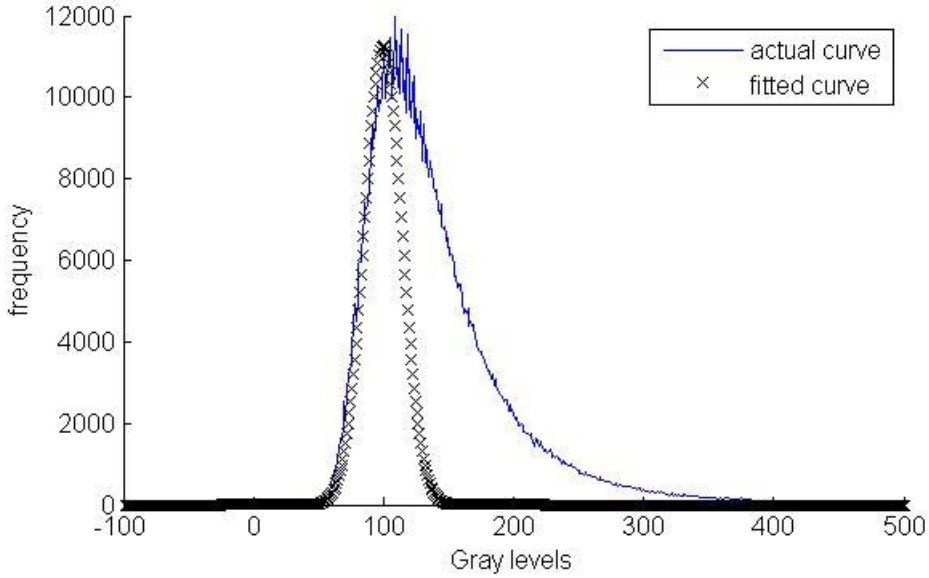

Figure 6-3 The fitted Gaussian function with left portion of the PDF

To improve the modelling, an alternative function was introduced as training data instead of the original PDF to generate the Gaussian curve. The function is defined as:

$$\mathbf{h(x)} = \begin{cases} \boldsymbol{h(x)} & \boldsymbol{x < m} \\ \boldsymbol{h(2m - x)} & \boldsymbol{x > m} \end{cases} \qquad \text{Equation 6-7}$$

where *h(x)* is the original probability density functions and *m* is its mode. Because some probability density functions tend to be jagged around their modes, the actual mode may prejudice the fitting result. In particular, the probability density function for high glint coating has the big jagged shape as shown in Figure 6-4. In practice, *m* is selected as the median value of a vector, which is composed of ten ray-level elements corresponding to the ten largest frequency values of the some probability density functions. This is equivalent to applying a median smooth filter on the curve at its peak section to exclude outliers from the training function in order to enhance modelling.

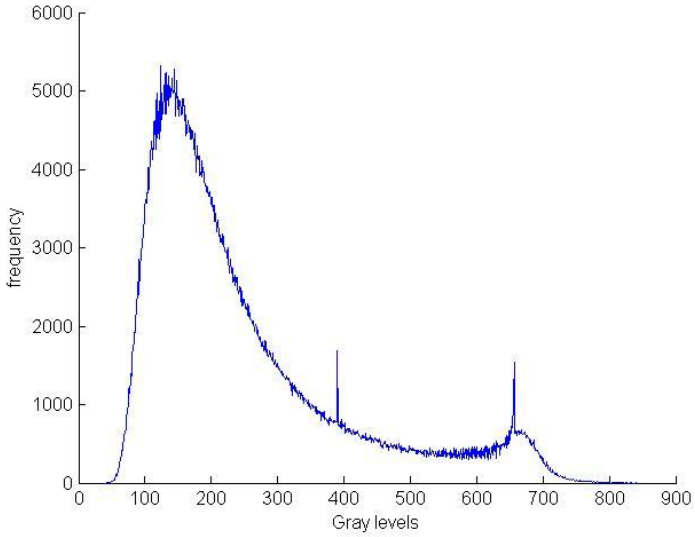

Figure 6-4 Probability density function for a high-glint coating

After going through the procedure above, a fitting curve was generated as shown in Figure 6-3. The fitting result considering the left portion of the PDF was vastly improved from the training function in Equation 5.6. The good fit testifies that the left portion of the PDF is connected to the normal distributed surrounding of the coating as pixels of the bright glint spot were not a portion of this side. Once the surrounding is modelled by a Gaussian function, the threshold value t was calculated to segment bright spots from the surroundings. The formula for this was:

$$\boldsymbol{t = m + k\sigma} \qquad \text{Equation 6-8}$$

where m and σ are the parameters of the Gaussian function computed in Equation 6-8, and the value k is a constant. The selection of k can be established by some properties of well-studied Gaussian distributions. For example, if the background was perfectly Gaussian distributed and we take $k=3$ in Equation 6-8, the expected misclassification rate of pixels of background (placed under the Gaussian curve beyond the threshold) as pixels of glint feature will be less than 0.14%. This is because, for a Gaussian distributed population, a span of width 3σ on either side of the mean will contain 99.73% of the total population (Lewis and Traill, 1999). On the basis of this assumption, we would have 99.87% confidence that pixels whose values are higher than t are related to glint features. As a matter of fact, the imposition of such a low error is reasonable enough to keep low the number of misclassified pixels of background. If the value of k is set to higher than 3, the

error of misclassification of background will clearly be lower, but also there will be higher possibility that too many pixels of glint feature would be misclassified as background. Therefore, *k=3* was chosen in the present study.

6.2.2. Statistical approaches

In section 6.2.1, the number of pixels corresponding to bright spots was separated from the background. This Section proposes various statistical approaches to extract glint features correlated with perceptual glint.

Equation 6-9 shows the calculation of the number of pixels that exceed a certain threshold *t. I(i, j)* is the luminance value of the image *I* at the pixel position *(i, j). P* is the mode value of the image *I* which was subtracted from every pixel in the image.

$$G1 = \boldsymbol{count}((\boldsymbol{I}(\boldsymbol{i},\boldsymbol{j}) - \boldsymbol{p}) \geq \boldsymbol{t}) \qquad \text{Equation 6-9}$$

Secondly, G2 was calculated as the sum of those pixel values that belonged to the bright spots.

$$G2 = \sum((\boldsymbol{I}(\boldsymbol{i},\boldsymbol{j}) - \boldsymbol{p}) \geq \boldsymbol{t}) \qquad \text{Equation 6-10}$$

The matrix *G3* counted the number of particles which consisted of one or more pixels that belonged to the bright spots. Particles were identified by labelling 8-connected components (Gonzalez *et al.*, 2004).

$$G3 = \mathbf{count}(\boldsymbol{particle}\ (\boldsymbol{I}(\boldsymbol{i},\boldsymbol{j}) - \boldsymbol{p}) \geq \boldsymbol{t}))) \qquad \text{Equation 6-11}$$

The metric G4 calculated the sum of mean value of each particle.

$$G4 = \sum \mathbf{mean}(\boldsymbol{particle}(\boldsymbol{I}(\boldsymbol{i},\boldsymbol{j}) - \boldsymbol{p}) \geq \boldsymbol{t}))) \qquad \text{Equation 6-12}$$

The metric *G5* computed the percentage of bright spots and background.

$$G5 = \frac{\boldsymbol{G1}}{\mathbf{count}(\boldsymbol{I}) - \boldsymbol{G1}} \qquad \text{Equation 6-13}$$

The metric *G6* computed the percentage of bright spots against the number of total pixel.

$$G6 = \frac{G1}{\text{count}(I)} \qquad G7 = \frac{G1}{p} \qquad G8 = \frac{G2}{p} \qquad G9 = \frac{G3}{p}$$

$$G10 = \frac{\boldsymbol{G4}}{\boldsymbol{p}} \qquad G11 = \frac{\boldsymbol{G5}}{\boldsymbol{p}} \qquad G12 = \frac{\boldsymbol{G6}}{\boldsymbol{p}} \qquad \text{Equation 6-14}$$

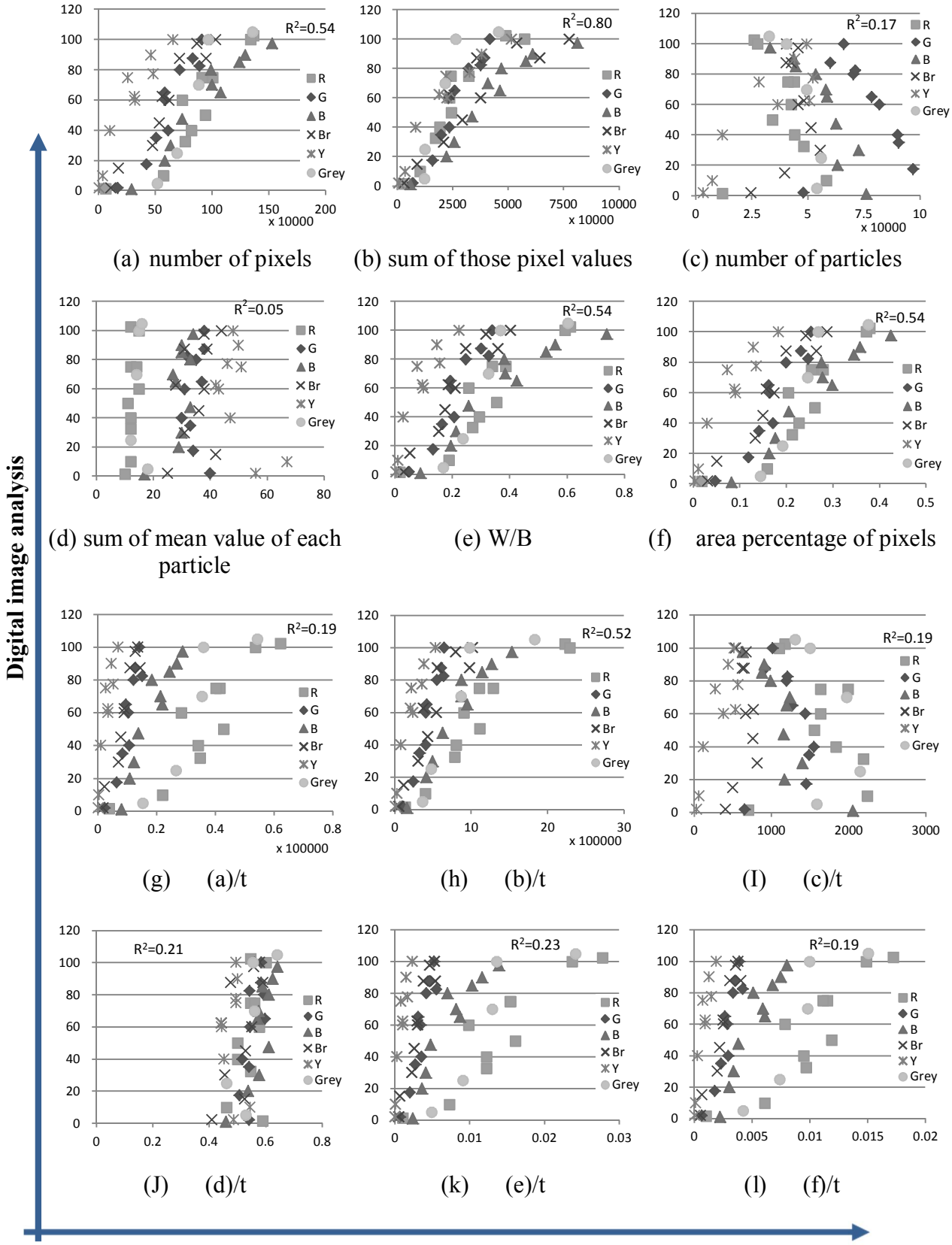

Figure 6-5 Observer grade VS digital image analysis

6.3. Coarseness feature extraction

Coarseness segmentation was attempted to extract meaningful features. This section aims to extract perceptual coarseness of the metallic coating panels. After preparing image processing in Chapter 5, the feature extraction was conducted using the following two steps:

1. Apply the discrete Fourier transform using the Fast Fourier Transform algorithm to reconstructed images (Gonzalez *et al.*, 2004). A set of octave band pass filters was applied to the images in the Fourier domain.
2. Compare these with the data from the visual assessment to find out what parameter relates to coarseness perception.

6.3.1. Octave band-passing filters

In computer vision, feature extraction aims to measure certain properties and features that are relevant to the task in hand (Duda *et al.*, 2001). In this section, the evenness of the intensity of metallic-coating panels was decomposed into regions of different sizes according to frequency in the power spectrum images.

Lindbergs S. *et al* (2002) examined the gloss level of printed papers by using octave band-pass filters to evaluate intensity using various octave bands. This image analysis method was employed to all 54 metallic-coating samples. The procedure can be explained in the following steps. It first transforms device dependent *RGB* data to device independent *CIE XYZ* data via a 3×20 matrix camera characterisation model. Two images, left and right image, were combined to reproduce stereoscopic vision as one image. A Discrete Fourier Transform was then applied to the *XYZ* images. An octave bandpass filter was then applied to the Fourier Spectra image, leaving the phase angle unchanged. In this step, the octave bandpass was automatically generated to separate the Fourier spectrum of each image in to 8 equal bands which are shown in Table 6-1. Finally, data analysis was carried out to achieve the "image variance value" for each band using the luminance data, *Y*. The assumption is that the larger image variance values of the luminance channel, the

higher the coarser of the sample. It means that the sample is perceived to be high coarseness with a larger variation in pixels. The image variance value can be calculated using Equation 6-15. This equation has the advantage of requiring only one pass through the image (Edelman, 1999).

Image variance = $\mathrm{Var}[f] = E[f^2] - E[f]]^2$

$$\left(\frac{1}{MN}\sum_{x=0}^{M-1}\sum_{y=0}^{N-1}\boldsymbol{f}(\boldsymbol{x},\boldsymbol{y})^2\right) - \left(\frac{1}{MN}\sum_{x=0}^{M-1}\sum_{y=0}^{N-1}\boldsymbol{f}(\boldsymbol{x},\boldsymbol{y})\right)^2 \qquad \text{Equation 6-15}$$

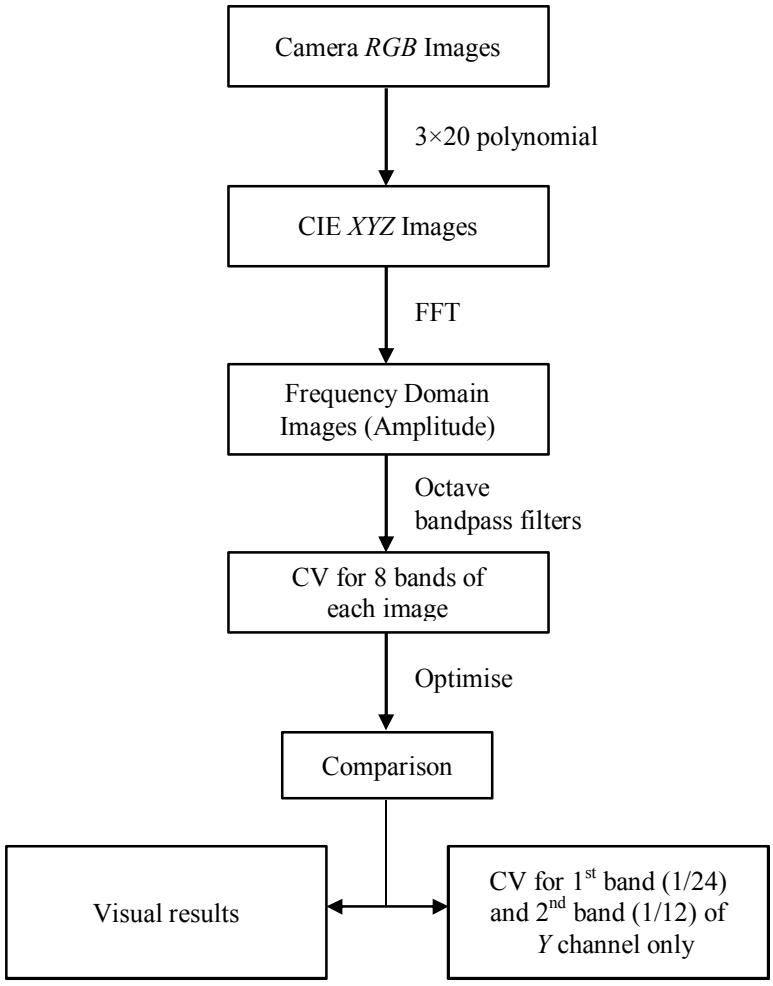

Figure 6-6 Computational procedure for octave bandpass filters

The evenness of the intensity of metallic-coating panels was decomposed into regions of different sizes according to frequency in the power spectrum images.

Lindbergs, *et al.* (2002) examined the gloss level of printed papers by using octave bandpass filters to evaluate the intensity using various size of octave bands (Table 6.1).

Table 6-1 Optimise band size of band

Band	1 & 2						3	4	5	6	7	8
Ratio of square of pixels	1/24	2/24	3/24	4/24	5/24	6/24	9/24	12/24	15/24	18/24	21/24	24/24

6.3.2. Correlation between octave bandpass filter results and visual assessment results

The best relationship with the observer results was for Band 1 and Band 2, with sizes 1/24 and 1/12 as seen in Figure 6-6. Each band was examined in terms of all samples, red, green, blue, brown, yellow and grey colour sample groups as shown in Table 6-2. In these results, the best correlation depends on band size and the worst samples were red.

Table 6-2 Results of optimising the size of bands 1 and 2

	1/24	1/12	1/18	1/6	5/24	1/4
all samples	0.69	0.79	0.42	0.27	0.24	0.23
Red	0.45	0.58	0.13	0.01	0.00	0.00
Green	0.50	0.84	0.69	0.35	0.10	0.24
Blue	0.56	0.94	0.74	0.03	0.16	0.43
Brown	0.80	0.86	0.43	0.04	0.04	0.07
Yellow	0.88	0.70	0.53	0.83	0.31	0.04
Grey	0.97	0.84	0.00	0.40	0.83	0.57

6.4. Conclusions and discussions

In Chapter 6, two major perceptual features of metallic-coating panels were characterised. The computational models were developed to predict two perceptual attributes, glint and coarseness. Two models for two perceptual properties were evaluated by comparing its output with the scaled value of the glint and coarseness from visual assessment respectively. The performance of two models was evaluated in comparison with previous study, Kitaguchi's results.

The best performance of the model was the sum of those pixel values, G2, in which the R^2 value of 0.80 and the RMS value of 0.144 are as shown in Figure 6-7.

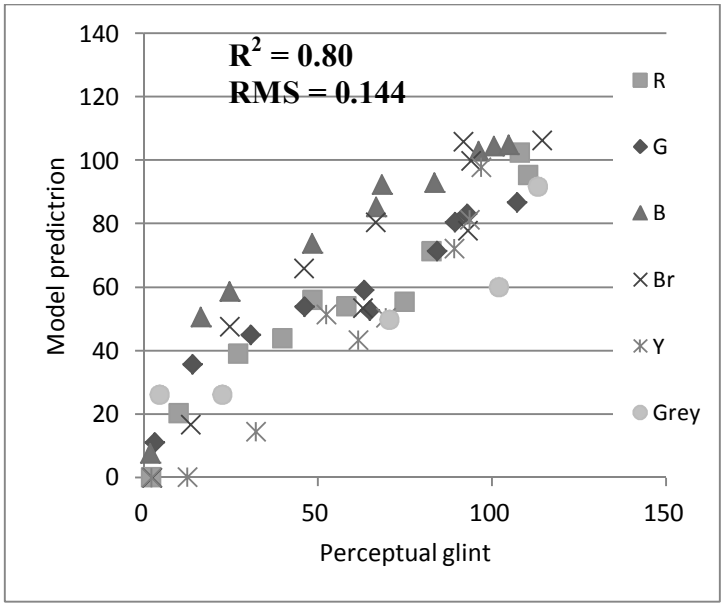

Figure 6-7 The model predictions against the perceptual glint

The results present slightly less accuracy in comparison with the best performance of Kitaguchi which the R^2 value of 0.85 and the RMS value of 0.116 as shown in Figure 6-8.

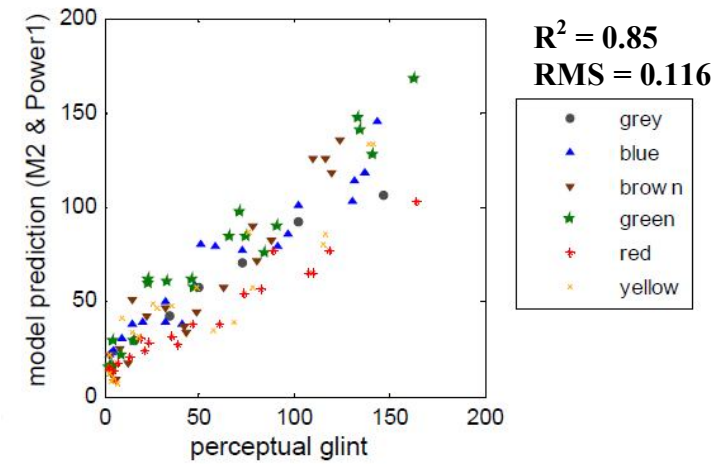

Figure 6-8 The model predictions against the perceptual glint (Kitaguch, 2008)

However, there are significant differences between both researches in terms of experiment condition which is the number of sample. A set of 106 metallic-coating panels were used in Kitaguchi's experiment, while half of the number, 54, were utilised as a sample in this research. In other words, Kitaguchi's method provides twice work to get the coefficient of determination, 0.85, whereas this proposed method do half effort to get 0.80 which is slightly lower, but similar with Kitaguchi's result. That means that the new method performs bigger impact of characterising perceptual glint of metallic-coating panels. Consequently, the proposed image capture system and model performance are considered to be more correct.

With regards to the model performance, the each colour set was examined in detail. Figure 6-8 shows that the model predictions against the perceptual glint for each coloured group. The correlation of determination, R^2, was 0.94, 0.93, 0.89, 0.88, 0.94 and 0.86 for the red, green, blue, brown, yellow and grey. Comparing with Kitaguchi's result in Figure 6-9, they are slightly low or similar to the values of 0.96, 0.94, 0.93, 0.93 0.85 and 0.97 which are same order. Dashed lines in each graph represent linear line regression lines between the model predictions and the scale values of all samples. Solid lines are linear regression lines of each coloured set. The difference between dashed and solid lines manifests the dispersion of the tendency of each coloured group. In accordance with the dispersions of each colours group, the degrees are quite small differences as shown in both Figure 6-8 and 6-9. That is, it can be said that the performance of the model was influenced by the colour of samples.

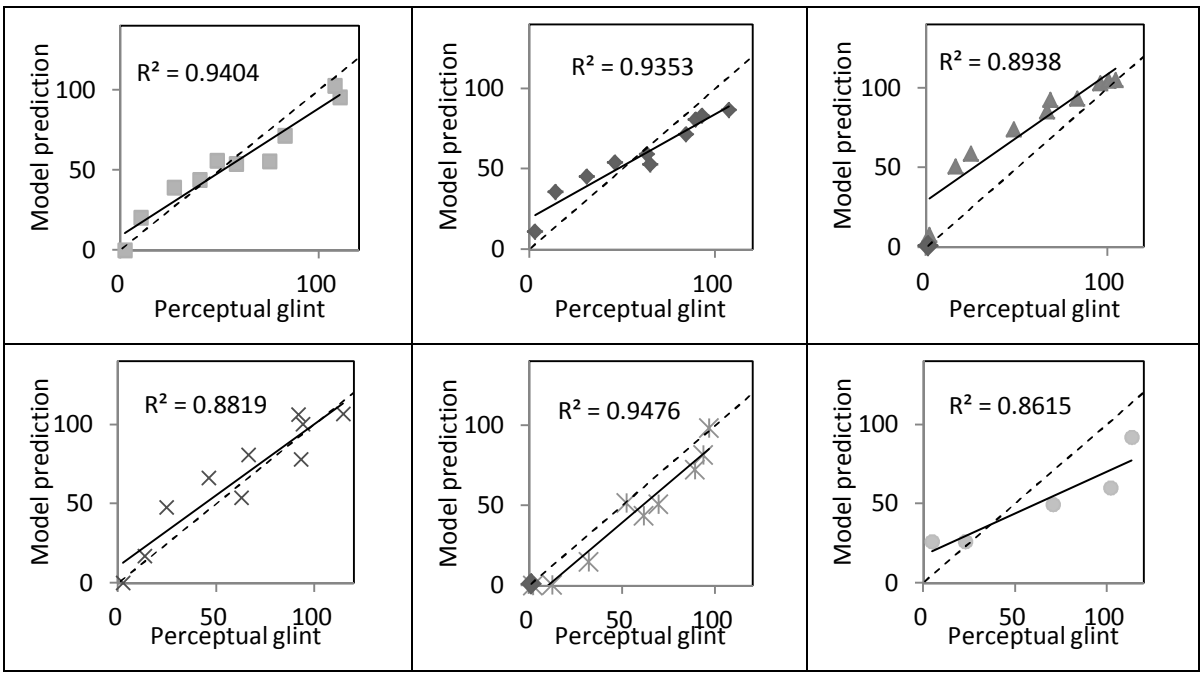

Figure 6-8 The model predictions against the perceptual glint for each coloured group

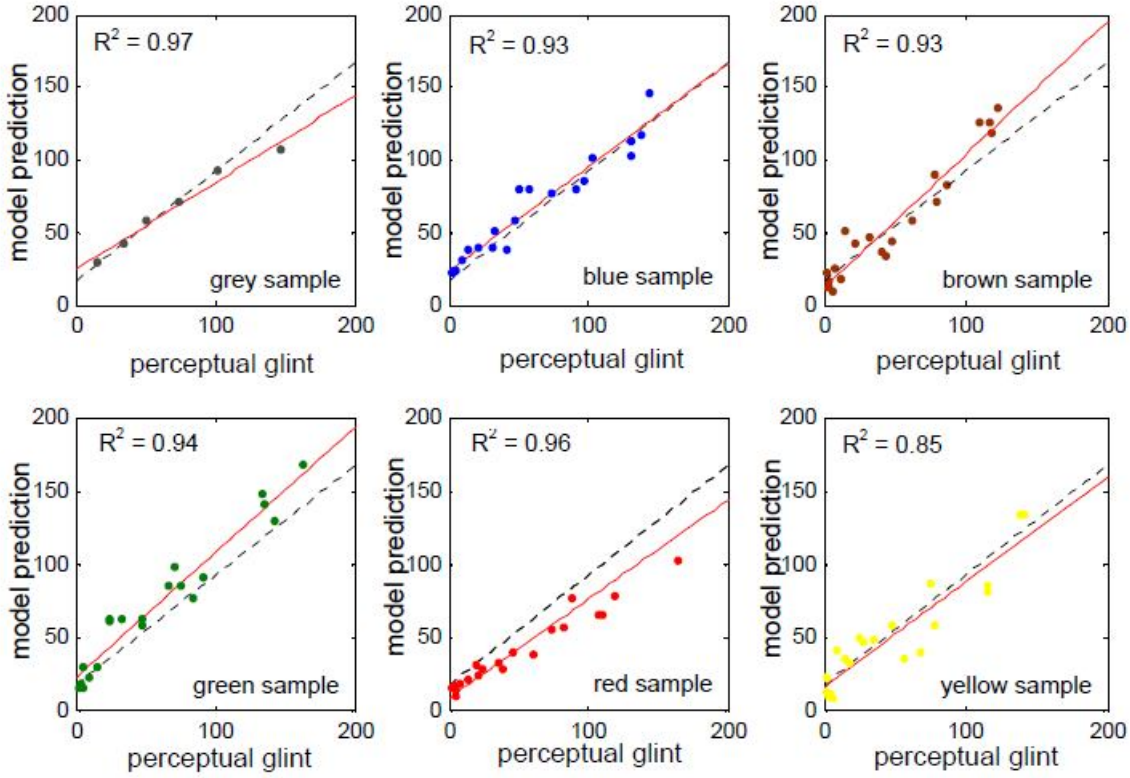

Figure 6-8 The model predictions against the perceptual glint for each coloured group (Kitaguch, 2008)

CHAPTER 7

CONCLUSION AND DISCUSSION

7.1. Conclusion and discussion

This research has developed to model the texture appearance of metallic- coating based on Kitaguchi (2008) study. We found out critical drawbacks of her as well as related researches to hers and provided the resolution of following problems with each chapter of this study. The study takes mainly five stages to accomplish the task. Visual assessment is basic for obtaining the standard data of the real human perception. Secondly, an image acquisition system is responsible for converting physical fabric samples into digital data. At preprocessing stage, some unwanted imaging defect caused form illumination non-uniformity is removed by image processing methods. Feature extraction means to modify the metallic coating image and to separate the perceptual features of coating surface and background of it. Finally, these features were compared with the visual assessment data to find out what parameters relate to the perceptual attribute of human vision. The stages were presented form Chapter 3 to 6 in this thesis.

In Chapter 3, this study investigated which appearance properties of gonio-apparent materials are influenced by stereoscopic and monocular vision using a psychophysical approach. With texture, glint typically has big differences between the results from stereoscopic and monocular vision for the same sample. It means that it is easier for observers to judge glint and this property can lead big different perception between two viewing modes. Therefore, it can be concluded that glint and texture are the best type of sample for verification of the difference between two modes of viewing.

- In psychophysical experiments, most importantly, visual acuity of observers makes a big influence to the result of visual assessment. Most researches have tested the normal vision of observers but haven't taken into account of the acuity vision condition. In the visual assessment, observers performed not only normal colour vision test but also visual acuity test by using a near visual acuity test chart before the assessment.

Chapter 4 was to study the interaction between three parameters affecting the total appearance of metallic-coating surfaces; glint, coarseness, and brightness under specific

viewing condition, in which 'glint' is represented as dominant texture property. Most of the studies have focus on one dominant perceptual attribute of metallic-coating panel under corresponding illumination geometry. It is means that they ignored a visually-complex nature of coatings which may have a various properties of perceptual attributes. This study investigated the interaction between three parameters affecting the total appearance of metallic-coating surfaces; glint, coarseness, and brightness under specific viewing condition. It is testified that brightness is not one of visual texture properties of metallic coatings under specific viewing condition.

- Visual fatigue is the negative effect caused by intensive use of the eyes in psychophysical experiment. Observers having this symptom perform the degradation of vision. This reason is directly related to the experiment time which depends on the number of sample. In this main experiment, 54 metallic coating of Kitaguchi samples were selected as optimum sampling and performance of observers was limited to 45 in visual assessment for total appearance (Chapter 4). In experiment for gonio-apparent surface, observer had a break for 5minutes to avoid fatigue (Chapter 3).

In Chapter 5, the hardware is introduced as the image acquisition system. A stereo illumination setup is proposed for the real image capture of the metallic-coating panels. This novel configuration was applied to outperform the conventional illumination systems in several ways. The stereo image acquisition system is comprised of a digital camera and two light sources. For preparing image processing, digital camera characterisation, illumination uniformity correction, normalisation and stereo image merger were applied to images.

- It is controversial that coloured light source such as yellowish is appropriate for visual and capturing experiment. To this, researchers have generally used some filter of light to reduce the effect of coloured light source. In this experiment, LED white spot light were used. Also, temporal stability of illumination was measured and considered in the experiment to reduce the effect of intensity variation of lighting.

- A vital drawback is that the existing methods for capturing some image of metallic-coating surface were designed not to take into account stereoscopic vison which refers to the human ability to view with both eyes. In particular, the metallic-coating strongly depends on the viewing geometry. Therefore, each of eyes capture slightly different image from a different point of view even though they focus on a same metallic since two eyes are posited with distance, about 64 mm. It means that the concept of many image acquisition systems is different to that of real perception of human. In this study, novel image acquisition system was designed to mimic stereo human vision.

- For stereoscopic vision, most studies have used two cameras which play role as two eyes. However those common methods using two cameras are not appropriate for this study dealing with small aluminum flakes because it is extremely challenging to do stereo matching (image registration). In the novel image acquisition system, one camera with particularly designed illumination setup reproduce stereo image of metallic-coating panel.

- From this point of view, it can be said that HDR progress is similar to stereo matching in terms of the combine of two or three images. In the study dealing with coatings including aluminium flakes, physical diameter ranges between 5 and 50 μm, camera stability is vital to achieving a sharp image due to micro appearance of perceptual attributes of metallic-coating samples. There were not any mentions for camera stability on capturing in most studies. In this experiment, a camera remote shutter release was used as trigger to activate the camera's shutter remotely without touching the shutter release button.

- The illumination setup is core of the novel image acquisition because it enables not only one camera paly role as two eyes of human vision but also two images register correctly. Two LED spot lights are located at different lateral positions and Each LED source function as each eye of human vision. Two scenes illuminated by two different lights are different due to illumination angle. The angle between a digital camera and light source was fixed as that of viewing

geometry in visual assessment. In practice, two slightly different images for one sample were captured under two different lighting conditions: each image with single light on.

- Some researchers have used the compressed format images captured form digital camera. However, in this capturing, a “raw” data which is uncompressed image format was obtained from the camera and converted to “tiff” file. It is indicate that the used images data were lossless in this experiment.

In the Chapter 6, glint and coarseness, were extracted in order to able to sufficiently characterise the total appearance of coatings.

- The segmentation method base on Gaussian fitting theory could be greatly developed by considering only half portion of the PDF. Glint feature were well identified.

- With regard to coarseness, the overall agreement between digital image and observer data was lower than for the glint feature; however it is similar to the reliability of the visual assessment results in which repeatability and accuracy of coarseness was lower than these of glint.

7.2. Future works

- This experiment was completed without HDR image process. However, it was empirical determination of optimal exposure. For reliability of the image process, it is need to find out what is optimal exposure for all metallic coating.

- It is need to evaluate the performance of glint.

REFERENCES

Akzo-Nobel (2004). Akzo-Nobel Internal Report.

Akzo-Nobel (2004-2006). Private Communication.

Allison, R., Wilcox, L. &Elder, J. (n.d.).Depth of Field in 3D Stereoscopic Images. Centre for Vision Research, York University.

Alspach, J. &Rodrigues, A. B. J. (2011). Measurement and Specification of Gonioapprarent Color and Appearance. du Pont de Numours and Company.

ASTM (2001). ASTM E284-07: Standard terminology of appearance. In *Annual book of ASTM Standards : Textiles 07-01*.

Bal, C., Jain, A. K. &Nguyen, T. Q. (2011). Detection and removal of binocular luster in compressed 3D images. In *2011 IEEE International Conference on Acoustics, Speech and Signal Processing (ICASSP)*, 1345-1348 Prague, Czech Republic: IEEE.

Bartleson, C. J. (1960). Memory colors of Familiar Objects. *Journal of Optical Society of America* 50: 73-77.

Bartleson, C. J. &Breneman, E. J. (1967). Brightness perception in complex fields. *Journal of Optical Society of America* 57: 953-957.

Cheung, T. &Westland, S. (2001). Color camera characterization using artificial neural networks. In *Proceedings of IS&T/SID 10th Colour imaging conference*, 117-120 Scottsdale, Arizona.

Cheung, T. L. V. (2004). Approaches to colour camera characterization. *PhD thesis*: University of Leeds.

CIE International Lighting Vocabulary (1987). *CIE International Lighting Vocabulary.*

Cooke, W. D. (1985). Pilling attribution and fatigue. *Textile Research Journal* 55(7): 409-414.

Dana, K. J., van Ginneken, B., Nayar, S. K. &Koenderink, J. J. (1999). Reflectance and texture of real-world surfaces. *ACM Transactions on Graphics (TOG)* 18(1): 1-34.

Dartnall, H., Bowmaker, J. &Mollon, J. (1983). *Human Visual Pigments.*

Department of Psychology University of Calgary (2005). Brightness, lightness, darkness & contrast: dark adaptaion. *http://pip.ucalgary.ca/psyc-369/mod3-light-and-colour/unit3.1-brightness-lightness-darkness-and-contrast/Dark-Adaptation.html.*

Duda, R. O., Hart, P. E., Stork, D. G., Duda, R. O. P. c. &scene, a. (2001). *Pattern classification.* New York ; Chichester: Wiley.

Durikovic, R. (2003). Simulation of sparkling and depth effect in paints. In *Proceedings of the 19th ACM spring conference on computer graphics-SCCG2003*, 193-198 Budmerice, Slovakia.

Durikovic, R. &Kolchin, K. (2001). Physically-based model of photographic effects for night and day scenes. *Journal of Three Dimensional Images* 15(4): 119-124.

Durikovic, R., Kolchin, K. &Ershov, S. (2002). Rendering of Japanese artcraft. In *Eurographics 2002* Saarbrücken, Germany: European Association for Computer Graphics.

E284, A. (2004). Standard terminology of appearance. American society for testing and materials.

Edelman, S. (1999). *Representation and recognition in vision.* Cambridge, Mass. ; London: MIT Press.

Ershov, S., Kolchin, K. &Myszkowski, K. (2001). Rendering Pearlescent Appearance Based On Paint-Composition Modelling. In *Computer Graphics Forum*, Vol. 20, 227-238: Blackwell Publishers Ltd.

Fairchild, M. D. (1999). A Victory for Equivalent Background – On average. *Proceedings of the 7th IS&T/SID Color Imaging Conference*: 87-92.

Fairchild, M. D. (2005). *Colour Appearance Models.* Chichester: John Wiley & Sons.

Ferwerda, J. A., Pellacini, F. &Greenberg, D. P. (2001). A Psychophysically-based model of surface gloss perception. In *Photonics West 2001-Electronic Imaging*, 291-301 San Jose, CA, USA: International Society for Optics and Photonics.

Fleming, R. W., Dror, R. O. &Adelson, E. H. (2003). Real-world illumination and the perception of surface reflectance properties. *Journal of Vision* 3(5): 347-368.

Gonzalez, R. C. (2002). *Digital image processing.* Prentice Hall.

Gonzalez, R. C., Woods, R. E. &Eddins, S. L. (2004). *Digital Image processing using MATLAB.* Upper Saddle River, NJ ; London: Pearson/Prentice Hall.

Haskell, B. G. &Netravali, A. N. (1997). *Digital pictures : representation, compression, and standards.* New York ; London: Plenum Press.

He, X. D., Torrance, K. E., Sillion, F. X. &Greenberg, D. P. (1991). A comprehensive physical model for light reflection. *ACM SIGGRAPH Computer Graphics* 25(4): 175-186.

Helson, H. (1934). Some factors and implications of color constancy. *Journal of Optical Society of America* 33: 555-567.

Holliman, N. (2005). 3D Display Systems*. in handbook of optoelectronics.* University Durham: Nick Holliman.

Hunt, R. W. G. (1952). Light and dark adaptation and the reception of colour. *Journal of Optical Society of America* 42: 190-199.

Hunt, R. W. G. (1998). Measuring Colour*. Fountanin press*: Kingston-upon-Thames.

Hunter, R. S. &Harold, R. W. (1987). *The Measurement of Appearance.* John Wiley & Sons, Inc.

Ignell, S., Kleist, U. &Rigdahl, M. (2009). On the relations between color, gloss, and surface texture in injection-molded plastics. *Color Research & Application* 34(4): 291-298.

Jameson, D. &Hurvich, L. M. (1961). Opponent chromatic induction: Experimental evaluation and theoretical Account. *Journal of Optical Society of America* 2: 135-154.

Judd, D. (1940). Hue, saturation, and lightness of surface colours with chromatic. *Journal of Optical Society of America B* 30: 2-32.

Kaiser, P. K. a. B., R.M (1996). Human color Vision. *Optical Society of America*.

Kim, Y. (2004). Characterisation of LCD colour monitors using a digital camera. *MSc thesis*;University of Derby.

Kirchner, E., Nko, L., Haas, K. d. &Rosler, M. (2006). Coarsencess and glints. *European Coatings Journal* (11): 46.

Kirchner, E. &Ravi, J. (2012). Predicting and measuring the perceived texture of car paints. In *Predicting Perceptions: The 3rd International Conference on Appearance*, 25 Edinburgh, UK.

Kirchner, E., van den Kieboom, G.-J. &Super, R. (2008). Accurate measurement of sparkle for effect coatings. In *AIC 2008 Interim Meeting of the International Colour Association, Colour-Effects and Affects*Stockholm, Sweden.

Kirchner, E., van den Kieboom, G. J., Njo, L., Super, R. &Cottenbos, R. (2007). Observation of visual Texture of Metallic and Pearlescent Materials. *Color Research and Application* 32(4): 256-266

Kitaguchi, S., Westland, S., Luo, R. M., Kirchner, E. J. J. &van den Kieboom, G.-J. (2008). Application of HDR colour imaging to modeling of glints in metallic coatings. In *AIC 2008 Interim Meeting of the International Colour Association, Colour-Effects and Affects*, 3 Stockholm, Sweden.

Kitaguchi, S. (2008). Modelling texture appearance of gonioapparent objects. *PhD thesis*; University of Leeds.

Land, E. H. (1977). The Retinex Theory of Color Vision. *Scientific American* 237(6): 108-129.

Land, E. H. (1986). Recent Advances in Retinex Theory. *Vision Research* 26(1): 7-21.

Lewis, J. P. &Traill, A. (1999). Statistics explained*. Harlow* : Addison-Wesley.

Li, C. J., Luo, M. R. &Hunt, R. W. G. (2002a). CMC 2000 chromatic adaptation transform: CMCCAT2000. *Colour Research Application* 27(1): 49-58.

Li, C. J., Luo, M. R., Hunt, R. W. G., Moroney, N., Fairchild, M. D. &Newman, T. (2002b). The performance of CIECAM02. In *IS&T/SID 11th Color Imaging Conference*, 28-32 Scottsdale, Arizona, USA.

Li, C. J., R., L. M. &Cui, G. H. (2003). Colour-difference evaluation using colour appearance models. In *IS&T/SID 11th Color Imaging Conference*, 127 Scottsdale, Arizona, USA.

Li, X., Ji, W., Li, C. J., Cui, G. H. &Luo, M. R. (2005). Further comparison study of the surface colour measurement data correlation. In *AIC 10th Congress of the International Colour Association*, 725-728 Granada, Spain.

Lindberg, S., Blend, M. &Johansson, P. (2002). Effect of sample orientation on perceived quality of print gloss. In *The 11th International printing and graphic arts conference*, 1-8.

Lindstrand, M. (2002). *Gloss: Measurement, Characterization and Visualization-in the Light of Visual Evaluation.* Sweden: Department of Science and Technology, Linköpings Universitet.

Lipton, L. (1997). StereoGraphic developer's handbook*. Stereographics coporation.*

Lozano, R. D. (2004). Appearance in paints: Gloss, spatial filtering and definition of image (DOI). In *AIC 2008 Interim Meeting of the International Colour Association, Color and Paints*Porto Alegre, Brazil.

Luo, M. R. (2002). The CIE 1997 colour appearance model: CIECAM97s. In *Colour Engineering*, 79-104 (Ed P. J. a. M. Green, L. W.). Chichester, UK: Wiley.

Luo, M. R., Clarke, A. A., Rhodes, P. A., Schappo, A., Scrivener, S. A. R. &Tait, C. J. (1991). Quantifying Colour Appearance. Part I. LUTCHI Colour Appearance Data. *Color Research and Application* 16: 166-180.

Luo, M. R., Cui, G. H. &Li, C. J. (2006). Uniform colour spaces based on CIECAM02 Colour Appearance Model. *Color Research and Application* 31: 320.

Luo, M. R. &Hunt, R. W. G. (1998). The Structure of the CIE1997 Colour Appearance Model (CIECAM97s). *Color Research and Application* 23(3): 138-146.

Müller, G., Meseth, J., Sattler, M., Sarlette, R. &Klein, R. (2004). Acquisition, synthesis, and rendering of bidirectional texture functions. In *Eurographics 2004*, 69-94 Grenoble, France: European Association for Computer Graphics.

Müller, G., Meseth, J., Sattler, M., Sarlette, R. &Klein, R. (2005). Acquisition, synthesis, and rendering of bidirectional texture functions. *Computer Graphics Forum* 24(1): 83-109.

Marcus, R. T. (2007). ASTM Standards on Color and Appearance. Sun Chemical Corporation.

McCamy, C. S. (1998). Observation and Measurement of the Appearance of Metallic Materials. Part II. Micro Appearance. *Color Research and Application* 23(6): 362-373.

Nadal, M. E. &Early, E. A. (2004). Color measurements for pearlescent coatings. *Color Research & Application* 29(1): 38-42.

Phillips, J. B., Ferwerda, J. A. &Luka, S. (2009). Effects of image dynamic range on apparent surface gloss. In *The 17th Color Imaging Conference*, Vol. 2009, 193-197 New Mexico: Society for Imaging Science and Technology.

Pointer, M. (2003). Measuring visual appearance - A Framework for the future. In *National physical laboratory report COAM*Teddington, Mdlx, UK.

Riddle, J. (1992). SEMATECH Provisional Test Method for Visual Characterization of Surface Roughness for Plastic Surfaces of UPW Distribution System. Austin, TX, USA: SEMATECH Technology Transfer.

Roy S, B. (2000). *Principles of Color Technology.* New York: John Wiley and Sons Inc.

Schanda, J. (2007) CIE Colorimetry, in Colorimetry: Understanding the CIE System (Schanda, J.Ed.) John Wiley & Sons, Chichester.

Simonot, L. &Elias, M. (2003). Color change due to surface state modification. *Color Research & Application* 28(1): 45-49.

Simonot, L., Hébert, M. &Dupraz, D. (2011). Goniocolorimetry: from measurement to representation in the CIELAB color space. *Color Research & Application* 36(3): 169-178.

Sivakumar, V. R. &Pillay, K. P. R. (1981). Study of pilling on polyester/cotton blended fabrics. *Indian Journal of Textile Research* 6: 22-27.

Sprouse, J. (2008). Magnitude estimation and the non-linearity of acceptability judgments. In *The 27th West Coast Conference on Formal Linguistics*Los Angeles, CA, USA.

Standards America (2002). ASTM D3512-02: Standard test method for pilling resistance and other related surface changes of textile fabrics: Random tumble pilling tester. .

Standards British (2000[a]). BS EN ISO 12945-1:2001:Textiles - Determination of fabric propensity to surface fuzzing and to pilling, Part 1: Pilling box method. .

Standards British (2000[b]).BS EN ISO 12945-2:2000: Textiles - Determination of fabric propensity to surface fuzzing and to pilling, Part 2: Modified Martindale method. .

Stevens, J. C. a. S., S.S. (1963). Brightness Functions: Effects of Adaptation. *Journal of Optical Society of America* 53: 375-385.

Tatler,S.(2007). Illustration portfolio. *http://illustration.stevetatler.co.uk/illustration6.htm*.

Torgerson, W. S. (1958). Theory and Methods of Scaling. *New York*: John Wiley & Sons, Inc.

Umbaugh, S. E. (1998). *Computer vision and image processing : a practical approach using CVIPtools.* Englewood Cliffs, N.J. ; London: Prentice Hall International.

Van der Lans, I., Kirchner, E. &Half, A. (2012). Accurate appearance-based visualization of car paints. In *Conference on Colour in Graphics, Imaging, and Vision*, 17-23 Amsterdam, The Netherlands: Society for Imaging Science and Technology.

Vangorp, P., Laurijssen, J. &Dutré, P. (2007). The influence of shape on the perception of material reflectance. *ACM Transactions on Graphics (TOG)* 26(3, Article 77): 1-9.

Von Kries, J. A. (1911). *In handbuch der Physiologisches* Leopold Voss, Hamburg.

Wei, J. (2006). Assessing the Appearance of Objects. *PhD thesis*; University of Leeds.

Westland, H. B. &Meyer, G. W. (2001). Applying appearance standards to light reflection models. In *The 28th Annual Conference on Computer Graphics and Interactive Techniques*, 501-551. Los Angelels, CA, USA: ACM.

Wyszecki, G. and Stiles, W. S. (1982) Color Science: Concepts and Methods, Quantitative Data andFormulae. John Wiley & Sons, Chichester.

Xiao, B. &Brainard, D. H. (2006). Color perception of 3D objects: Constancy with respect to variation of surface gloss. In *The 3rd symposium on Applied perception in graphics and visualization*, 63-68 Boston, MA, USA: ACM.

Xiao, B. &Brainard, D. H. (2008). Surface gloss and color perception of 3D objects. *Visual Neuroscience* 25(3): 371-385.

Xin, J. &Shen, H.-L. (2005). Proposal for color management of LCD. In *Proceedings of the 9th Color Imaging Conference: Color science and engineering: Systems, technologies, applications*, 341-347 Arizona, USA.

Yamamotoa, S., Sawabe, M., Yokoya, M. &Tsumura, N. (2012). Enhancement of gloss perception by using binocular disparity. In *Conference on Colour in Graphics, Imaging, and Vision*, 226-230 Amsterdam, The Netherlands: Society for Imaging Science and Technology.